NATIONAL CENTER FOR EARTHQUAKE ENGINEERING RESEARCH

ISSN 1088-3800

Deterministic Model for Seismic Damage Evaluation of Reinforced Concrete Structures

by

J.M. Bracci, A.M. Reinhorn, J.B. Mander and S.K. Kunnath

Technical Report NCEER-89-0033

September 27, 1989

This research was conducted at the University at Buffalo, State University of New York and was supported in whole or in part by the National Science Foundation under grant number ECE 86-07591.

NOTICE

This report was prepared by the University at Buffalo, State University of New York as a result of research sponsored by the National Center for Earthquake Engineering Research (NCEER) through a grant from the National Science Foundation, and other sponsors. Neither NCEER, associates of NCEER, its sponsors, the University at Buffalo, State University of New York nor any person acting on their behalf:

a. makes any warranty, express or implied, with respect to the use of any information, apparatus, method, or process disclosed in this report or that such use may not infringe upon privately owned rights; or

b. assumes any liabilities of whatsoever kind with respect to the use of, or the damage resulting from the use of, any information, apparatus, method, or process disclosed in this report.

Any opinions, findings, and conclusions or recommendations expressed in this publication are those of the author(s) and do not necessarily reflect the views of NCEER, the National Science Foundation, or other sponsors.

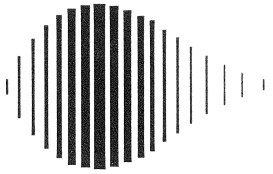

DETERMINISTIC MODEL FOR SEISMIC DAMAGE EVALUATION OF REINFORCED CONCRETE STRUCTURES

by

J.M. Bracci[1], A.M. Reinhorn[2], J.B. Mander[3] and S.K. Kunnath[4]

September 27, 1989

NCEER Technical Report NCEER-89-0033

NCEER Contract Number 88-1002A

NSF Master Contract Number 86-07591

1 Graduate Research Assistant, Dept. of Civil Engineering, State University of New York at Buffalo
2 Associate Professor, Dept. of Civil Engineering, State University of New York at Buffalo
3 Assistant Professor, Dept. of Civil Engineering, State University of New York at Buffalo
4 Research Assistant Professor, Dept. of Civil Engineering, State University of New York at Buffalo

NATIONAL CENTER FOR EARTHQUAKE ENGINEERING RESEARCH
State University of New York at Buffalo
Red Jacket Quadrangle, Buffalo, NY 14261

PREFACE

The National Center for Earthquake Engineering Research (NCEER) is devoted to the expansion and dissemination of knowledge about earthquakes, the improvement of earthquake-resistant design, and the implementation of seismic hazard mitigation procedures to minimize loss of lives and property. The emphasis is on structures and lifelines that are found in zones of moderate to high seismicity throughout the United States.

NCEER's research is being carried out in an integrated and coordinated manner following a structured program. The current research program comprises four main areas:

- Existing and New Structures
- Secondary and Protective Systems
- Lifeline Systems
- Disaster Research and Planning

This technical report pertains to Program 1, Existing and New Structures, and to two of the components of this program, system response, and reliability analysis and risk assessment.

The long term goal of research in Existing and New Structures is to develop seismic hazard mitigation procedures through rational probabilistic risk assessment for damage or collapse of structures, mainly existing buildings, in regions of moderate to high seismicity. This work relies on improved definitions of seismicity and site response, experimental and analytical evaluations of systems response, and more accurate assessment of risk factors. This technology will be incorporated in expert systems tools and improved code formats for existing and new structures. Methods of retrofit will also be developed. When this work is completed, it should be possible to characterize and quantify societal impact of seismic risk in various geographical regions and large municipalities. Toward this goal, the program has been divided into five components, as shown in the figure below:

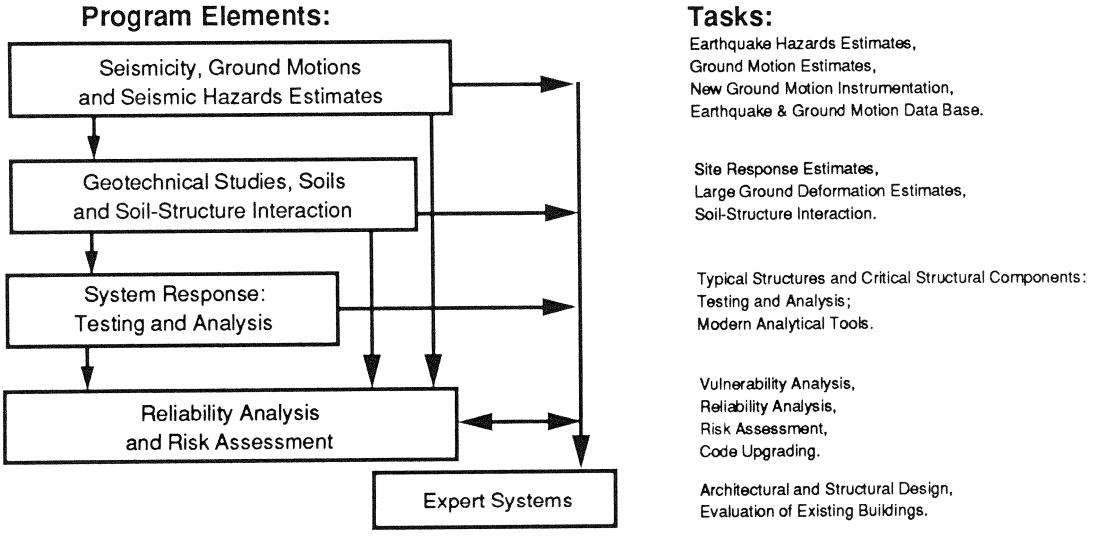

ABSTRACT

A new normalized damage index for evaluation of structural damage of reinforced concrete was developed based on the relation of demand and capacity. The proposed formulation combines two sources of damage: permanent deformation and strength deterioration due to cyclic loading during dynamic events.

The new damage model is first verified for single components. Based on the compressive strains in the core concrete, tensile strains in the transverse hoops and a good photographic record of the component during stages of testing, damage limit states for serviceability, repairability/irrepairability and collapse are identified and correlated with the damage model.

A global damage index is also proposed based on individual member damage indices, which uses a weighting scheme that assigns importance as a function of gravity loading. The global damage model is used for evaluation of structural damage in a three story frame that was tested to failure.

The new damage model is compared with the Park and Ang damage model for a six story structure designed for gravity loads only using Monte Carlo simulations of earthquake ground motion with appropriate local characteristics. The new model compares favorably, but shows additional flexibility in assigning damage states of repairability and irrepairability to structures.

Finally, an inelastic design spectra is recommended for code development wherein the relationship between the natural period of the structure and the response reduction factor is quantified in terms of incurred structural damage.

ACKNOWLEDGEMENTS

Funding for this work was provided through the National Center for Earthquake Engineering Research (NCEER) Contract No. 88-1002A under the National Science Foundation Master Contract No. 86-07591 and the State of New York. The support is gratefully acknowledged.
This report is based on the graduate work of the first author completed under the supervision of the other authors.

TABLE OF CONTENTS

TABLE OF CONTENTS (Cont'd)

LIST OF FIGURES

LIST OF FIGURES (Cont'd)

LIST OF TABLES

SECTION 1

INTRODUCTION

Current practice in earthquake-resistant design of reinforced concrete structures relies on the energy dissipation of components through inelastic cyclic deformation. Consequently, the design of reinforced concrete structures calls for adequate analytical tools that can evaluate the inelastic response of the system. Since inelastic deformations imply some degree of damage, it must be possible, following a nonlinear analysis, to express the response quantities in terms of the damage sustained not only by the components but also by the overall structure. It must also be possible to relate the degree of seismic demand for "damage" as a function of the reserve structural capacity, thereby permitting an assessment of structural integrity in terms of damage limit states, such as serviceability or collapse. This damage estimate can also be used in risk assessment of structures.

The earliest references to damage are ductility based. Newmark and Rosenblueth (1974), who proposed the idea of ductility ratio as a quantitative measure of damage, established the simplest notion of structural integrity. A second source of damage finds its roots in steel models of low-cycle fatigue. Energy-based indices for damage prediction have been used particularly for reinforced concrete since experimental observations point to a correlation between dissipated energy and strength loss. However, energy dissipation mechanisms in reinforced concrete are complex. They depend upon several parameters ranging from the composition and properties of the constituent materials to fluctuations in axial force, the magnitude of critical shear span ratios, and the nature of loading. Hence, a damage index based purely on dissipated energy would tend to be ambiguous. Yet another approach to damage prediction is based on the degradation of certain structural parameters such as stiffness and/or strength. Since no attention is paid either to cumulative damage or the effect of load

history, such indices cannot account for the distinction between capacity, consumption and reserve strength. A synthesis of the essential ingredients in damage prediction was provided by Park, Ang, and Wen (1985) who investigated the physical implication of deformation demand. They came to the conclusion that the deformation capacity of an element is reduced as a consequence of dissipated hysteretic energy caused by cyclic load reversals. Their model (Park et al. 1985) has also been used to evaluate overall damage of buildings using an energy weighting scheme.

Numerous variations of the above mentioned models may be found in the literature. Comprehensive reviews of damage indexing techniques have also appeared in Chung et al.(1987) and Allahabadi et al.(1988). Chung et al.(1987) also go on to define a new accelerated damage index, as an extension of a modified Miner's hypothesis. An important concept coming from their damage model is the development of a lower bound failure curve for low cycle fatigue.

In summary, it may be stated that all of the models listed above are unable to physically relate the quantitative measure of the model to the actual damaged state of the structure. Nor are these models capable of expressing a measure of strength or energy reserve in the structure following a seismic event.

The scope of the work presented in this report consists of the development of a conceptual damage model and its application to reinforced concrete members. Concepts such as damage potential and consumption, deformation and strength damage, will be introduced. A procedure for defining a global damage index based on local damage indices is also proposed.

Verification for the new damage model is presented first with an implementation to individual component members. Hollow column members tested by Mander et al.(1983) are used for the verification due to the availability of an accurate identification of failure and a good photographic collection showing visual damage of the column specimens during testing.

The new damage model is then used for the evaluation of a three story frame, tested to failure by Yunfei et al.(1986). Story level and structural damage indices were determined based on local damage indices.

The new damage model was also used for a comparative evaluation with the damage model of Park and Ang (1985), used in the work by Seidel et al.(1989), for a typical six story reinforced concrete frame structure designed for gravity loads only and subjected to ground motion estimated for the eastern United States. Due to a complete lack of natural earthquake data for the eastern United States, the ground motion was simulated as a nonstationary process of filtered white noise based on given response spectrum characteristics suitable for that area. Story level and structural damage indices were calculated for both maximum and mean earthquakes of magnitude 6.5 and epicentral distance of 20 km.

Finally, from the results of this investigation, conclusions are drawn regarding the future use and application of damage modeling in evaluation of structures that are induced to seismic loading.

SECTION 2

DEVELOPMENT OF A CONCEPTUAL DAMAGE MODEL

2.1 Generalized Damage Model and Definitions

In this section, a conceptual model of damage is developed which utilizes the concepts of *damage consumption* and *available damage potential*. These terms are defined as follows:

> Damage potential, (D_p), is the total capacity of the component to sustain damage.
>
> Damage consumption, (D_c), is that portion of the available capacity that is lost or dissipated during the course of the applied load history.

These basic terms will now be further detailed in a physical sense.

A component that is failed by purely monotonic loading represents an upper bound phenomenon since it is unlikely that any alternative load path will exceed the bounds of the monotonic envelope. At the other extreme of the loading scenario is low cycle fatigue which constitutes repeated cycling at a given amplitude of deformation (Chung et al. 1987). Fig. 2-1 shows an envelope connecting all failure points of inelastic fatigue testing at different deformation levels. This envelope defines a new curve representing a lower bound phenomenon.

The damage potential, D_p, of a reinforced concrete structural component is hereby defined as the total **area** enclosed by the monotonic and the failure envelopes as shown in Fig. 2-1.

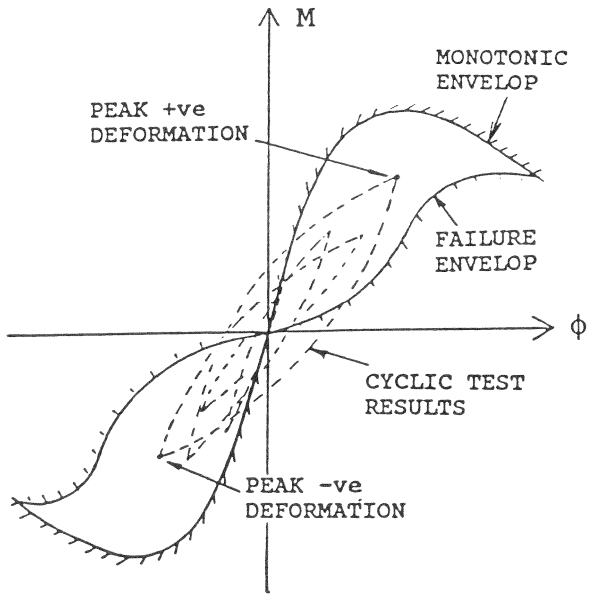

(a) Cyclic Test Data

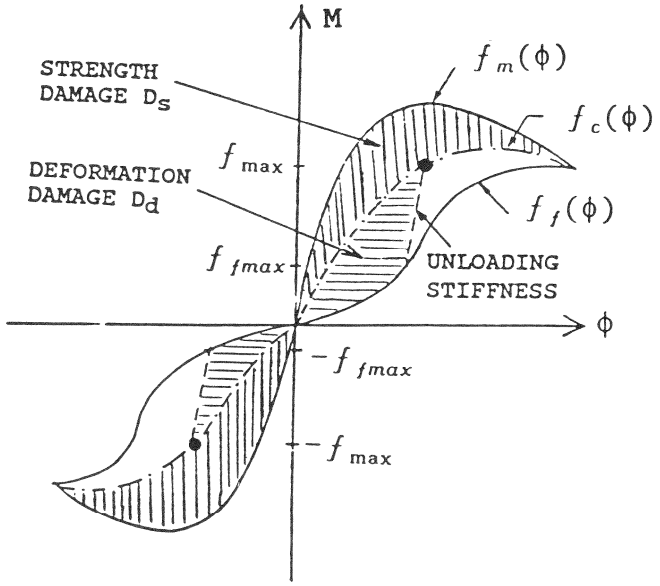

(b) Damage Estimation

FIGURE 2-1 Conceptual Model of Damage

Assuming that the monotonic envelope is specified by some function $f_m(\phi)$ and the failure envelope is defined by another function $f_f(\phi)$, then the damage potential is determined from:

$$D_p = \int_{-\phi_u}^{+\phi_u} \{f_m(\phi) - f_f(\phi)\} d\phi \qquad (2.1)$$

where ϕ is the curvature (displacement) and ϕ_u is the ultimate curvature (displacement) for monotonic loading.

Consider a reinforced concrete component for which the results of a cyclic test are available. Fig. 2-1a shows such a sample test superimposed on the bounding envelopes. A new curve needs to be defined representing the current damage level of the component based on the current positive and negative peak deformations. This is accomplished by defining $f_c(\phi)$ which assumes an intermediate path between the upper and lower bound curves. This function, $f_c(\phi)$, represents *a dynamic upper-bound envelope that is constantly dropping as a consequence of inelastic cyclic deformation. It further implies that this dynamic bounding curve cannot be exceeded in any future traversing of the load-deformation path.* To complete the modeling scheme, two lines, representing the positive and negative unloading stiffness paths, are drawn to intersect the deformation axis.

Fig. 2-1b shows the isolation of areas which constitute the two components of damage demand: the first area corresponding to strength-loss; and the second area arising from deformation related damage. These are defined as follows:

Strength damage is defined as the loss of damage potential due to strength deterioration and dissipated hysteretic energy. This accounts for the lowering of the monotonic or upper-bound curve, $f_m(\phi)$, to the now upper-bound curve, $f_c(\phi)$. Strength damage, D_s, is determined as:

$$D_s = \int_{-\phi_u}^{+\phi_u} \{f_m(\phi) - f_c(\phi)\} d\phi \tag{2.2}$$

Deformation damage accounts for the remainder of the loss of the damage potential. It corresponds to irrecoverable permanent deformations and is evaluated from the area bounded by the current damage level curve, $f_c(\phi)$, and the inelastic failure curve, $f_f(\phi)$, up to the current maximum deformation levels:

$$D_d = \int_{-\phi_a}^{+\phi_a} \{f_c(\phi) - f_f(\phi)\} d\phi \tag{2.3}$$

where ϕ_a represents the line joining f_{max} and f_{fmax} in Fig. 2-1b.

Damage consumption (D_c) can thus be defined as the cumulative effect of strength damage (D_s) and deformation damage (D_d) as follows:

$$D_c = D_s + D_d \tag{2.4}$$

Therefore, a normalized structural Damage Index (D.I.) is defined as the ratio of the damage consumption to the damage potential:

$$D.I. = \frac{D_c}{D_p} \tag{2.5}$$

2.2 Application of Damage Model to Reinforced Concrete Members

The conceptual model of structural damage developed herein is applied to an idealized hysteretic system to demonstrate the applicability of the scheme to practical analysis of reinforced concrete structural systems.

Consider a component whose force-deformation history at member ends is known following a regular response analysis. The peak moment and deformation attained are denoted as $M_{\phi max}$, $\phi_{\phi max}$ with positive and negative superscripts as shown in Fig. 2-2. A prerequisite for evaluating the Damage Index of a component is knowledge about the force and deformation at yield and ultimate levels for monotonic loading. This is established either through the use of empirical equations or some micro-modeling (fiber analysis) scheme. The backbone (upperbound) curve for a reinforced concrete member can now be developed based on an idealized bi-linear relationship.

The next step involves the setting up of the inelastic failure envelope, $f_f(\phi)$. Strictly speaking, the lower bound envelope should come directly from experimental testing of low cycle/inelastic fatigue. However, the task of building experimental lower bound curves as a function of component parameters was considered to be too time-consuming and exceeded the purposes of this study. Consequently, only theoretical possibilities based on observed patterns of low cycle fatigue failure for metals, and some limited data on concrete can be postulated. By assuming the backbone (upper bound) curve for a reinforced concrete member from an idealized bi-linear relationship, one possibility for the lower bound failure envelope is a transposed form of the monotonic yield surface shown in Fig. 2-2a. The second possibility for the lower bound envelope is a simple straight line shown in Fig. 2-2b. It is quite likely that the actual lower bound curve may lie somewhere between the two, suggesting the notion that

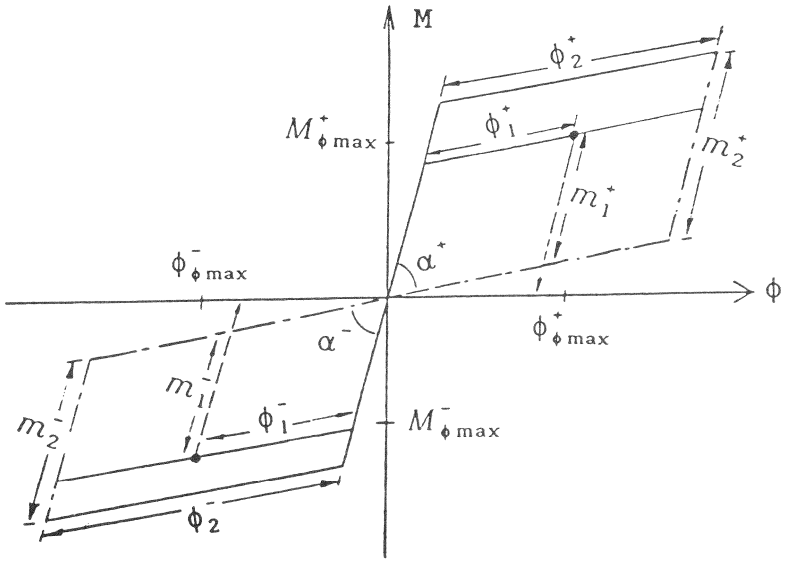

(a) Option #1

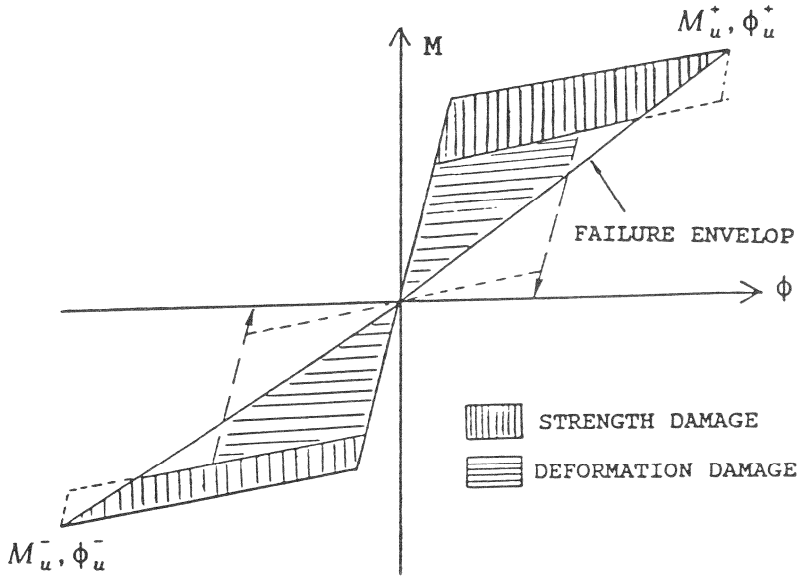

(b) Option #2

FIGURE 2-2 Implementation of Model for Bilinear Hysteresis

the two proposed options could represent an upper and a lower bound of the failure envelope. An analysis using each of the failure criteria could, therefore, yield a range of damage values in which the boundaries represent the least and maximum probable damage.

The formulation of the damage index requires merely the evaluation of Eqs. 2.1 to 2.3. From Fig. 2-2a, the transposed failure envelope (Option #1), the following expressions are derived:

$$D_s = (m_2^+ - m_1^+)\phi_2^+ \sin\alpha^+ + (m_2^- - m_1^-)\phi_2^- \sin\alpha^- \tag{2.6}$$

$$D_d = (m_1^+)\phi_1^+ \sin\alpha^+ + (m_1^-)\phi_1^- \sin\alpha^- \tag{2.7}$$

$$D_p = (m_2^+)\phi_2^+ \sin\alpha^+ + (m_2^-)\phi_2^- \sin\alpha^- \tag{2.8}$$

Generally, the initial and post-yielding stiffnesses in forward displacement are assumed to be the same as in reverse displacement. Hence, $\alpha^+ = \alpha^-$. In addition, if the envelope characteristics are assumed to be the same in forward and reverse displacements, as in the case of typical columns, the following simplified expression results on one side of the member:

$$D.I. = \frac{(m_2 - m_1)\phi_2 + m_1\phi_1}{m_2\phi_2} \tag{2.9}$$

$$D.I. = \frac{m_2 - m_1}{m_2} + \frac{m_1\phi_1}{m_2\phi_2} \tag{2.10}$$

$$D.I. = D_2 + D_1(1 - D_2) \tag{2.11}$$

$$D.I. = D_1 + D_2 - D_1 D_2 \tag{2.12}$$

where $D_1 = \phi_1 / \phi_2 = \{\phi_{max} / \phi_u\}$

$D_2 = (m_2 - m_1)/m_2 = \{\Delta M / M_y\}$

In the case of Option #2, the above formulations still remain valid with the change that the excess areas shown in dotted lines (Fig. 2-2b) must be neglected. This can be achieved with ease if the slope of the failure line is established.

In a T-beam where the initial and post-yielding stiffnesses and the envelope characteristics are not necessarily the same in forward and reverse displacements, the *damage index* can be calculated using Eq. 2.12 in each respective direction of loading with the corresponding parameters for each direction.

The validity of Eq. 2.12 exists only if the *deformation and strength damage indices*, D_1 and D_2, respectively, are less or equal to 1.0. Once either of these indices exceed 1.0, the member has consumed the strength available and will fail. Therefore, a member can fail through either deformation damage (D_1), strength damage (D_2) or a combination of the two as suggested in Eq. 2.12.

2.3 Combining Local Damage Indices

Eq. 2.5 corresponds to the damage at a member end where inelastic rotations are being monitored. The next task is to formulate a simple scheme that can be used to extend the indexing procedure first for the complete member and subsequently for story levels and the entire structure. At the member level, the maximum of the two joint indices (either i or j) is used to represent the *component* damage index:

$$(D.I.)_{member} = \max \{(D.I.)_i, (D.I.)_j\} \qquad (2.13)$$

At the story level, the component indices are combined using a self-weight procedure wherein the local indices themselves are used as weighting parameters:

$$(D.I.)_{total} = \frac{\sum_{i=1}^{N} w_i (D.I.)_i^{(m+1)}}{\sum_{i=1}^{N} w_i (D.I.)_i^{m}} \qquad (2.14)$$

where i = the component

m = the control weighting factor for the component

w_i = the importance factor for the component

The importance factors satisfy the condition:

$$\sum_{i=1}^{N} w_i = 1 \qquad (2.15)$$

so that the damage index $(D.I.)_{total}$ is always normalized.

This procedure can also be extended to the structure level. It is important to survey both story level and overall structure damage since story collapses due to panel mechanisms may not be reflected in the total structure index.

The idea of assigning importance to members and story levels is suggested in assessing the quality of damage (Bertero et al. 1974). Conventional wisdom for seismic design of structures implies that column elements are more *important* than beams in a structure. Likewise, lower story levels may be considered of greater structural importance than upper levels, since if a lower level of structure collapses, it is likely the whole structure will also collapse. On the

other hand, it is possible for an upper story level to collapse (soft story) with the lower structure remaining undamaged. Therefore, the method proposed herein uses *the total tributary gravity load* as the criterion for assigning importance factors for a member. Therefore,

$$w_i = (\text{Total tributary gravity load})_i \; / \; (\text{Total tributary gravity load})_{\text{all members}}$$

Therefore, columns will be weighted more than beams and lower story levels will have greater importance than upper story levels.

2.4 Summary

In this section, a conceptual damage model was developed based on the concept that reinforced concrete members may be damaged by a combination of plastic deformation and cyclic loading. The conceptual model was generalized assuming a bilinear representation for the monotonic loading envelope and two possible options which depict the failure loads under cyclic loading. Also presented in this section is a way of combining local damage indices to quantify the story level and structural damage that was sustained during cyclic loading.

SECTION 3

FORMULATION OF PARAMETERS FOR THE DAMAGE INDEX

3.1 Introduction

Fig. 3-1 shows the parameters, ultimate deformation, stiffness loss and strength degradation[1], that need to be determined when carrying out a damage analysis. This section outlines the methods used to calculate these parameters.

Firstly, the member's ductility capability needs to be assessed as if the member were to be loaded to failure in a monotonic fashion, Fig. 3-1a. It should be noted that under cyclic loading some of the component's ductility capability will be consumed which implies that the maximum displacement which the component can withstand under cyclic loading will be less than the ultimate displacement (Δ_u).

Secondly, the members stiffness change due to plastification needs to be evaluated. This can be identified from component tests by using the parameter α as shown in Fig. 3-1b.

Thirdly, the strength loss due to cyclic loading shown in Fig. 3-1c must be evaluated. In this study the following relationship was used based on the absorbed energy of the member (the meaning and effect of the parameters selected to reflect strength loss is discussed in detail in Section 3.3):

$$\Delta F = \frac{S_{sd} \int dE}{\Delta_y} \qquad (3.1)$$

1 These generalized parameters of force and displacement correspond to the generalized parameters of moment and curvature mentioned in Section 2 for flexural members.

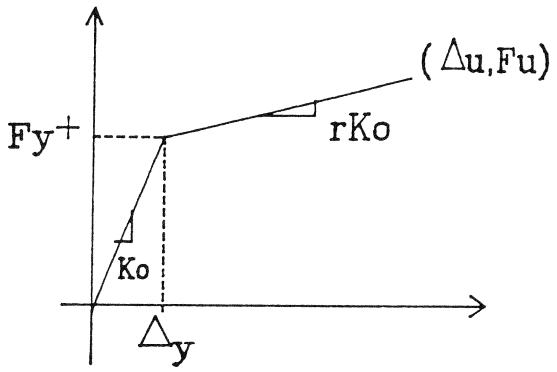

(a) Ultimate Displacement, Δ_u

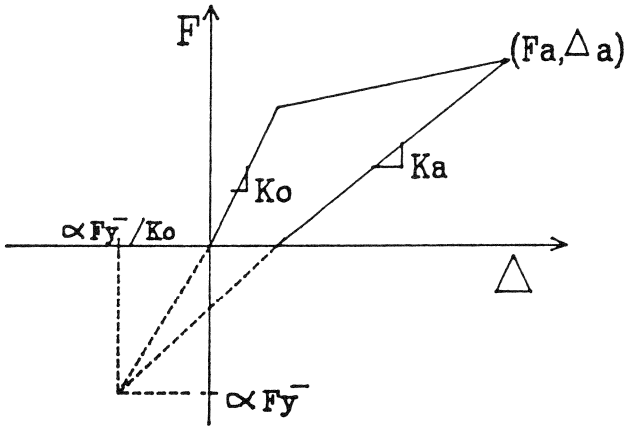

(b) Unloading Stiffness, k_α

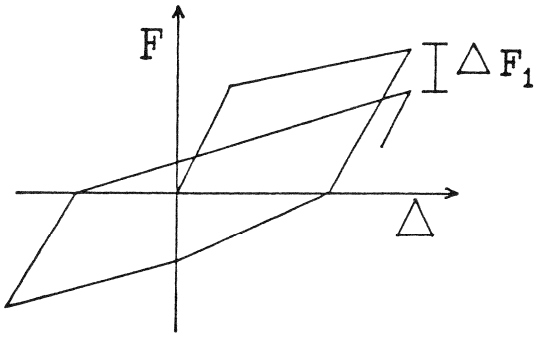

(c) Strength Loss due to Cyclic Loading

FIGURE 3-1 Parameters for Damage Analysis

where ΔF = strength drop on each cycle of loading

Δ_y = yield displacement

$\int dE$ = the total energy absorbed by the member, which is equal to the sum of the area enclosed within the hysteresis curves

S_{sd} = strength deterioration factor

3.2 Evaluation of Deformation Damage

In the development of the proposed damage model, deformation damage is defined to be the *irrecoverable permanent deformation* at a particular displacement level divided by the *permanent irrecoverable deformation at ultimate (failure)* for a member. For the evaluation of the deformation damage, the **ultimate deformation for monotonic loading** and the **unloading stiffness** must be determined.

3.2.1 Determining the Ultimate Deformation for Monotonic Loading

In this study, a standard analytical approach outlined in Park and Paulay (1975) was used for predicting the ultimate displacement for monotonic loading of a member, Δ_u. The method has been advanced by Mander, Priestley, and Park (1984) for confined members under combined axial load and bending.

"Failure" of a component was defined as when: a transverse hoop fractures; the longitudinal steel fractures or buckles; or when the member's strength capacity is reduced by more than 20% due to spalling of the concrete cover.

The data required in terms of the member's geometry and material characteristics for the ultimate deformation analysis is summarized as follows:

Specimen Details:	Member Length	= L
	Gross Concrete Area	= A_g
	Core Concrete Area	= A_{cc}
	Plain Concrete Strength	= f'_c
	Peak Confined Concrete Strength	= f'_{cc}
	Axial Load	= P_e
	Column Width	= H
Longitudinal Steel:	Steel Area	= A_{st}
	Yield Strength	= f_y
	Clear Bar Spacing	= w'
	Number of Bars	= n
	Bar Diameter	= d_b
Tranverse Steel:	Steel Area in Short Direction	= A_{sx}
	Steel Area in Long Direction	= A_{sy}
	Bar Spacing	= s
	Clear Bar Spacing	= s'
	Length in Short Direction	= d_c
	Length in Long Direction	= b_c
	Yield Strength	= f_{yh}

The procedure for calculating the ultimate displacement for monotonic loading using the above data as input is outlined below:

STEP #1 *Determining the confinement effectiveness coefficient*

Based on section geometry, determine the confining stresses along the two orthogonal axes:

$$f'_{lx} = k_e \rho_x f_{yh} \qquad (3.2)$$

$$f'_{ly} = k_e \rho_y f_{yh}$$

where ρ_x and ρ_y are the volumetric steel ratios along each respective axis and defined as follows:

$$\rho_x = \frac{A_{sx}}{s d_c} \quad \text{and} \quad \rho_y = \frac{A_{sy}}{s b_c} \tag{3.3}$$

The total volumetric ratio of the transverse steel, ρ_h, is obtained from:

$$\rho_h = \rho_x + \rho_y \tag{3.4}$$

The confinement effectiveness coefficient (k_e) is given by:

$$k_e = \left(\frac{1 - \frac{1}{6} n w'^2 / A_{cc}}{1 - \rho_{cc}} \right) \left(1 - \frac{0.5 s'}{d_c} \right) \left(1 - \frac{0.5 s'}{b_c} \right) \tag{3.5}$$

in which $\rho_{cc} = A_{st} / A_{cc}$ is the volumetric ratio of the longitudinal steel in the confined core.

STEP #2 *Determine the confining stress ratios*

The provided confined strength f'_{cc}

is obtained as follows:

$$f'_{cc} = K f'_c \tag{3.6}$$

where K is found by using the smallest and largest confining stress ratios from Fig. 3-2 developed by Mander et al.(1984). Note that in this diagram, f'_{co} is the plain concrete strength and may be taken as f'_c. The smallest and largest confining stress ratios are determined as follows:

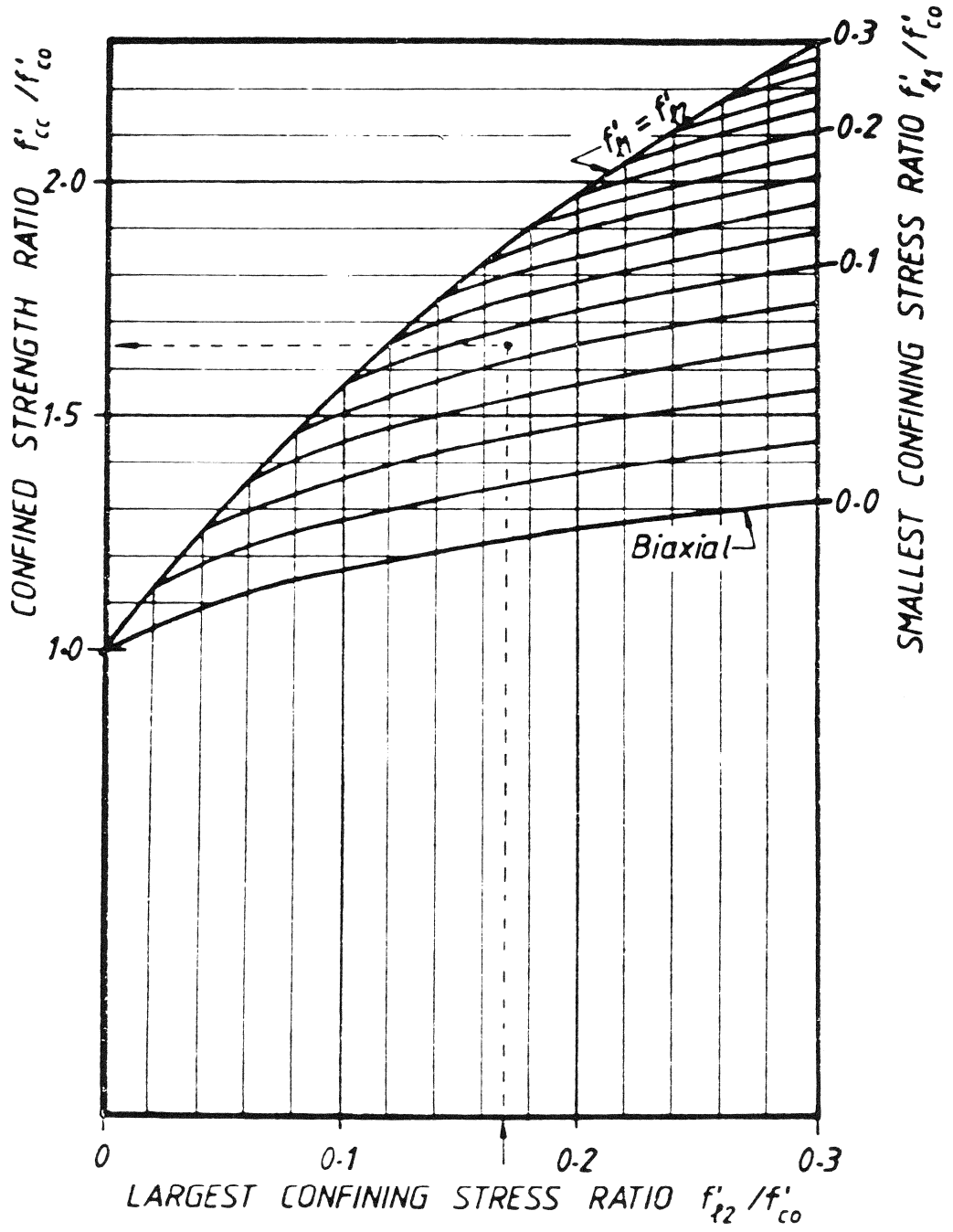

FIGURE 3-2 Relationship Between the Two Principal Confining Stresses and Confined Strength (Mander et al. 1984)

$$\frac{f'_{l1}}{f'_c} \quad \text{and} \quad \frac{f'_{l2}}{f'_c} \tag{3.7}$$

where f'_{l1} is the smaller of f'_{lx} and f'_{ly}

f'_{l2} is the larger of f'_{lx} and f'_{ly}

STEP #3 *Determine the plastic hinge rotation*

Using the axial load ($P_e / f'_c A_g$) and confined strength (K) ratios, the plastic curvature ($\phi_u - \phi_y$) of a concrete section is determined first. Fig. 3-3 shows the normalized plastic curvature for various section shapes with a longitudinal steel ratio of 0.01. These results need to be modified if the section possesses a steel volume different than 0.01 by using Fig. 3-4. The plastic hinge rotation, (θ_p), is then calculated as follows:

$$\theta_p = \left(\frac{\theta_p(\rho_{act})}{\theta_p(\rho = 0.01)}\right)\left(\frac{L_p}{H}\right)((\phi_u - \phi_y)H) \tag{3.8}$$

$$\theta_p = \left(\frac{\theta_p(\rho_{act})}{\theta_p(\rho = 0.01)}\right)\left(\frac{L_p}{H}\right)\left(\left(\frac{\phi_u}{\phi_y} - 1\right)H\phi_y\right)$$

where the plastic hinge length, (L_p), is determined by:

$$L_p = 6d_b + 0.08L \tag{3.9}$$

This formula was suggested by Priestley and Park (1987) based on the test results of Mander et al. (1983).

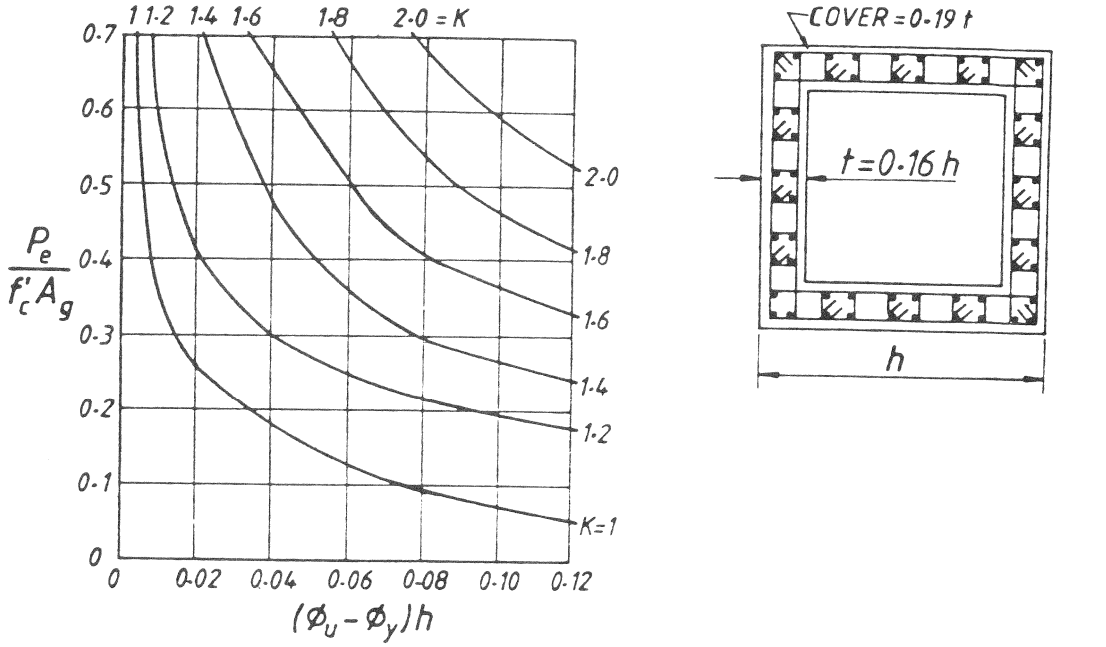

(a) SQUARE HOLLOW COLUMN

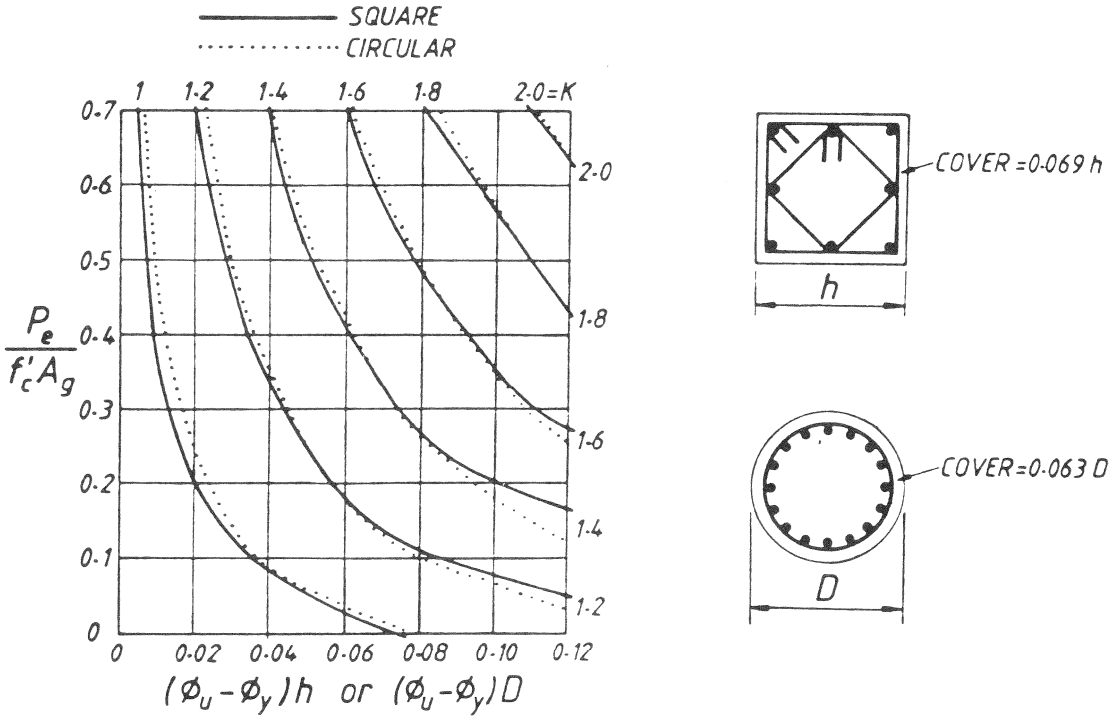

(b) SQUARE AND CIRCULAR COLUMNS

FIGURE 3-3 Ductility Capacity of Concrete Columns with a Longitudinal Steel Ratio of 0.01 (Mander et al. 1984)

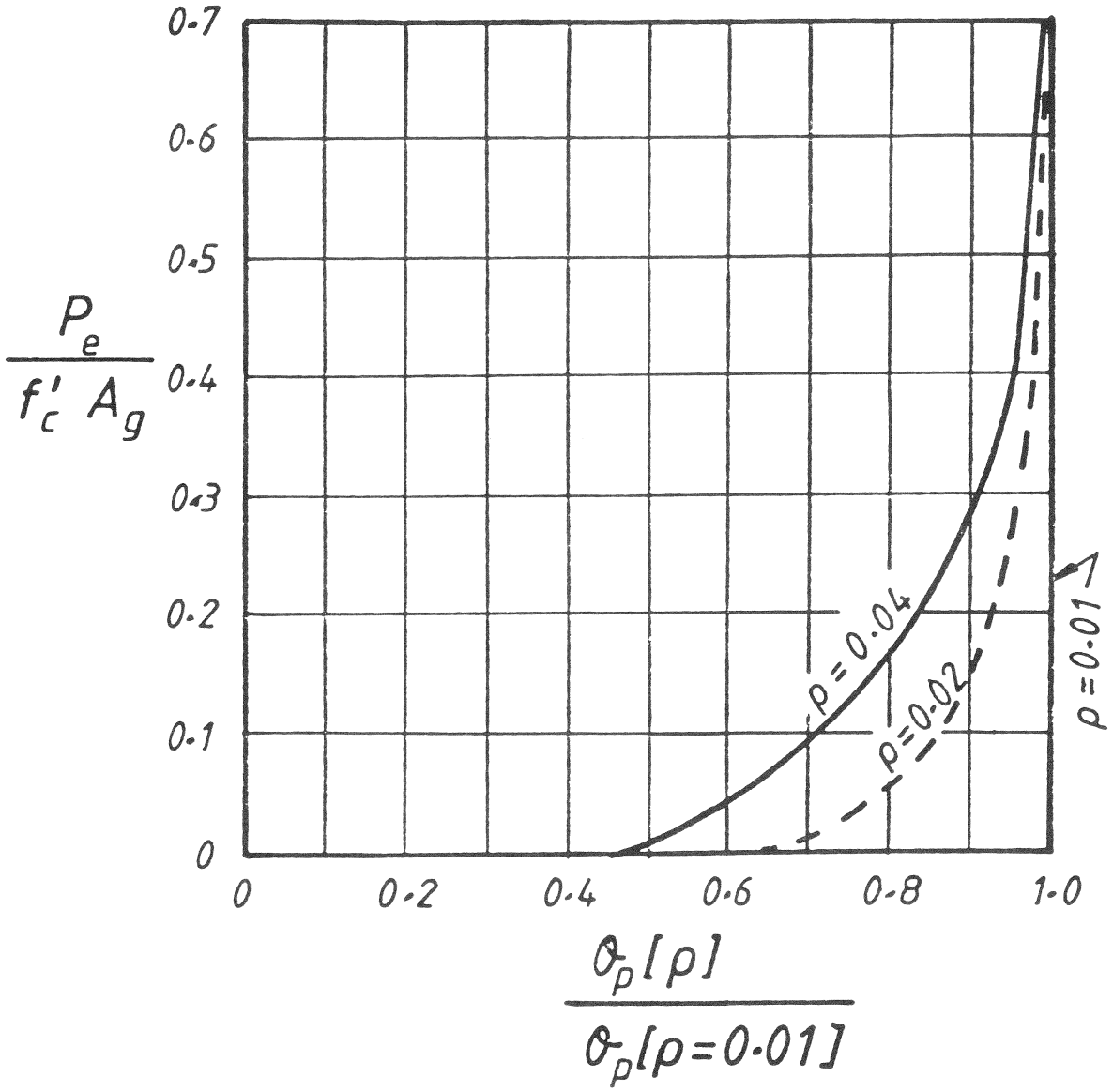

FIGURE 3-4 Effect of the Longitudinal Steel Volume (ρ) on the Plastic Hinge Rotation (θ_p) (Mander et al. 1984)

STEP #4 *Determine the ultimate displacement*

The ultimate displacement is determined from the sum of the plastic displacement Δ_p and the yield displacement Δ_y. Thus,

$$\Delta_u = \Delta_p + \Delta_y \tag{3.10}$$

where the plastic displacement (Δ_p) is determined as follows:

$$\Delta_p = \theta_p (L - 0.5 L_p) \tag{3.11}$$

3.2.2 Determining the Unloading Stiffness

The determination of the unloading stiffness can be found through the use of a stiffness reduction factor (α). Fig. 3-1b shows that α is a factor which distinguishes a direction of the hysteresis loops during unloading. The unloading stiffness can be determined in terms of the unloading stiffness reduction factor as follows:

$$k_a = \frac{F_a + \alpha F_y^-}{\Delta_a + \alpha F_y^- / k_0} \tag{3.12}$$

where F_a = current level of force

F_y^- = yield force for negative displacement

Δ_a = current level of displacement

k_0 = initial stiffness

k_a = unloading stiffness for the current deformation level

The stiffness reduction factor (α) can be determined through a system identification analysis of the actual digitized data or graphically from the hysteresis curves.

3.2.3 Formulation of Deformation Damage

With the evaluation of the two control parameters, deformation damage (D_1) can now be determined from:

$$D_1 = \frac{\phi_a - M_a / k_a}{\phi_u - M_u / k_u} \tag{3.13}$$

where ϕ_a = current level of curvature (displacement)

ϕ_u = ultimate curvature (displacement) for monotonic loading

M_a = current level of moment (force)

M_u = moment (force) at ultimate deformation

k_a = unloading stiffness at current level

k_u = unloading stiffness at ultimate deformation

3.3 Evaluation of Strength Loss with Cyclic Loading

In the development of the proposed damage model (section 2.1), the strength deterioration damage was defined as the strength consumed divided by the strength available. For cyclic loading with constant displacement amplitudes, the strength drop can be computed based on the observed moment loss at the peak deformation of each cycle. However, under random loading where peak deformations are irregular for each cycle, the strength loss can not be found in such a trivial manner.

Previous experiments on reinforced concrete components under cyclic loading show that energy dissipation contributes to the strength loss for a component. Park, Ang and Wen (1985) proposed that the amount of strength deterioration that is consumed by a component is defined in terms of a strength deterioration factor (S_{sd}) as follows:

$$D_s = \frac{S_{sd} \int dE}{\delta_y \Delta F} \qquad (3.14)$$

in which D_s = strength damage

$\int dE$ = dissipated energy (area enclosed between cyclic loading loops)

S_{sd} = strength deterioration factor

δ_y = yield curvature (displacement)

ΔF = available strength at a particular displacement level (defined also in Fig. 2-2 as ΔM for flexural elements)

For Eq. 3.14 to be dimensionless, the yield curvature (or generalized displacement) and moment (or generalized force) are used to normalize the strength loss of a component. Note that the Park, Ang and Wen model (1985) uses δ_u and M_y to normalize the strength loss of a component. The yield curvature (δ_y) was selected over the ultimate curvature (δ_u) to normalize the strength loss of a component primarily due to a better prediction of the yield curvature in this report.

The amount of energy dissipated by a component is known to be a function of many parameters. Some of which are confinement, axial load, longitudinal reinforcement, and the shear span ratio. Experimental data from Nmai et al.(1984), Bertero et al.(1974), Atalay et al.(1975), and Gill et al.(1979) was used to formulate an empirical expression for the strength deterioration factor (Table 3-1). The members from Nmai et al.(1984) were lightly reinforced concrete beams. In contrast, members from Bertero et al.(1974) were strongly reinforced beams. Atalay et al.(1975) and Gill et al.(1979) had column specimens with varying axial load. Thus the experimental data selected for this study consisted of various members in a typical reinforced concrete structure and formulates the strength deterioration factor for beam

TABLE 3-1 Data for Evaluation of the Strength Deterioration Factor, S_{sd}

Author	Specimen	F_{yl} (ksi)	ρ_l (%)	F_{yh} (ksi)	ρ_h (%)	f'_c (psi)	$P_e / f'_c A_g$	$S_{sd\ exp}$	$S_{sd\ th}$ Eq. 3.19
Nmai & Darwin (1984)	F-3	73.8	0.69	32.5	0.909	4260	0.0000	0.00875	0.00707
	F-4	73.8	0.69	38.2	0.799	4330	0.0000	0.00551	0.00708
	F-5	73.8	0.69	38.2	0.609	4370	0.0000	0.00873	0.00717
	F-6	73.8	0.69	32.5	0.909	4320	0.0000	0.00509	0.00709
	F-7	73.8	0.69	38.2	0.650	4220	0.0000	0.01104	0.00710
Bertero et al. (1974)	33	69.0	3.14	71.7	2.115	5400	0.0000	0.00376	0.00378
	35I	69.0	3.14	71.7	1.269	5500	0.0000	0.00396	0.00415
Atalay & Penzien (1975)	2	55.2	2.00	55.0	1.022	4450	0.0937	0.01122	0.01196
	3	55.2	2.00	55.0	1.703	4235	0.0984	0.00686	0.01125
	4	55.2	2.00	55.0	1.022	4005	0.1040	0.01509	0.01195
	5	55.2	2.00	55.0	1.703	4260	0.1957	0.02020	0.01740
	6	55.2	2.00	55.0	1.022	4610	0.1808	0.01129	0.01813
	7	55.2	2.00	55.0	1.703	4615	0.1806	0.02019	0.01721
	8	55.2	2.00	55.0	1.022	4440	0.1877	0.01938	0.01828
	9	55.2	2.00	55.0	1.703	4825	0.2591	0.02733	0.02280
	10	55.2	2.00	55.0	1.022	4700	0.2660	0.02562	0.02418
	11	55.2	2.00	55.0	1.703	4500	0.2778	0.02983	0.02321
Gill et al. (1979)	1	54.4	1.80	43.1	1.540	3350	0.2597	0.01680	0.01952
	2	54.4	1.80	45.8	2.360	6004	0.2140	0.02113	0.02222
	3	54.4	1.80	43.1	2.130	3104	0.4199	0.02184	0.02567
	4	54.4	1.80	42.6	3.170	3408	0.6000	0.03692	0.03393

and column members. Fig. 3-5 shows a typical moment-curvature diagram for a cyclically loaded member. The actual strength deterioration factor at a point can be computed based on the known strength loss at that point as follows:

$$S_{sd} = \frac{\Delta F_1 \delta_y}{\int dE} = \frac{\Delta M_1 \phi_y}{\int dE} \qquad (3.15)$$

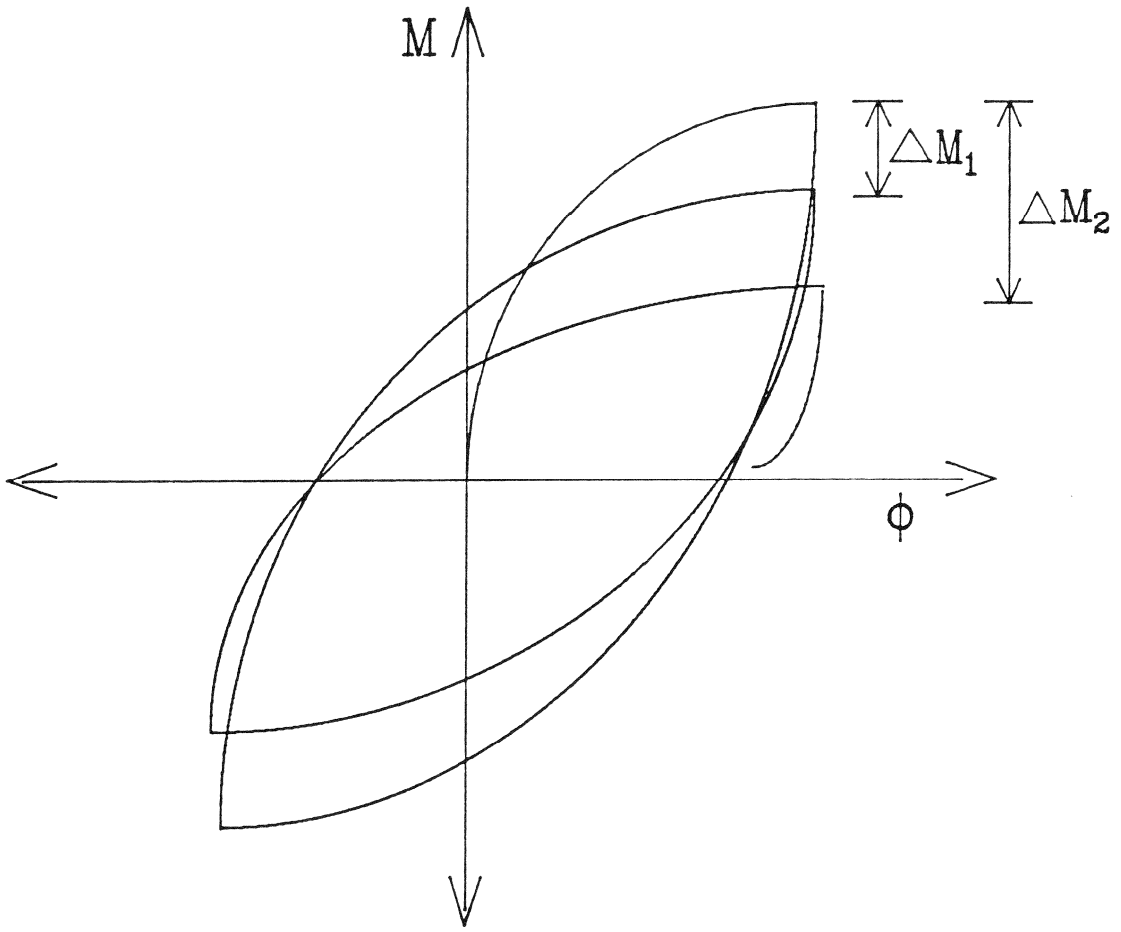

FIGURE 3-5 Strength Deterioration Factor

where ΔM_1 = strength loss up to point 1

$\int dE$ = total dissipated energy (area enclosed between all previous cyclic loading loops) up to point 1

Likewise, the strength deterioration factor can be computed at point 2 and also from the reverse load side. An average strength deterioration factor for a particular member induced to cyclic loading was determined and used in a regression analysis.

The regression analysis was performed on test results from 21 specimens with the influencing parameters mentioned above. It was considered that this minimum amount of specimen data was sufficient to obtain the basis of an empirical equation for the strength deterioration factor.

Three types of regression analyses were considered and tested in order to correlate the strength deterioration factor (S_{sd}) with the parameters influencing the energy dissipation:

$$S_{sd} = R_0\left(1 + \frac{P_e}{A_g f_c'}\right)^{R_1}\left(1 - \frac{\rho_h f_{hw}}{0.85 f_c'}\right)^{R_2}\left(1 - \frac{\rho_l f_y}{0.85 f_c'}\right)^{R_3}\left(1 + \frac{Vd}{M}\right)^{R_4} \qquad (3.16)$$

$$S_{sd} = R_0 + R_1\left(1 + \frac{P_e}{A_g f_c'}\right) + R_2\left(1 - \frac{\rho_h f_{hw}}{0.85 f_c'}\right) + R_3\left(1 - \frac{\rho_l f_y}{0.85 f_c'}\right) + R_4\left(1 + \frac{Vd}{M}\right) \qquad (3.17)$$

$$S_{sd} = R_0\left(1 + \alpha\frac{P_e}{A_g f_c'}\right)\left(1 - \beta\frac{\rho_h f_{hw}}{0.85 f_c'}\right)\left(1 - \gamma\frac{\rho_l f_y}{0.85 f_c'}\right)\left(1 + \delta\frac{Vd}{M}\right) \qquad (3.18)$$

where R_0, R_1, R_2, R_3, R_4 = constants

$\alpha, \beta, \gamma, \delta$ = expansion constants

P_e = Axial load

A_g = gross concrete area

f_c' = unconfined concrete strength

$\rho_h = \rho_x + \rho_y$ = volumetric ratio of the transverse reinforcement

f_{yh} = yield strenth of lateral reinforcement

$\rho_l = A_{st} / A_g$ = longitudinal reinforcement ratio

f_y = yield strength of longitudinal reinforcement

M/Vd = shear span ratio (L/d for a cantilever column)

The forms of these equations were postulated on the basis that strength loss due to cyclic loading will: increase with increasing axial load; decrease as confinement increases; decrease with increasing longitudinal reinforcement ratio; and increase with an increase in shear.

Each equation gave reasonable correlation coefficients. However, Eq. 3.18 was determined to be the most appropriate with δ set to 0.0 due to insufficient data for the shear span ratio. The shear span ratio is known to influence the amount of damage that occurs in a component, but the data available had insufficient variation in the shear span ratio and was therefore neglected in the empirical formulation for the strength deterioration factor in this study. It should be noted that this form of the equation can easily be modified by including other influencing effects, such as shear span ratio, when sufficient data becomes available. The strength deterioration factor was best correlated with the form of Eq. 3.18 as:

$$S_{sd\,th} = 0.00857\left(1 + 12\frac{P_e}{A_g f_c'}\right)\left(1 - 0.5\frac{\rho_h f_{yh}}{0.85 f_c'}\right)\left(1 - \frac{\rho_l f_{yl}}{0.85 f_c'}\right) \qquad (3.19)$$

Fig. 3-6 shows a plot of theoretical versus experimental S_{sd} values. It can be seen that the scatter is minimal. The coefficient of variation was determined to be 24 %.

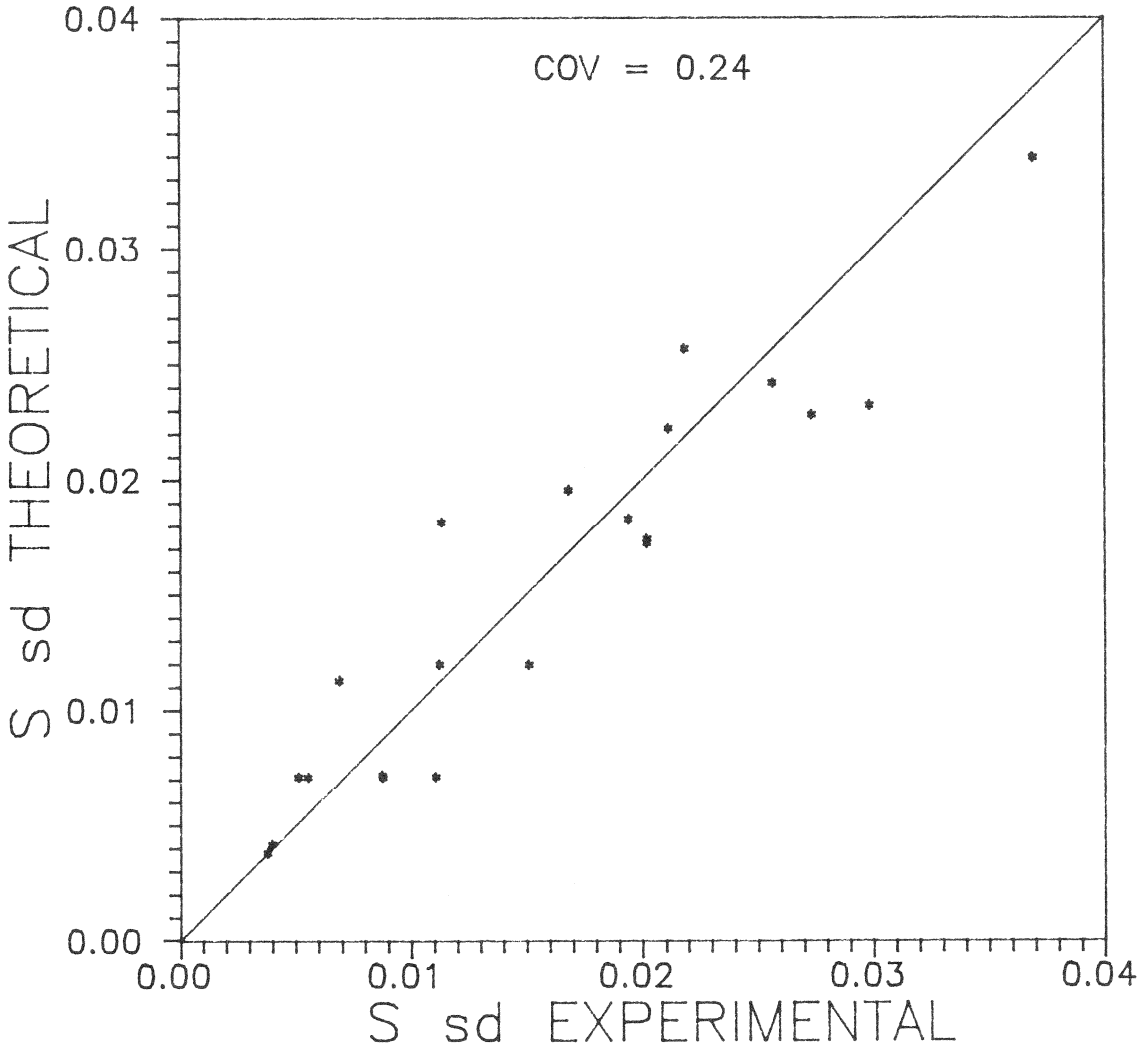

FIGURE 3-6 S_{sd} Theoretical versus S_{sd} Experimental

Fig. 3-7 shows the strength deterioration factor (S_{sd}) plotted against the longitudinal reinforcement ratio(ρ_l) for different amounts of confinement(ρ_h) in a beam($P_e = 0.0$) . As the confinement ratio of a member increases, the strength deterioration factor decreases. Fig. 3-7 also shows that as the longitudinal reinforcement ratio increases, the strength deterioration factor decreases. With the strength deterioration factor decreasing in both of the cases from above, the amount of strength damage also decreases for both cases. Note that as the longitudinal reinforcement ratio approaches 0.07, S_{sd} becomes less than zero. For such a high level of longitudinal steel, the member can behave as a steel member. The implication is that the moment is resisted entirely by a steel couple where work hardening of the steel is possible, therefore showing a negative value for S_{sd}.

Fig. 3-8 shows the strength deterioration factor (S_{sd}) for a column member plotted against the axial load ratio ($P_e / A_g f'_c$) for different amounts of confinement with a constant longitudinal reinforcement ratio(ρ_l) of 0.01. As the axial load on a column member increases, the strength deterioration factor also increases, which implies an increase in strength damage.

3.4 Conclusions

This section has outlined the quantification of the control parameters required in the proposed damage model:

Deformation Damage depends largely on an accurate assessment of the *ultimate displacement under monotonic loading* (ϕ_u *or* Δ_u). A method proposed by Park and Paulay (1975) and advanced for confined members by Mander, Park, and Priestley (1984) has been adopted in this study. The deformation damage also requires the quantification of the *unloading stiffness* (k_α). System identification programs or graphical techniques may be used for the determination of the parameter α, which in turn can be used to find the unloading stiffness.

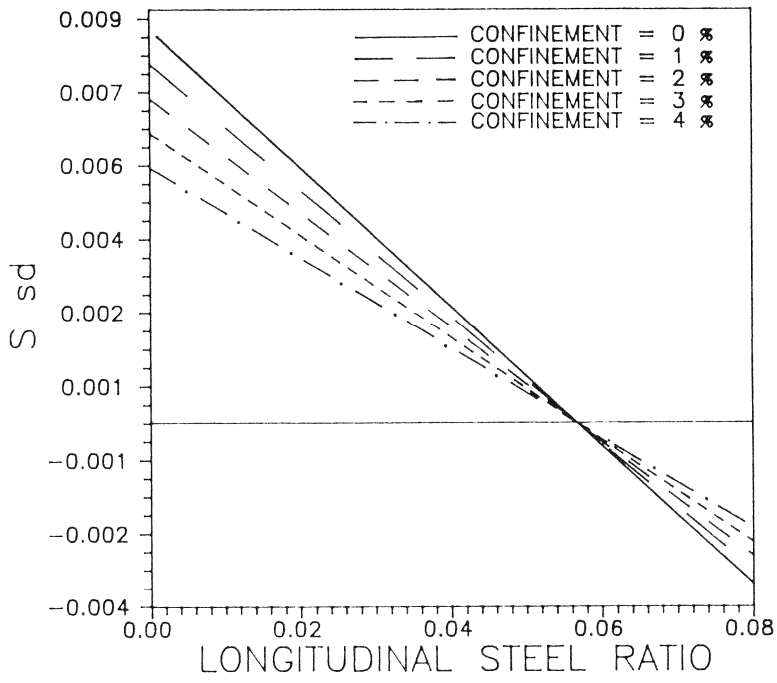

FIGURE 3-7 Strength Deterioration Factor for Beams

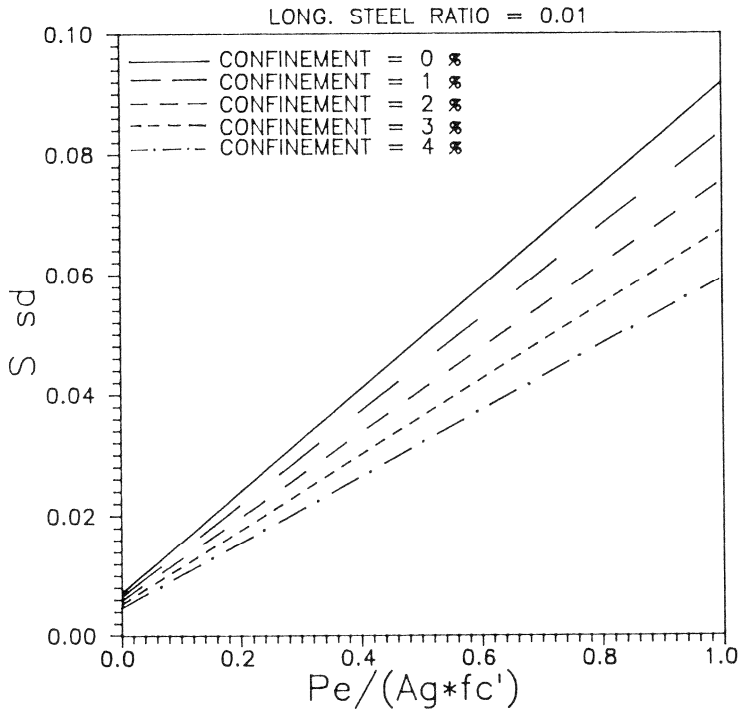

FIGURE 3-8 Strength Deterioration Factor for Columns

Strength Damage depends on an accurate assessment of the loss of strength, ΔM, with each cycle of loading. This may be calculated using the expression:

$$\Delta M = \frac{S_{sd} \int dE}{\delta_y} \qquad (3.20)$$

where S_{sd} is an empirically defined *strength reduction factor* which was calibrated in this study and shown in Eq. 3.19.

SECTION 4

VERIFICATION OF DAMAGE MODEL FOR SINGLE COMPONENTS

4.1 Introduction

Before utilizing the proposed damage model to evaluate damaged frames and complete structures, the damage model was verified against component tests in which the experimental failure characteristics could precisely be determined. It was found necessary to test the model independently of those specimens used to define the strength deterioration factor (S_{sd}). Mander, Park and Priestley (1983) tested four near full-sized hollow column specimens (Columns A,B,C,D) under varying levels of axial load with differing amounts of confining steel. Column B was not considered in this verification since the specimen failed prematurely outside the plastic hinge region during testing. The other three columns were used to study the contributing effects of cyclic loading on damage of reinforced concrete members. A good photographic record of the tests at various levels of ductility was available, thereby enabling a visual description of damage at various stages of loading to be correlated with the Damage Index. The amount of damage that occurred can also be viewed from the longitudinal compression strains in the core concrete and transverse tensile strains in the flange hoops. With the use of these visual aids, together with the observed experimental longitudinal compression strains in the core concrete and the transverse tensile strains in the flange hoops, engineering judgement was applied to identify Damage Indices corresponding to levels of *"serviceability"*, *"repairability"* and *"irrepairability"*. This concept is useful when translating quantified damage into a heuristic knowledge based system.

4.2 Description of the Test Specimen

Fig. 4-1 shows a typical column specimen and the test setup for the experiments conducted by Mander et al. (1983). Each column specimen tested had the same height, cross section and wall thickness of 3.2 m, 750 mm and 120 mm, respectively. Likewise, the longitudinal reinforcement ratio (ρ_l) was held constant at 0.0155 for all column members tested. The varying test parameters were the level of axial load and the transverse confining steel ratio. Columns A and D had the same amount of transverse reinforcement (0.021) but were tested at axial loads of $0.1 f_c' A_g$ and $0.3 f_c' A_g$, respectively. Columns C and D were tested at an axial load of $0.3 f_c' A_g$, but Column C had about 50% more confining steel than Column D (0.031).

Each of the specimens were tested in a quasi-static fashion consisting of two complete cycles each at displacement ductility factors of $\mu = \pm 2, \pm 4, \pm 6$, and ± 8, unless premature failure of the specimen occurred. The force-displacement hysteresis for each respective column is shown in Figs. 4-2, 4-3 and 4-4.

4.3 Calculation of Required Variables

Section 3 outlined the procedures for calculating the control parameters used in the damage analysis. The damage analysis requires knowledge of the strength deterioration factor, S_{sd}. In section 3.3, evaluation of strength loss with cyclic loading, the strength deterioration factor was formulated independently of the column specimens tested by Mander et al.(1983). Table 4-1 shows the calculation of the strength deterioration factor for the column members tested.

Other variables needed for the damage analysis are the initial yielding stiffness (k_0), yield deformation(Δ_y), and yield force(F_y). These variables can be determined quite accurately

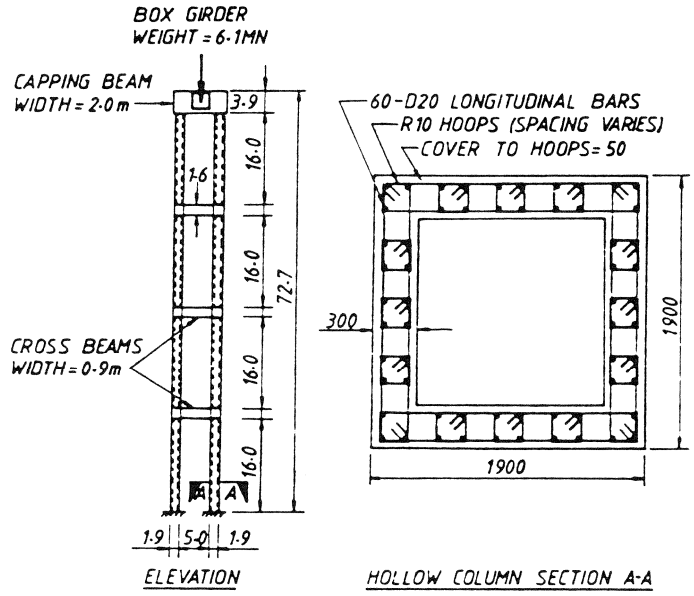

(a) PROTOTYPE PIER WITH DUCTILE HOLLOW COLUMNS

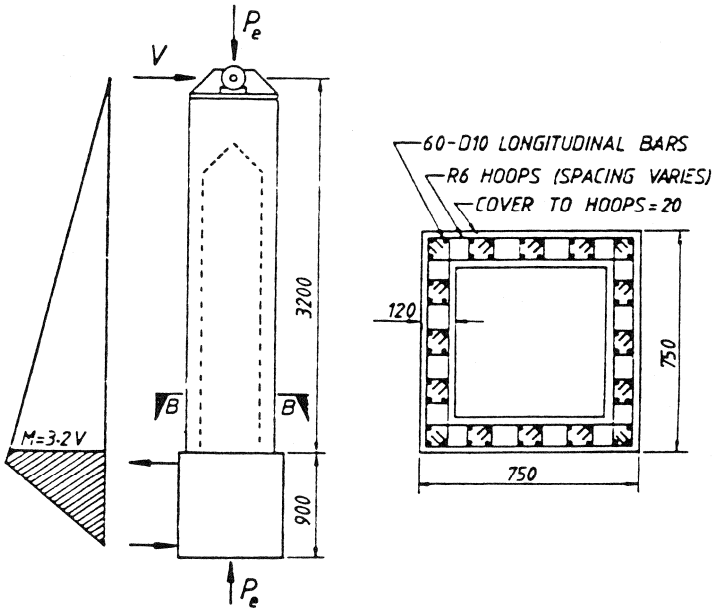

(b) SCALE MODELLING OF PROTOTYPE HOLLOW COLUMNS

Hoop set spacings in the hinge region were 60, 40 and 60 mm for Columns A, C and D, respectively. Outside the hinge region, hoop spacing was 120 mm.

FIGURE 4-1 Specimen Model (Mander, Park and Priestley 1984)

(25.4 mm = 1 inch)

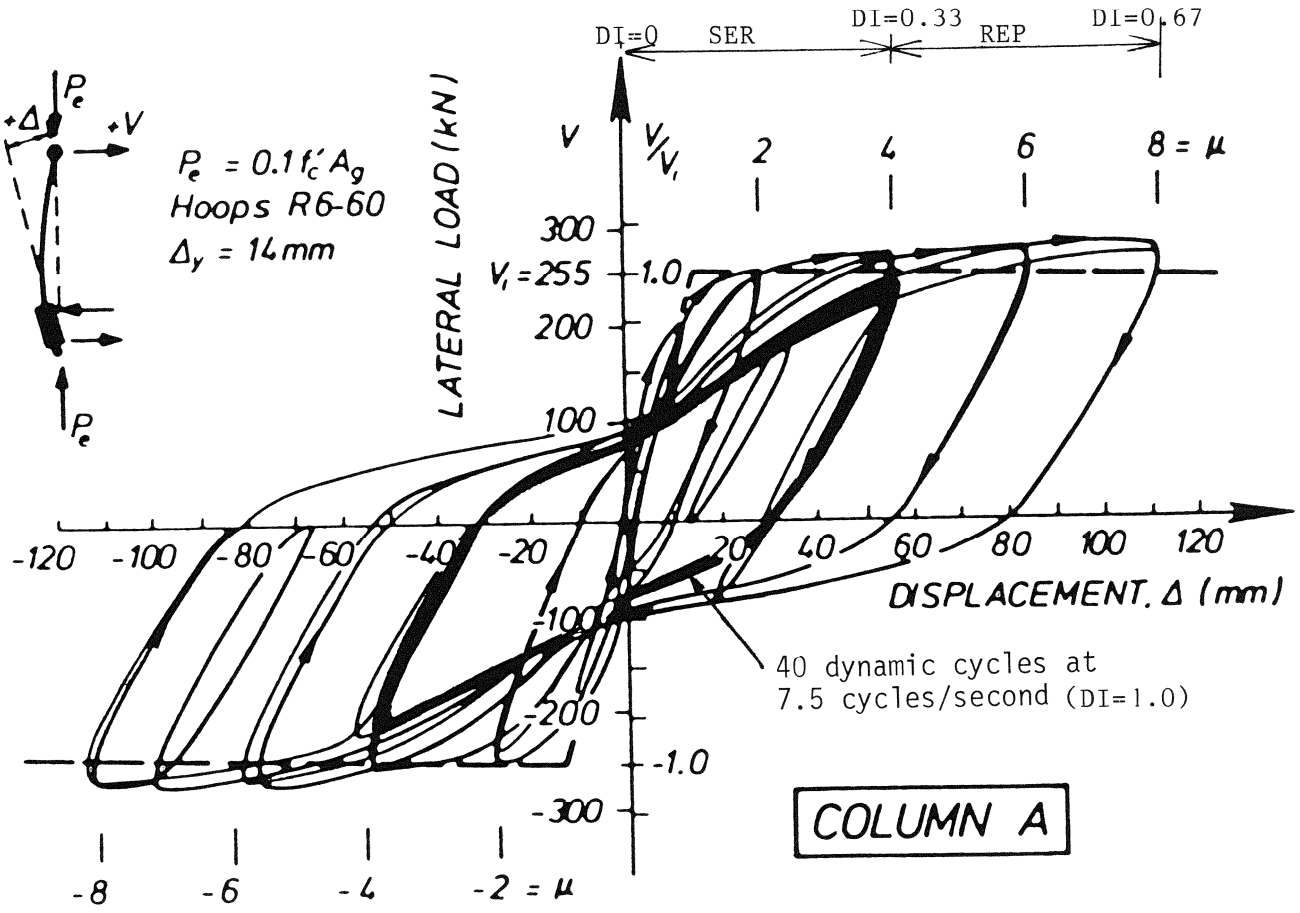

SER = SERVICEABLE
REP = REPAIRABLE

FIGURE 4-2 Force-Displacement Hysteresis for Column A

(Mander, Park and Priestley 1984)

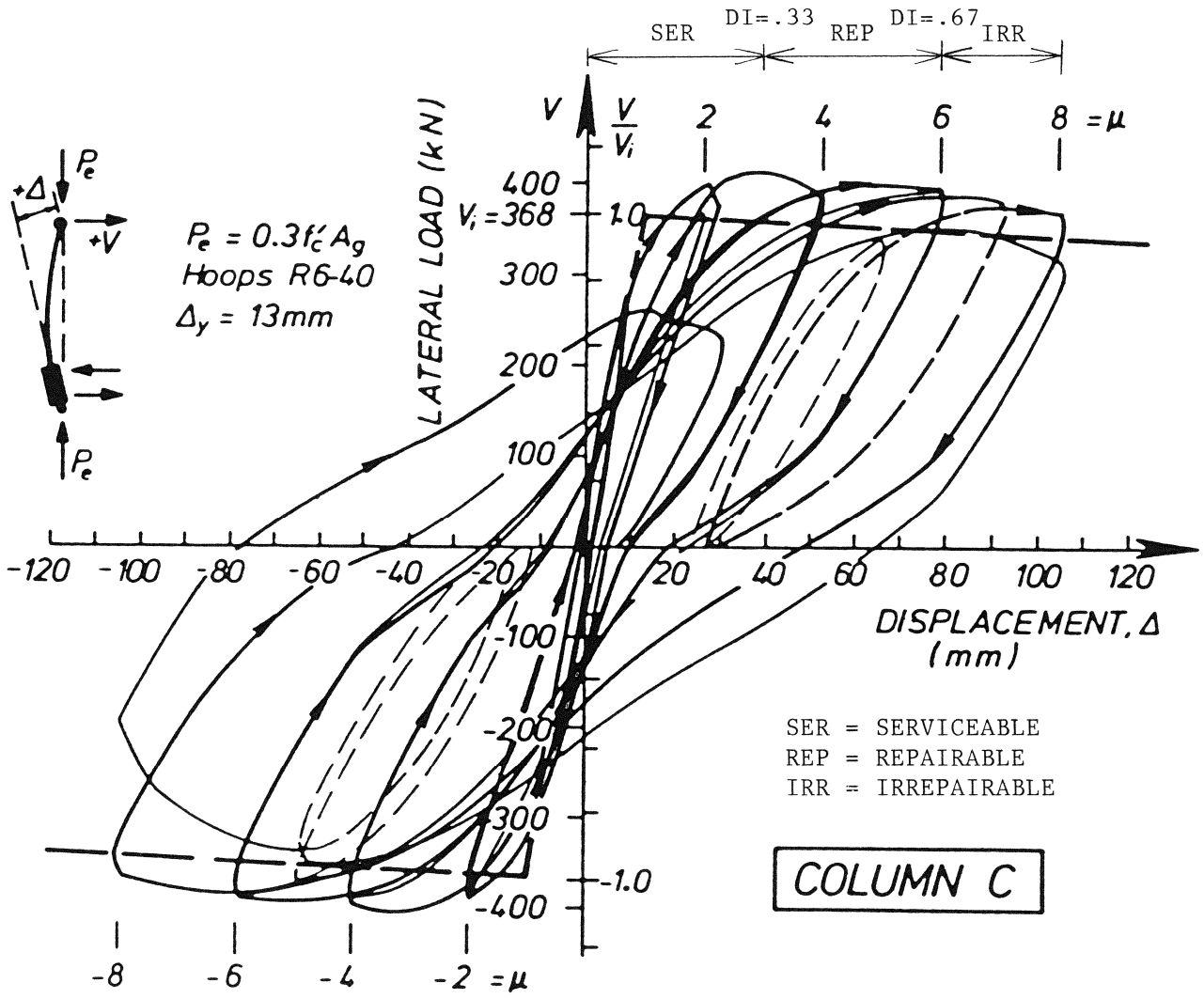

FIGURE 4-3 Force-Displacement Hysteresis for Column C

(Mander, Park and Priestley 1984)

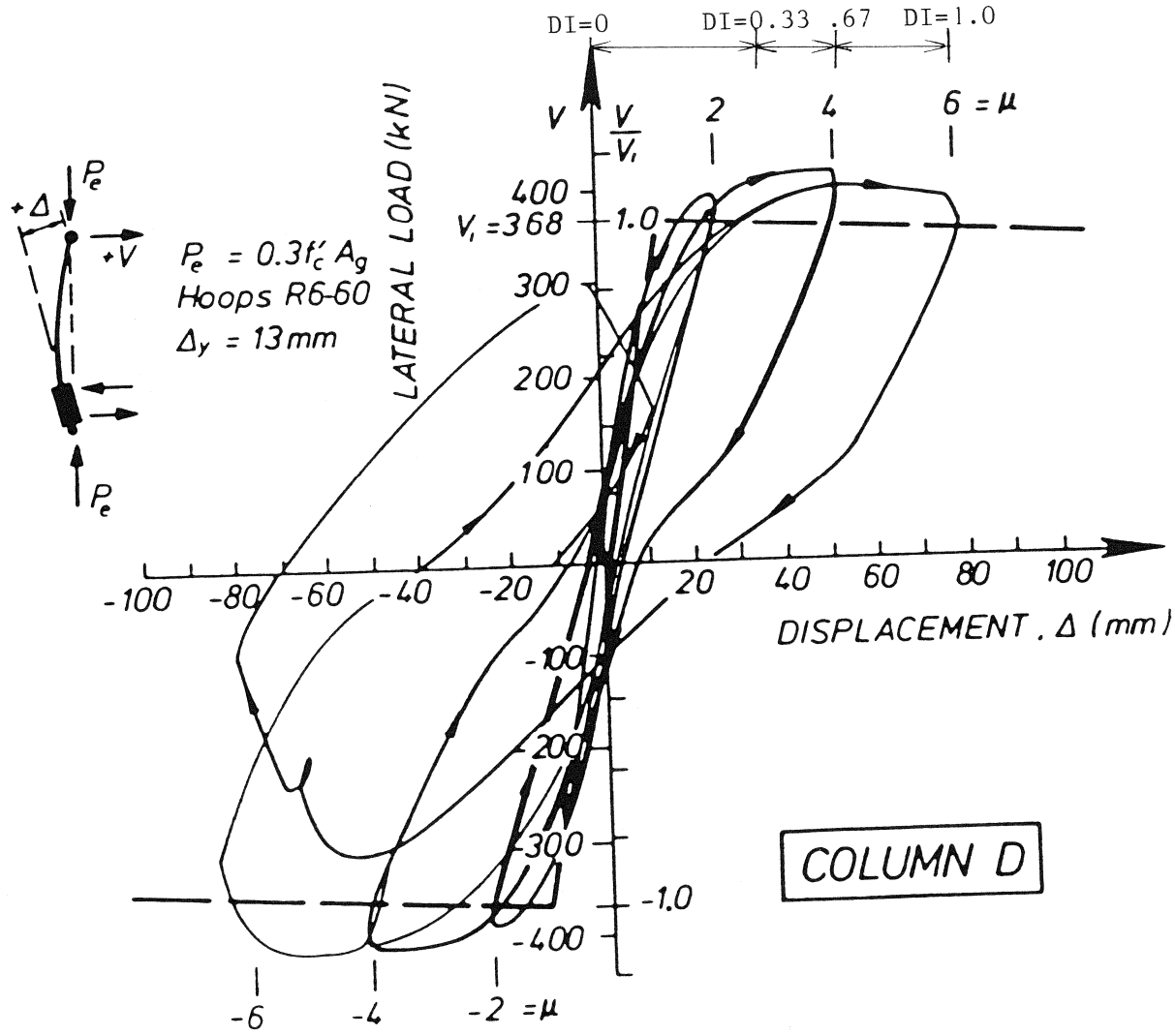

FIGURE 4-4 Force-Displacement Hysteresis for Column D

(Mander, Park and Priestley 1984)

TABLE 4-1 Determination of S_{sd} and Δ_u

Parameter	Units	Source	Column A	Column C	Column D
Axial load, $P_e/f_c'A_g$		Test	0.1	0.3	0.3
Transverse steel ratio, ρ_h		Data	0.021	0.031	0.021
Longitudinal steel ratio, ρ_l		Data	0.0155	0.0155	0.155
S_{sd}		Eq.3.19	**0.0067**	**0.0112**	**0.0123**
1. k_e		Eq.3.5	0.473	0.578	0.473
Volumetric steel ratios:		Eq.3.3			
(a).ρ_x			0.012	0.019	0.012
(b).ρ_y			0.008	0.012	0.008
2. Confining Stress ratio:		Eqs.3.2, 3.7			
(a). larger (f'_{l2}/f'_c)			0.063	0.119	0.065
(b). smaller (f'_{l1}/f'_c)			0.041	0.077	0.042
3. Confined Strength Ratio (K)		Fig.3-2	1.31	1.54	1.32
$\theta_p(\rho_l = 0.01)$		Fig.3-3	0.21	0.115	0.065
$\theta_p(\rho_l(act))$		Fig.3-4	0.195	0.111	0.063
L_p/H		Eq.3.9	0.4	0.4	0.4
θ_p		Eq.3.8	0.078	0.0444	0.0252
4. Δ_p	mm	Eq.3.11	239	136	77
Δ_y	mm	Test	14	13	13
Δ_u	mm	Eq.3.10	**253**	**149**	**90**
$\mu = \Delta_u/\Delta_y$		Test	18	11.5	6.9

through the use of empirical formulations. However, the actual experimentally observed values of Δ_y and F_y were used in this study, with $k_o = F_y/\Delta_y$. These variables are also shown in Table 4-2.

The final variables required for the damage analysis are the ultimate displacement for monotonic loading (Δ_u) and the unloading stiffness factor (α). Table 4-1 shows the calculation of Δ_u as outlined in section 3.2.1. The level of force at the ultimate monotonic displacement (F_u) was calculated from the observed post-yielding stiffness of the respective column test result. The unloading stiffness factor was determined graphically. These values are tabulated in Table 4-2.

4.4 Results of Damage Analysis

Using the control parameters in Table 4-2 together with the digitized data of the force-displacement hysteresis loops, the amount of damage that occurred in each component was analyzed using both Options #1 and #2 from Fig. 2-2. The results are tabulated in Table 4-3. Option #2 showed very high strength damage when the member was displaced near the ultimate monotonic deformation. This implies that the amount of strength consumed exceeds the amount of strength available, i.e. failure. For example, Column D has a calculated strength damage of 3.2 during a point in loading, but experimentally the member had not yet failed. Therefore, Option #2 will be disregarded as being a possible lower bound curve due to the very high strength Damage Index that is calculated when the displacement approaches the ultimate monotonic displacement. The following discussion will only pertain to Option #1.

Figs. 4-5a, 4-6a and 4-7a present the results of the damage analysis with respect to displacement ductility, $\mu = \Delta_a/\Delta_y$ where Δ_a is the current maximum displacement. Figs. 4-5b, 4-6b and 4-7b are the results of the damage analysis with respect to cumulative ductility ($\sum\mu$).

TABLE 4-2 Control Parameters for Damage Analysis

Column	F_u	α	Δ_y	Δ_u	F_y	k_o	S_{sd}
	(KN)		(mm)	(mm)	(KN)	(KN/mm)	Eq. 3.19
A	300	3.00	14	260	255	18.2	0.0067
C	432	2.00	13	150	368	28.3	0.0112
D	445	3.60	13	90	368	28.3	0.0123

TABLE 4-3 Results of Damage Analysis at Failure Stage

Column	Option #1			Option #2		
	D_1	D_2	DI	D_1	D_2	DI
			Eq. 2.10			Eq. 2.10
A	0.50	1.35	1.18	0.50	1.75	1.38
C	0.84	0.69	0.96	0.84	2.20	1.10
D	0.94	0.34	0.96	0.94	3.20	1.20

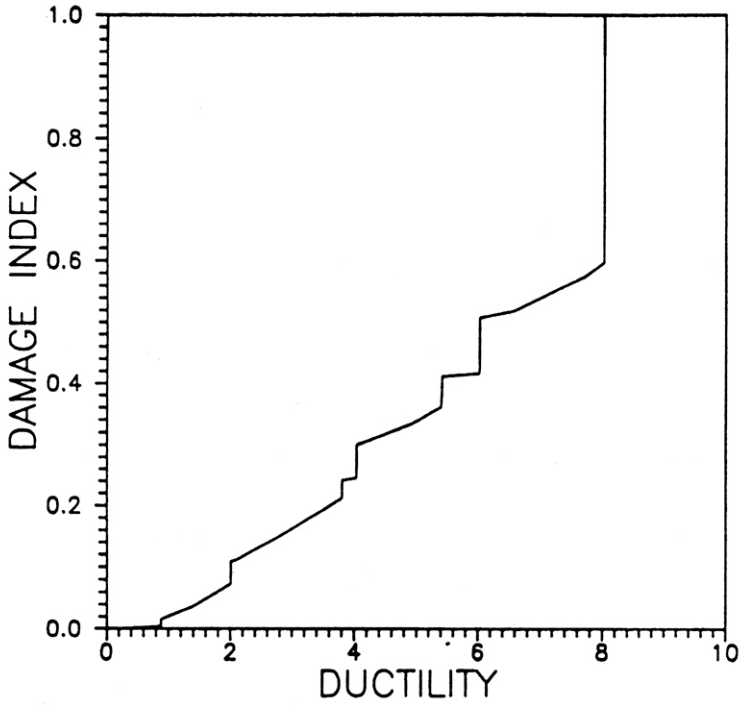

(a) DI versus μ

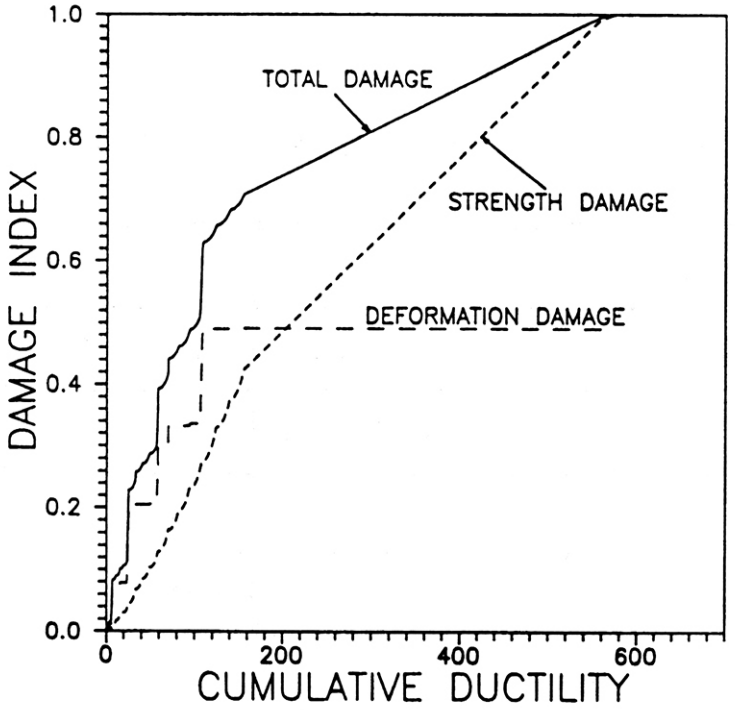

(b) DI versus $\sum \mu$

FIGURE 4-5 Damage Analysis for Column A

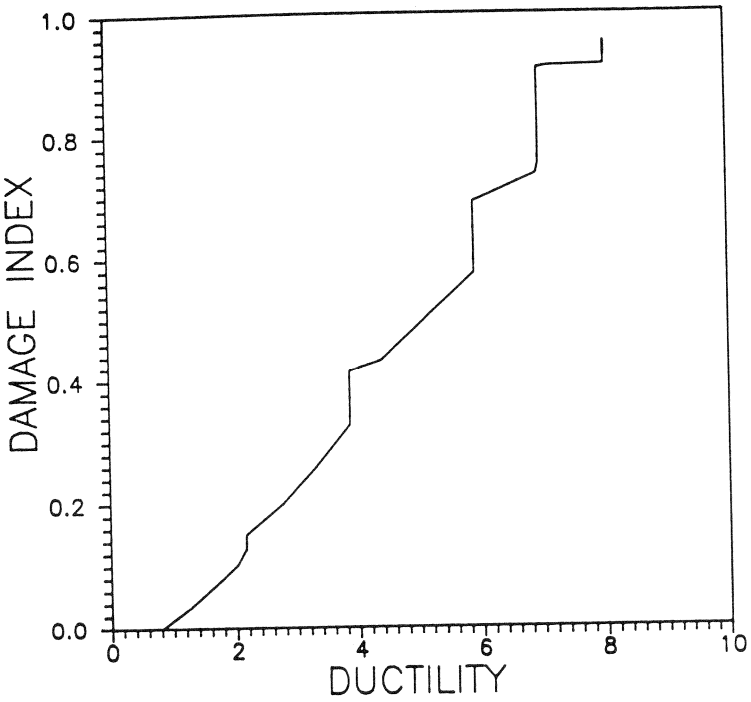

(a) DI versus μ

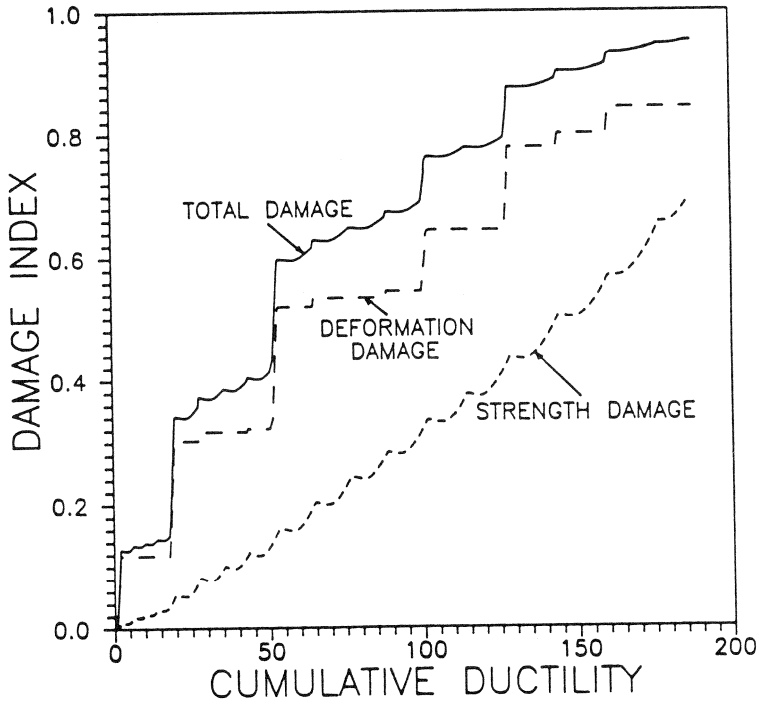

(b) DI versus $\sum \mu$

FIGURE 4-6 Damage Analysis for Column C

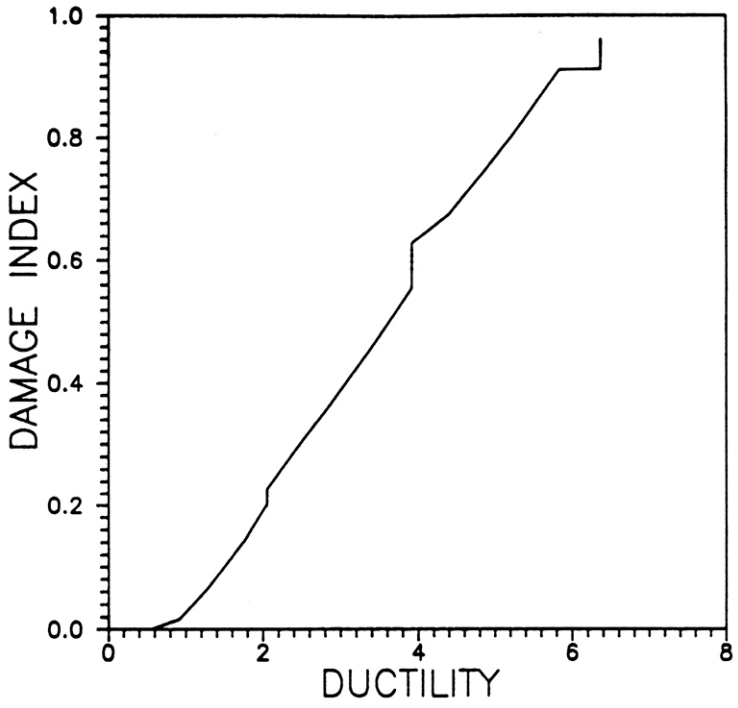

(a) DI versus μ

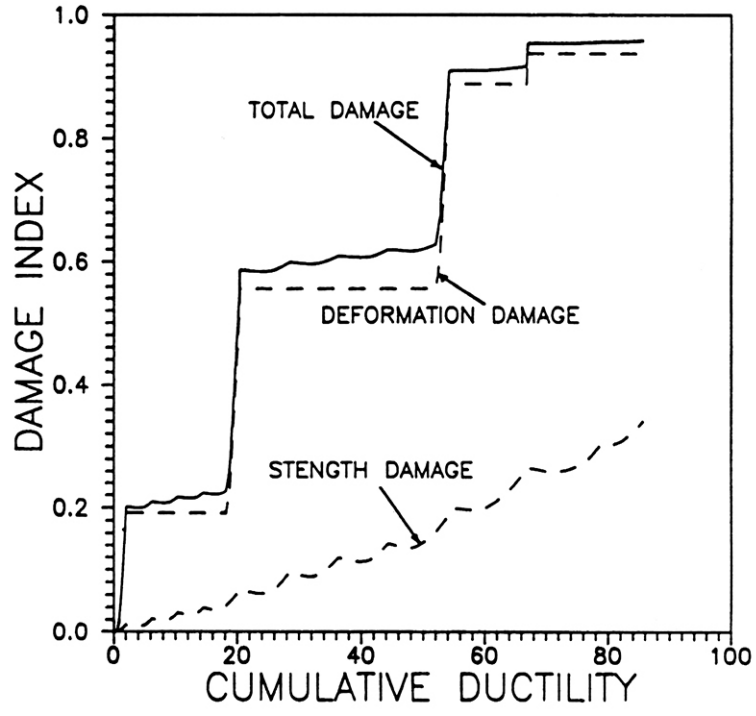

(b) DI versus $\sum \mu$

FIGURE 4-7 Damage Analysis for Column D

Table 4-4 Results of Sensitivity Analysis with 25 % Change in S_{sd}

Column	Result for 25 % *decrease* in S_{sd} using Option #1			Results for 25 % *increase* in S_{sd} using Option #1		
	D_2	DI	% change in DI with Option #1	D_2	DI	% change in DI with Option #1
A	1.02	1.01	14	1.69	1.35	14
C	0.52	0.93	3	0.86	0.98	3
D	0.25	0.95	1	0.43	0.97	1

For Column A after two cycles at $\mu = \pm 8$, Fig. 4-5a shows that the damage index was found to be 0.63. Since the component had not yet failed, the column was placed in dynamic cyclic loading at $\mu = \pm 4$ until failure occurred due to low cycle fatigue of the longitudinal reinforcement after 40 dynamic cycles. Fig. 4-5b also shows the strength damage (D_2) continuously increasing until the member failed (DI = 1.0) due to low cycle fatigue. On the other hand, the deformation damage (D_1), previously loaded to a ductility level of ± 8 and then reduced to a ductility level of ± 4 for the dynamic cycling, remained constant at about 0.5 due to the loading at $\mu = \pm 8$. It should be noted the deformation damage (D_1) could only be increased if the specimen was displaced beyond $\mu = \pm 8$.

Fig. 4-5b shows that the cumulative ductility at failure was determined to be about 600, which corresponds to failure after about 25 dynamic cycles at $\mu = \pm 4$. The observed failure for Column A occurred after 40 dynamic cycles, where the cumulative ductility was about 800. This moderately conservative prediction of failure was due to the strength deterioration factor (S_{sd}). In the formulation of the strength deterioration factor, the coefficient of variation was 24%. The results of a sensitivity study of the damage analysis for a 25% change in S_{sd} (approximately one standard deviation) are shown in Table 4-4 . Failure was accurately predicted

after 40 dynamic cycles at $\mu = \pm 4$ for Column A with a 25% reduction in S_{sd}. This resulted in a 14% change in the Damage Index. Therefore, this analysis provides a verification of the sensitivity of the strength deterioration factor used in finding the amount of strength damage.

The observed failure in Column C occurred at the completion of the second cycle of loading at $\mu = +8$. Fig. 4-6a shows that failure occurred in Column C at a displacement ductility factor $\mu = \pm 8$. Fig. 4-6b shows that the deformation damage (D_1) was the primary cause of failure ($D_1 = 0.84$) combined with a significant amount of strength damage (D_2) of 0.69 that accumulated until failure.

After two cycles at displacement ductilities of $\mu = \pm 2$ and ± 4, Column D was then loaded to $\mu = -6$ where observed failure occurred due to transverse hoop fracture. Fig. 4-7a shows that Column D failed at $\mu = 6$ due mostly to deformation damage ($D_1 = 0.94$), while the strength damage (D_2) was 0.34 (Fig. 4-7b).

Columns C and D failed primarily due to deformation damage. But, the results clearly show that the strength damage due to cyclic loading had a contributing effect on the damage that occurred. By viewing the displacement ductility factor at failure, the member's ductility capacity was reduced due to cyclic loading. Under monotonic loading, the calculated ultimate displacement ductility factor for Column C from Table 4-1 was $\mu = 11.5$. However under cyclic loading test patterns, Column C failed at $\mu = 8.0$. Similarly, Column D had a calculated ultimate displacement ductility factor of $\mu = 7.0$, but actually failed at $\mu = 6$ due to cyclic loading damage. Also from Table 4-4, the 25% variation in S_{sd} has only a 3% and 1% change in the Damage Index. This implies that the strength deterioration factor has little effect for a member governed by irrecoverable deformation damage.

4.5 Experimental Observations of Component Testing

Actual damage in members that have been cyclically loaded can be evaluated based on the experimentally observed longitudinal compression strains in the core concrete and the transverse tensile strains in the flange hoops. However, following an earthquake in which members suffer damage, an inspecting engineer does not have strain gages available during the time of inspection to determine the extent of damage that may have occurred to the member. A decision must be based on a visual observation of damage. The amount of cracking and concrete cover spalling can be used to evaluate the damage of a specimen. Visual accounts of longitudinal steel buckling, transverse hoop fracture, etc. can also be used for inspection purposes. Mander et al.(1983) kept a good photographic record of the test specimens at various levels of displacement ductilities. Therefore, from engineering judgement, the state of damage in each specimen was determined from the measured strains and visual evaluation.

Figs. 4-8, 4-10, and 4-13 show the measured longitudinal strains in the core concrete and the transverse tensile strains in the flange hoops for each respective column during the domain of cycling. When the longitudinal strains for the concrete core have reached 0.008, it can be considered that unconfined cover concrete will be completely lost by spalling. Therefore when the strains in the concrete core are less than 0.008, the member's concrete cover is still mostly intact and the member can sustain the required moment and axial load. Also when the measured transverse tensile strains in the flange hoops are less then the corresponding yield strains, the transverse reinforcement behaves elastically, implying concrete strains are small with stresses not exceeding f_c'.

4.6 Damage Analysis Correlation with Experimentally Observed Damage

COLUMN A:

Column A was cycled twice at a displacement ductility, $\mu = \pm 2$ and then at $\mu = \pm 4$. Fig. 4-8 shows the measured longitudinal strains in the concrete core and transverse tensile strains in the flange hoops at different levels of displacement ductility for Column A. After two cycles at $\mu = 4$, the compressive strain in the core concrete near the base was about 0.008, implying cracks and minor spalling have formed. Fig. 4-9b is a photograph of Column A after two cycles at $\mu = \pm 4$. Minor cracking at the base of the column can be identified, but the member remained intact. The opening cracks that occurred near the base is due to tensile strains in the longitudinal reinforcing steel. The calculated damage index (DI) after two cycles at $\mu = \pm 4$ was determined to be 0.3. Therefore from the measured strains in the concrete core of one flange and tensile cracks visually observed near the base of the other flange, it was concluded that the member is in a *"serviceable"* state at this point in loading.

Column A was then cycled two times at $\mu = \pm 6$ and then $\mu = \pm 8$. The calculated DI after two cycles at $\mu = \pm 8$ was determined to be 0.63. Fig. 4-8 shows that the compressive strain in the concrete core was about 0.02 near the base of the column at $\mu = 8$ with Fig. 4-9c visually confirming this result showing a region of spalled concrete cover near the base of the column with large tensile cracks open above this area. From a visual standpoint, it was considered that the member has entered an unserviceable state but could be *"repaired"* to restore serviceability of the member.

Column A was then placed in dynamic cycling at $\mu = \pm 4$ until failure occurred after 40 dynamic cycles. Fig. 4-9d shows Column A at failure where large amounts of concrete cover had spalled and some longitudinal bars had fractured. At this point, the member was con-

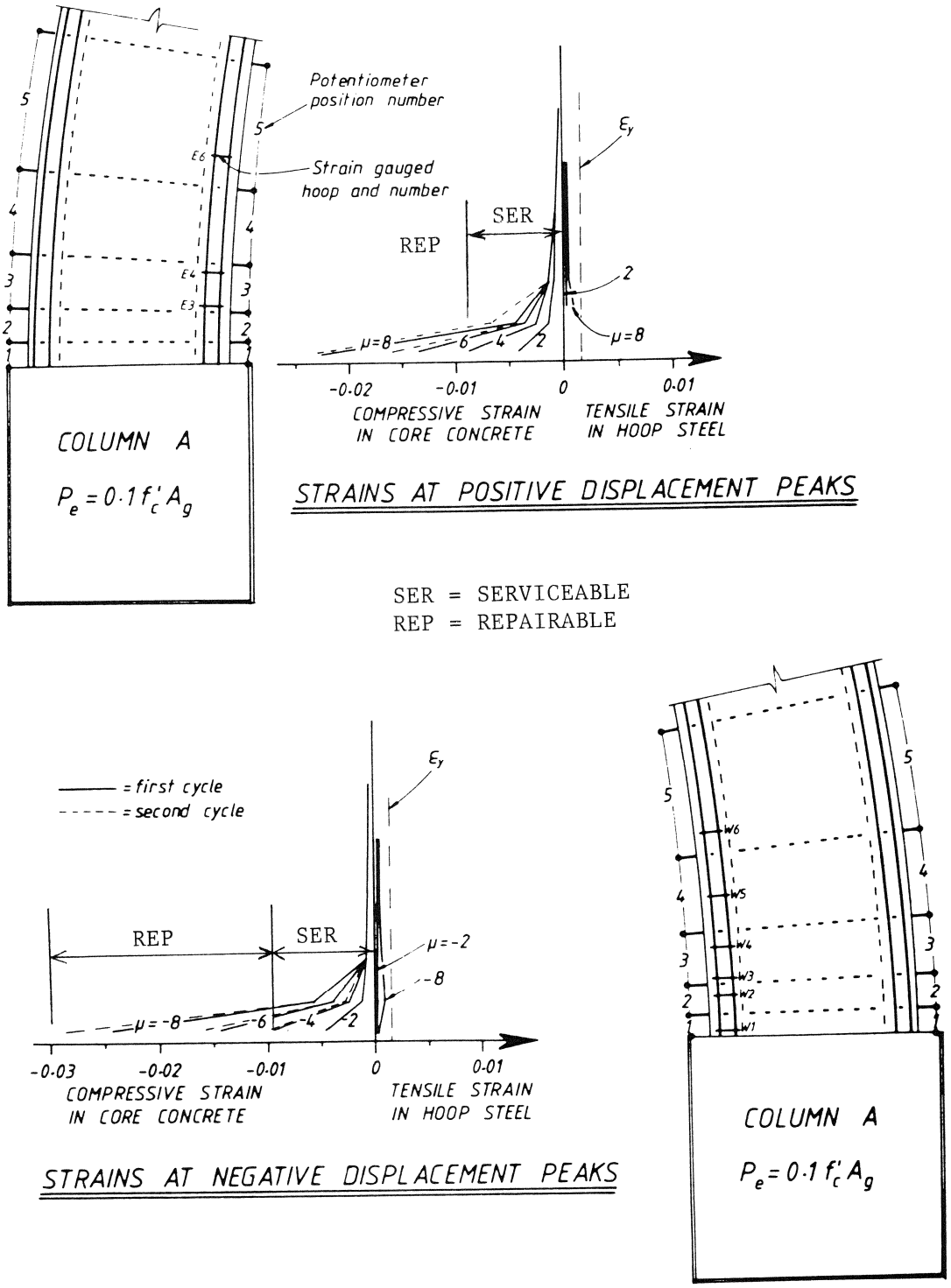

FIGURE 4-8 Measured Longitudinal Strains in the Core Concrete and Transverse Tensile Strains in the Flange Hoops of Column A (Mander et al. 1983,1984)

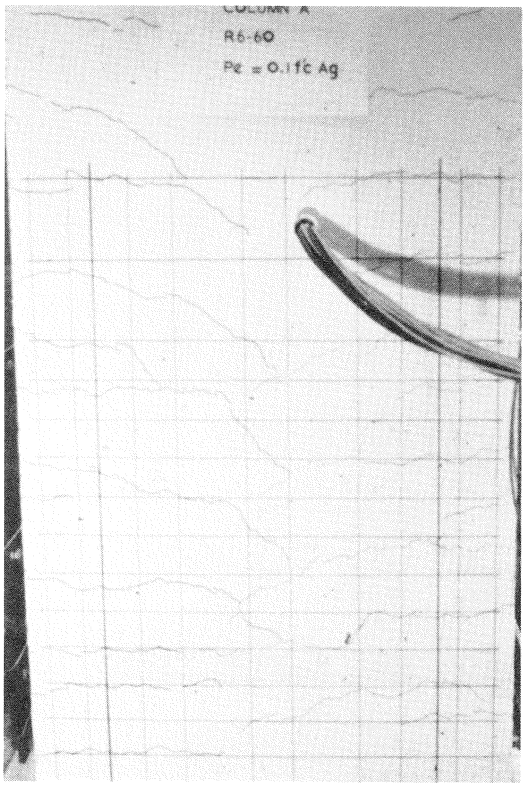

(a) End of elastic cycles

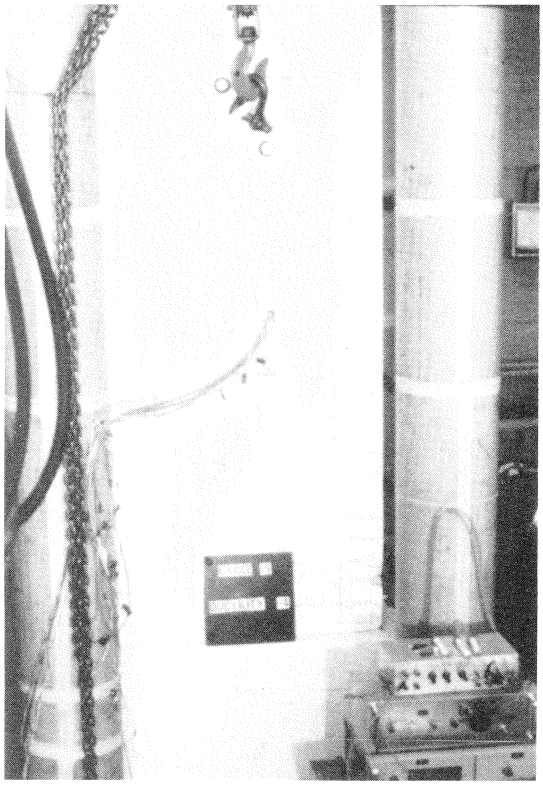

(b) After 2 cycles at $\mu = \pm 4$

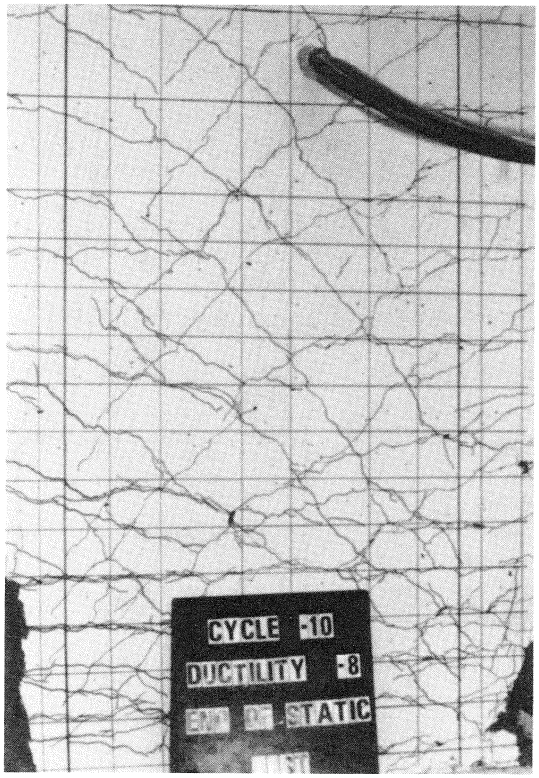

(c) After 2 cycles at $\mu = \pm 8$

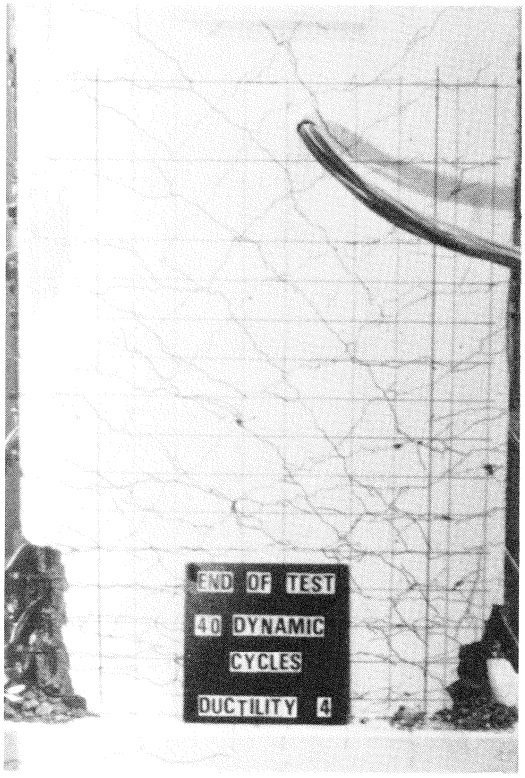

(d) End of testing, after 40 dynamic cycles at $\mu = \pm 4$

FIGURE 4-9 Photographs of Column A during Quasi-Static Testing (Mander, Park and Priestley 1984)

sidered to have failed and was beyond repair. Note that the transverse tensile strain in the flange hoops was still well below yield. This implied for the axial load level used in this test ($P_e = 0.1 f_c' A_g$) that the specimen was well confined.

COLUMN C:

Column C was loaded for two cycles at $\mu = \pm 2$ where the DI was calculated to be 0.17. Fig. 4-10 shows the measured longitudinal compressive strain in the concrete core at a peak negative displacement was 0.009. This correlates with Fig. 4-11b where significant cracking had formed near the column base, but remained mostly intact. Again, the member can be considered to be *"serviceable"* at this point in loading.

Column C was then loaded for two cycles at $\mu = \pm 4$, when the concrete core compressive strains were about 0.02 at a peak negative displacement. Small amounts of concrete cover spalling and large tensile/shear cracks were beginning to form. The DI was calculated to be 0.41 at this stage. It was considered the member would be unserviceable at this stage but could be *"repaired"* to restore serviceability. Therefore, the *"serviceability"* limit state for this specimen should lie between DI = 0.15 and DI = 0.4.

At $\mu = \pm 6$ with DI = 0.7, the member had a large amount of cracking with concrete cover spalling as shown in Fig. 4-12a. The compressive strains in the concrete core were 0.03 for a peak negative displacement. Note that the transverse tensile strains in the flange hoops are beyond yield and were behaving inelastically. It was considered that the member was beyond the extent of being repaired ("irrepairable") at this stage, although it still had some reserve strength. Hence the member was in an *"irrepairable"* state when $\mu = \pm 6$ with a DI = 0.7.

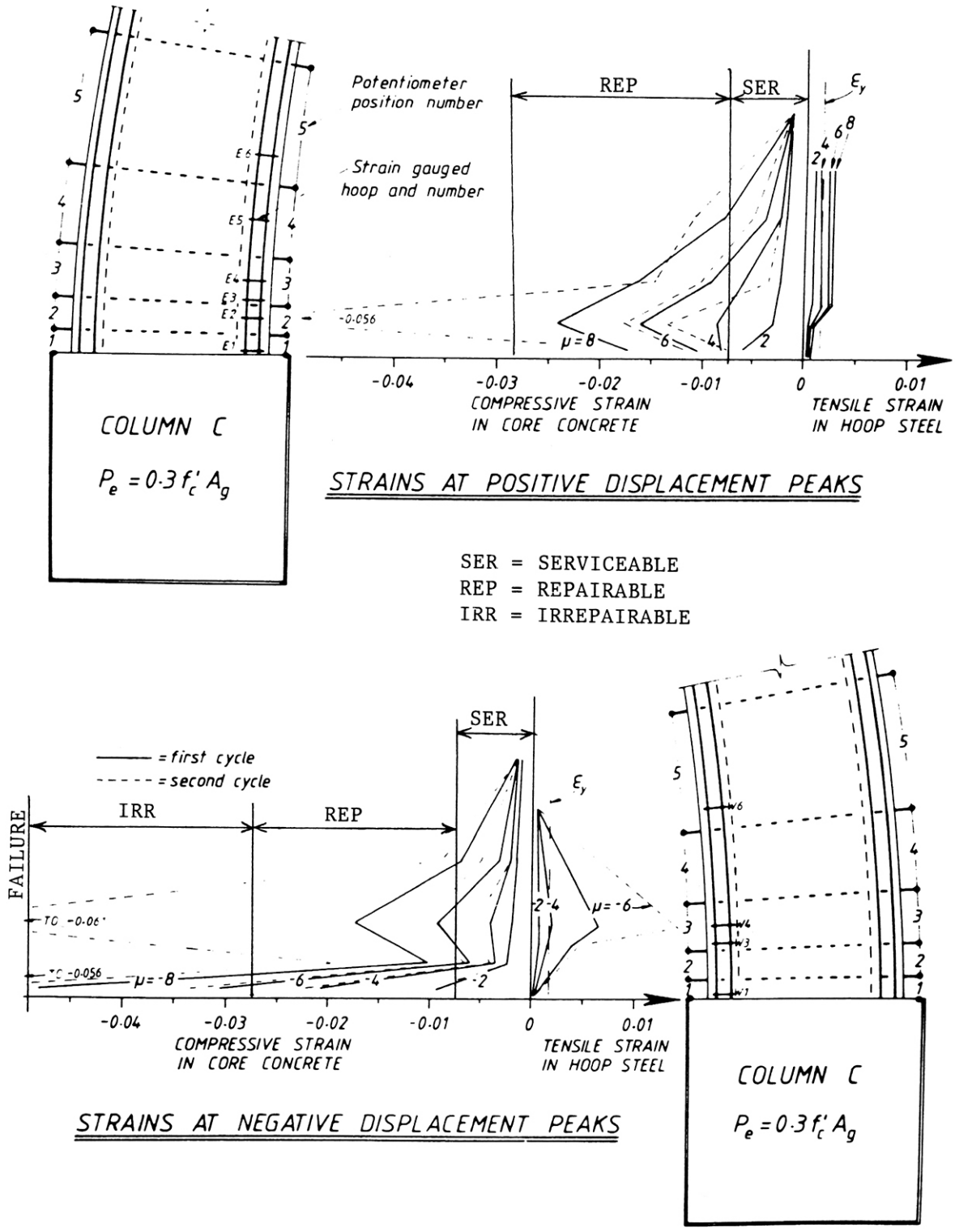

FIGURE 4-10 Measured Longitudinal Strains in the Core Concrete and Transverse Tensile Strains in the Flange Hoops of Column C (Mander, Park and Priestley 1983, 1984)

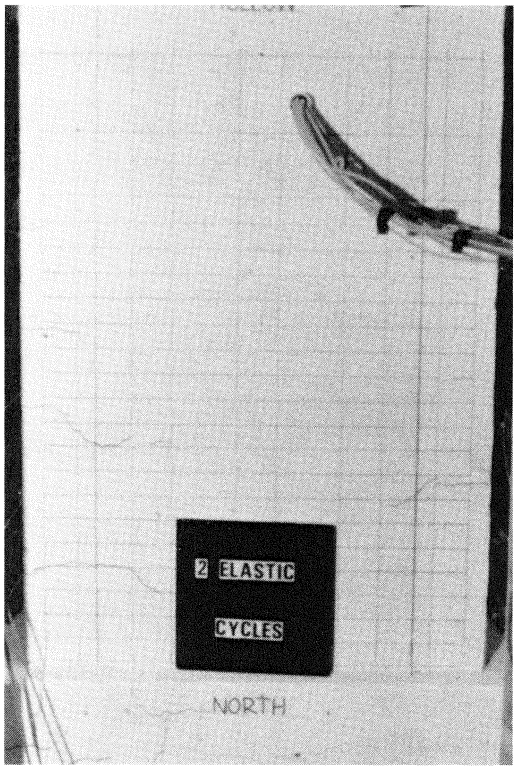

(a) End of elastic cycles

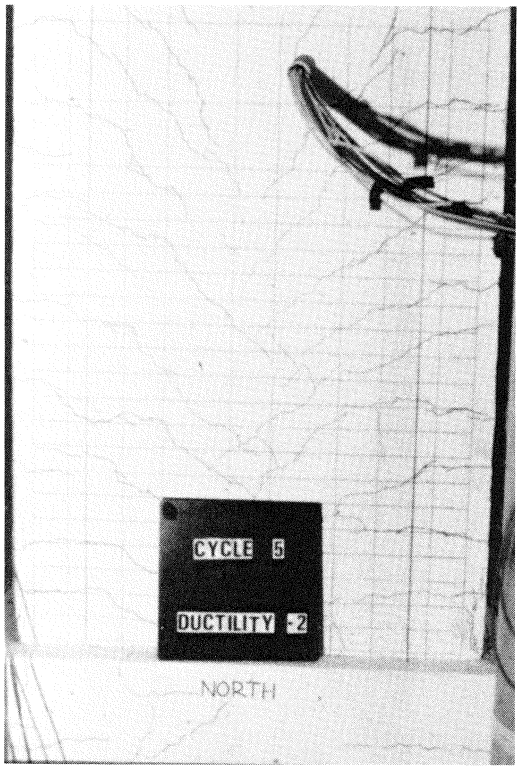

(b) After 2 cycles at $\mu = \pm 2$

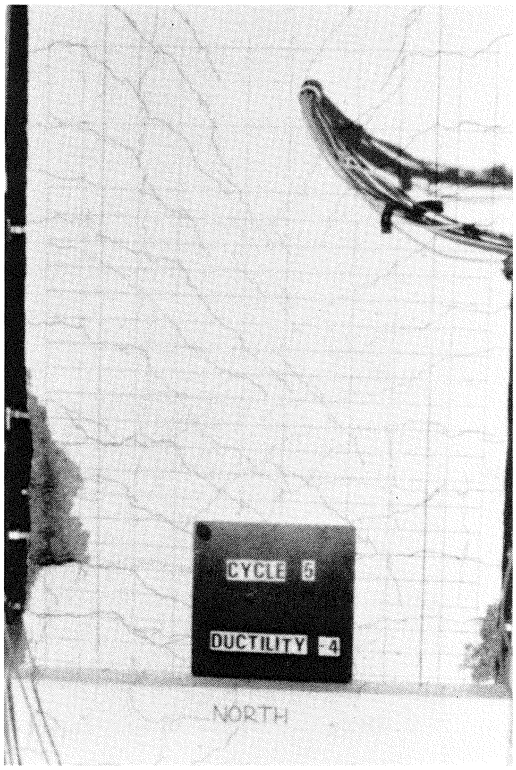

(c) After 2 cycles at $\mu = \pm 4$

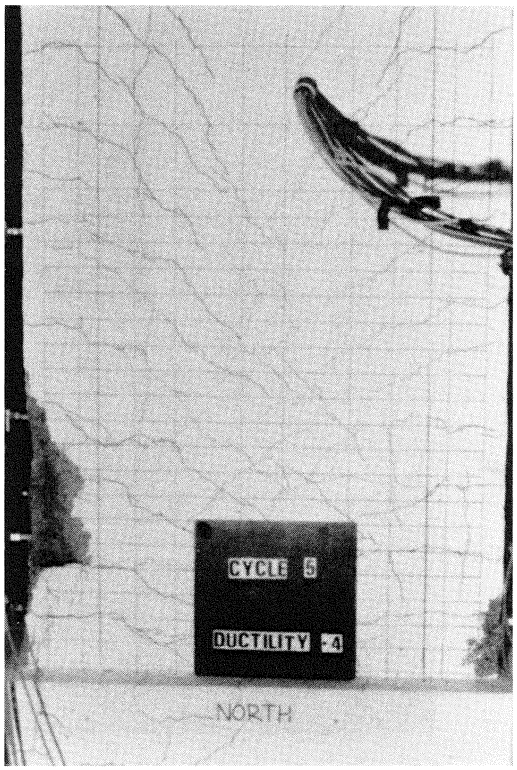

(d) Extent of cracking at $\mu = 4$

FIGURE 4-11 Photographs of Column C during Early Stages of Quasi-Static Testing (Mander, Park and Priestley 1984)

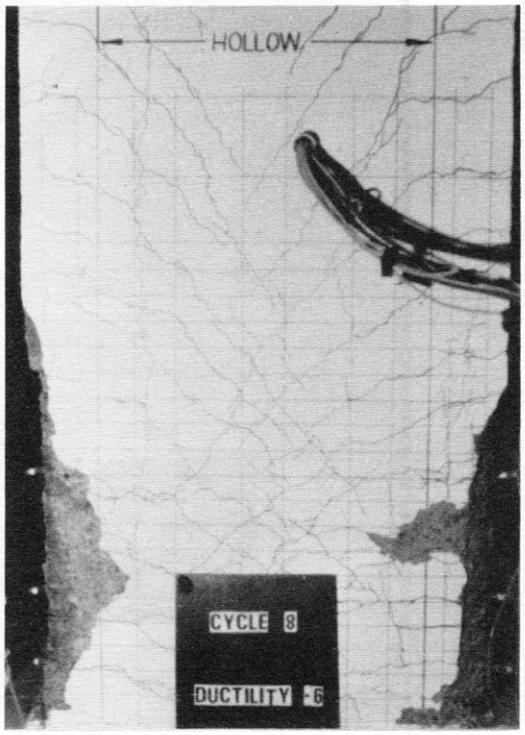

(a) Cracking and spalling after 2 cycles at $\mu = \pm 6$

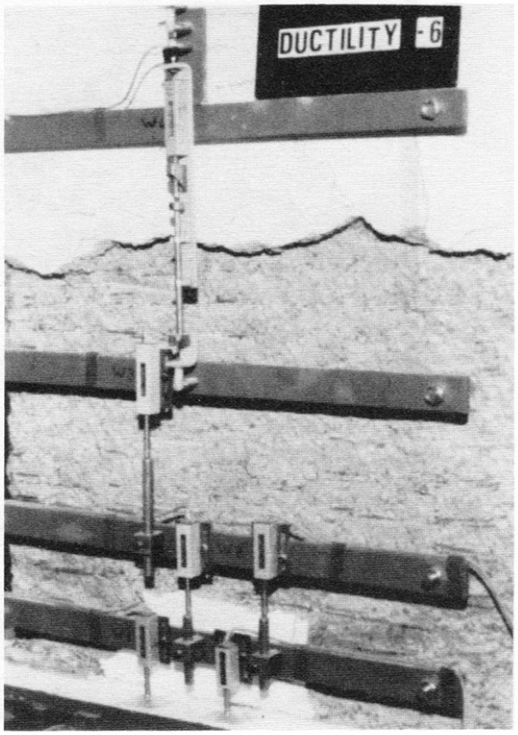

(b) Spalling in column at $\mu = -6$

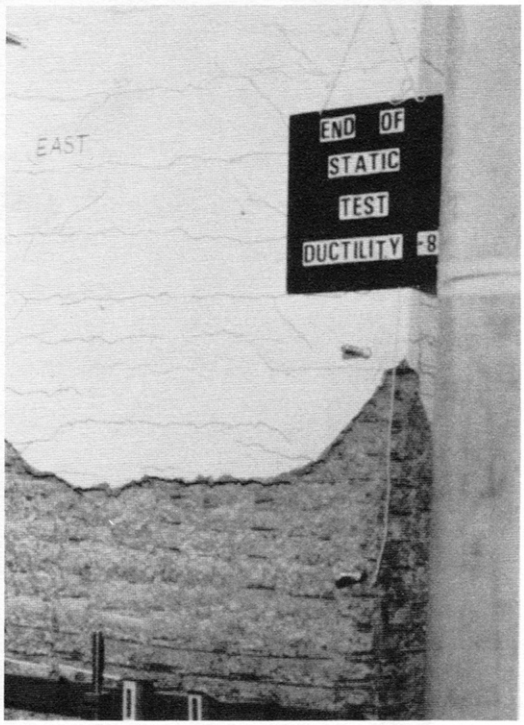

(c) End of quasi-static testing, after 2 cycles at $\mu = \pm 8$

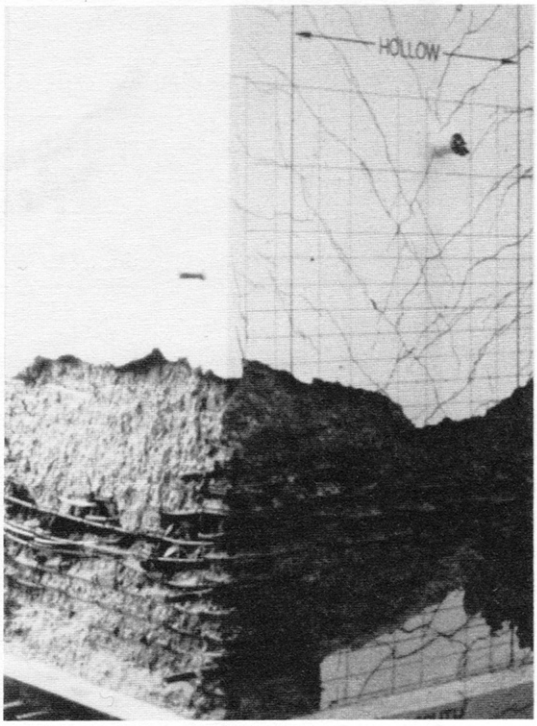

(d) Spalling in column, $\mu = -8$

FIGURE 4-12 Photographs of Column C during Later Stages of Quasi-Static Testing (Mander, Park and Priestley 1984)

Finally when the member was loaded to $\mu = \pm 8$, very large tensile strains occurred in the flange hoops as shown in Fig. 4-10. Transverse hoop fracture occurred leaving the flanges unconfined and unable to sustain the high level of axial load and bending moment causing failure.

COLUMN D:

Column D after two cycles at $\mu = \pm 2$ had a DI = 0.2. Fig. 4-13 shows a longitudinal concrete core compressive strain of 0.007 and small tensile strains in the transverse hoops. Fig. 4-14b shows minor tensile cracking at the base of the column. The member was considered to be "*serviceable*" at this stage.

At $\mu = \pm 4$ with DI = 0.67, the concrete core compressive strain was 0.015 near the column base with still small tensile strains in the flange hoops. Fig. 4-14c shows tensile cracking at the base and small amounts of spalling cover. At this stage, the member was considered to be in a *"repairable"* state.

When Column D was loaded to $\mu = \pm 6$ with DI = 0.96, the compressive strain in the core concrete was 0.02 and the tensile strain in the transverse hoops were well beyond yield. The member was considered to have failed due to transverse hoop fracture of the flange hoops leaving the concrete unconfined, which also led to substantial buckling of the longitudinal bars.

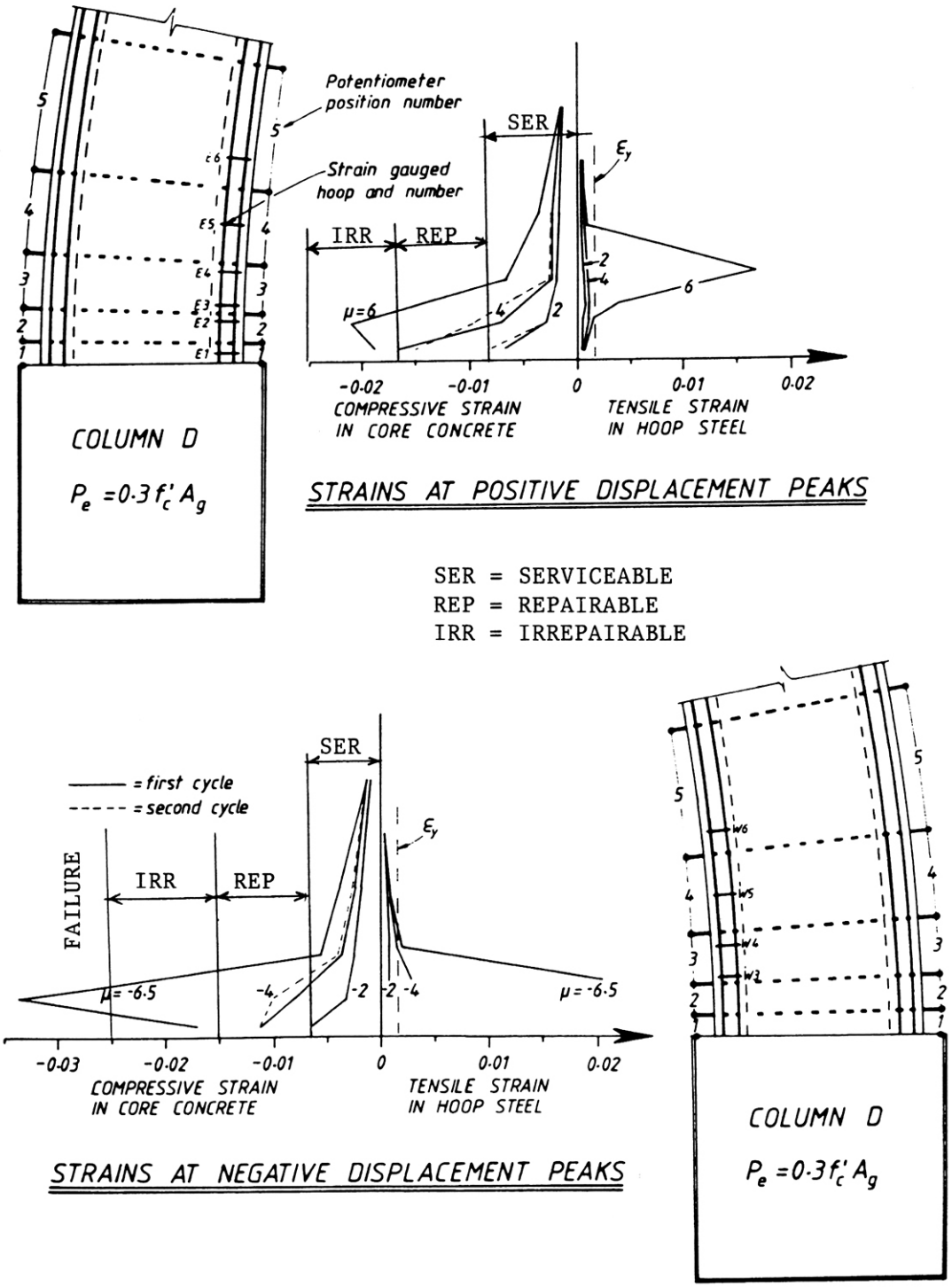

FIGURE 4-13 Measured Longitudinal Strains in the Core Concrete and Transverse Tensile Strains in the Flange Hoops of Column D (Mander, Park and Priestley 1983, 1984)

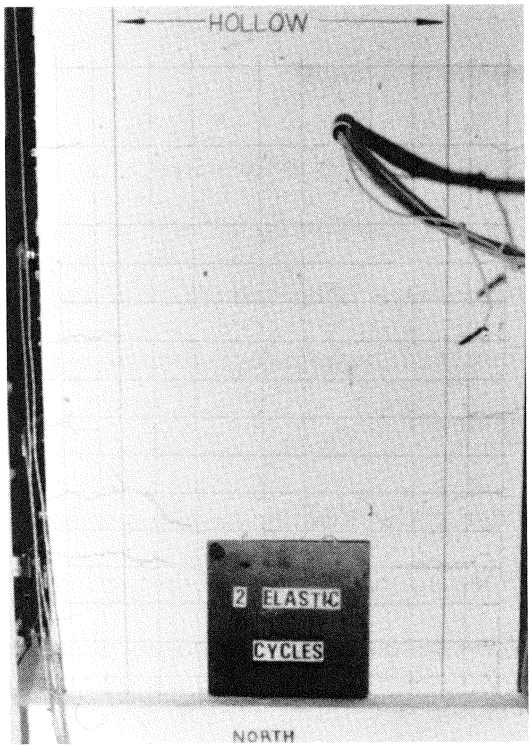

(a) End of elastic cycles

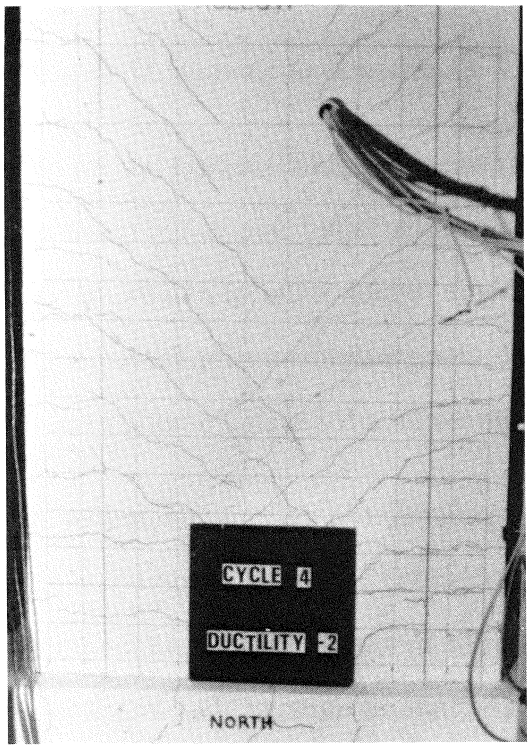

(b) After 2 cycles at $\mu = \pm 2$

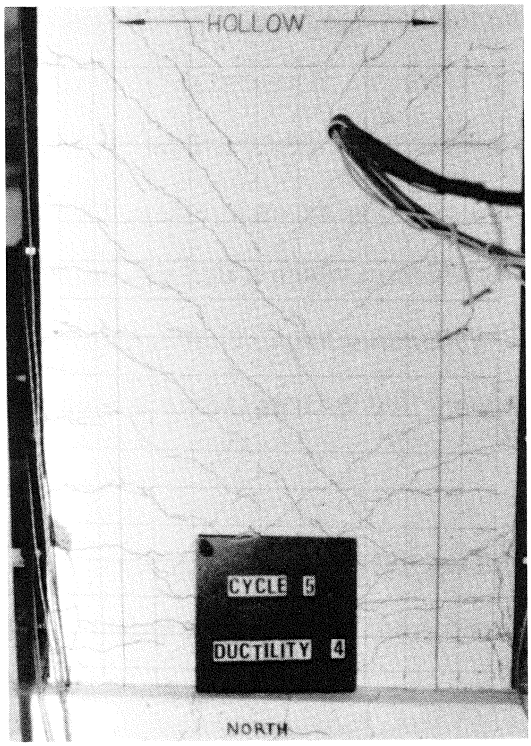

(c) After 2 cycles at $\mu = \pm 4$

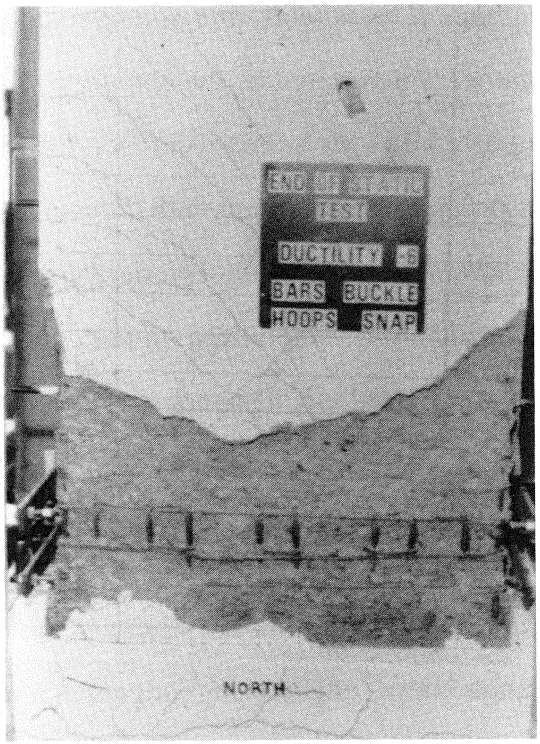

(d) First hoop fracture, $\mu = -6.5$

FIGURE 4-14 Photographs of Column D during Quasi-Static Testing (Mander, Park and Priestley 1984)

4.7 Conclusion of Damage Evaluation for Component Testing

Mander et al.(1983) tested hollow columns with varying levels of axial load and confinement. Column A failed due to repeated cyclic loading at a ductility factor of $\mu = \pm 4$ (low cycle fatigue) which is defined in this study as strength damage. This test provided verification of the strength deterioration factor (S_{sd}) and the concept of strength damage using a lower bound failure curve for cyclic loading as described in section 2.1.

In general, the columns tested by Mander under cyclic loading clearly demonstrate that members fail due to the combined effects of deformation damage and strength loss damage caused by cyclic loading, which confirms the foundation of the proposed damage model. Deformation damage (D_1) is primarily related to the maximum deformation (or maximum displacement ductility factor (μ) and the unloading stiffness coefficient (α). The strength damage (D_2) is related to strength deterioration factor (S_{sd}) from Eq. 3.19 and the amount of energy dissipated by the component ($\int dE$). In principle, it was established that the study reported in this section verifies the damage model. Further verification testing of an assortment of specimens with differing characteristics should be undertaken. However, it will be stressed here the importance of selecting specimens in which a definite failure could be identified and pin-pointed on the experimental hysteresis curves. Unfortunately, this is not often reported, or the specimens are so overdesigned that no true failure is obtained during testing.

By using photographs of the specimens at different ductility levels together with the observed experimental longitudinal strains in the core concrete and the transverse tensile strains in the flange hoops, engineering judgements can be applied to define several damage limit states: *(i) "serviceability"*; *(ii) "repairability"*; and *(iii) "irrepairability"* correlated with the damage index. On the basis of the results of this study, these states may be defined as:

Serviceable state:	$DI \leq 0.33$
Repairable state:	$0.33 < DI \leq 0.66$
Irrepairable state:	$0.66 < DI \leq 1.0$
Collapse state:	$DI > 1.0$

Thus with ranges of damage determined in the Damage Index, structural components can be designed to allow for a certain amount of damage for certain earthquakes. For a low magnitude earthquake or minor tremors, the structural components should be designed to allow only minor damage so that they remain *"serviceable"* after the earthquake ($0.0 \leq DI \leq 0.33$). For a moderate type earthquake (e.g. Elcentro), the components should allow moderate damage but should also be *"repairable"* ($0.33 < DI \leq 0.66$). Finally for a maximum type of earthquake (e.g. Pacoima Dam or Mexico City), the design of the structure should allow for "irrepairable" damage or possibly collapse ($DI > 0.66$).

With the verification of component testing, the damage index can now be used to analyze frames and structures.

SECTION 5

DAMAGE MODEL EVALUATION USING A THREE STORY FRAME

5.1 Introduction

In this section, the proposed damage model is applied to a 2-bay, 3-story reinforced concrete frame structure that was tested to failure by Yunfei et al.(1986) . The test structure and the load history is shown in Fig. 5-1. Loading comprised of three preliminary cycles up to yield after which the structure was subjected to three cycles each at consecutive displacement ductility factors of $\mu = \pm 1, \pm 2, \pm 3, \pm 4$, and ± 5.

The structure was analyzed under the prescribed displacement history using the program IDARC initially developed by Park et al.(1987) and revised by Kunnath (1988). Fig. 5-2 shows the experimental and simulated response of the top story displacement. These results indicate satisfactory agreement between the analytical simulation and experimental testing. The discrepancy under reverse displacements was caused by the fact that most of the beams in the test structure had different amounts of reinforcement at each end of the member, while the version of IDARC used in this study allowed only constant properties at each end.

5.2 Evaluation of Damage

The evaluation of damage will first be discussed for a typical component where a large amount of damage was known to occur. The amount of damage that occurred in the structure will follow.

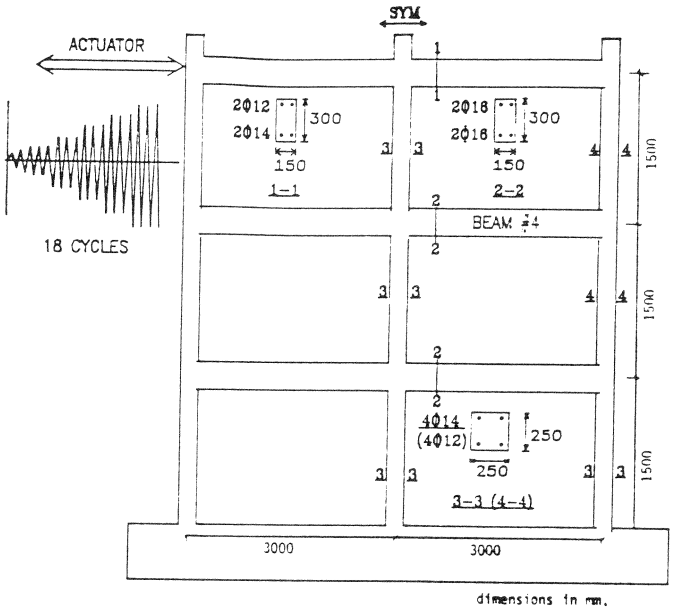

FIGURE 5-1 Test Structure

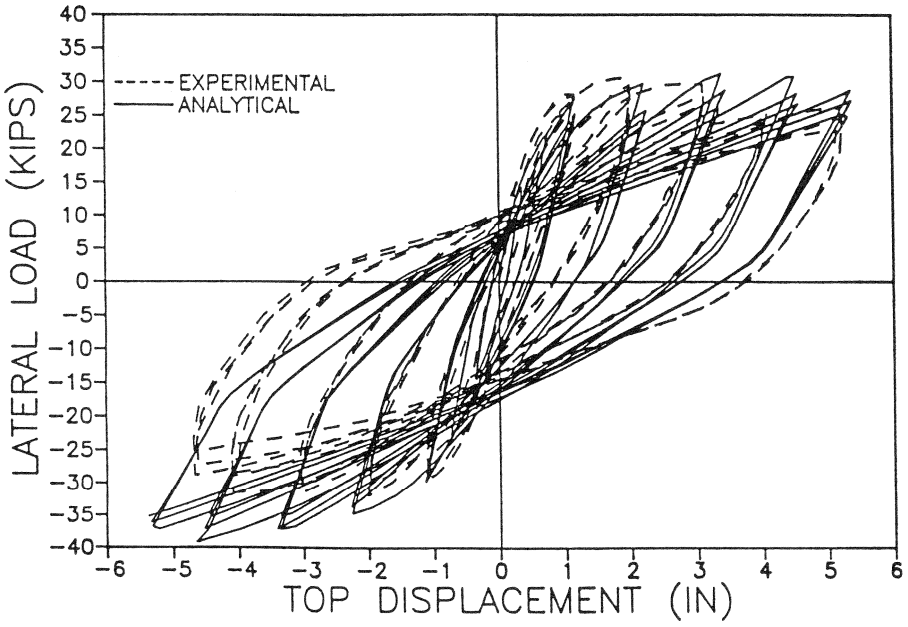

FIGURE 5-2 Experimental versus Analytical Response
(Top Story Displacement)

5.2.1 Evaluation of Damage in a Typical Member of the Structure

Fig. 5-3 shows the moment-curvature hysteresis loops for the left joint of beam #4 (Fig. 5-1). The member curvature ductility factor after the sixth cycle of loading was 1.0. As the structural displacement ductility factor was increased to $\mu = \pm 2$ on the seventh cycle of loading, the member curvature ductility factor for the left joint of beam #4 increased to 4.0. The reason the member curvature increased disproportionately was because beam #4 was one of the first members to yield as the structure was displaced into the inelastic range. After the rest of the members began to yield, an increase in structural displacement caused curvature rotations in this joint comparable with other joints.

Fig. 5-4 shows the progressive damage of the left joint of beam #4 using Option #1 (transposed bilinear option). The three lines on the graph correspond to deformation (D_1), strength (D_2), and total damage (D.I.) as outlined in the development of the damage model. On the seventh cycle of loading for the structure, the damage index for the joint *jumped* from 0.1 to 0.5 due to the sudden increase in the curvature ductility factor at the joint (deformation damage). As the loading on the structure continued, the failure mechanism began to form in the total structure causing all members to become inelastic.

Fig. 5-4 also shows that deformation damage ($D_1 = 0.84$) controls the overall damage index for beam #4, while having a strength damage of $D_2 = 0.15$ using Option #1.

Fig. 5-5 shows the progressive damage for the left joint of beam #4 using Option #2, the triangular option. The difference between the options is the evaluation of the strength damage discussed in section 2.2. Near failure, the strength damage strongly influenced the amount of total damage in the component with $D_2 = 0.73$.

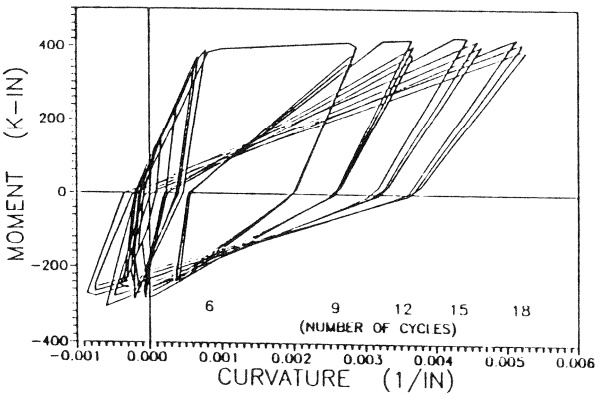

FIGURE 5-3 Force-Deformation
(Left Joint, Beam #4)

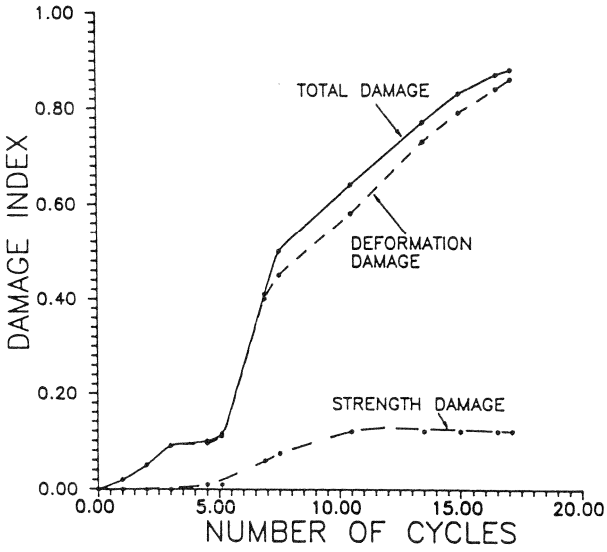

FIGURE 5-4 Progressive Damage
(Option #1, Transposed Bilinear)

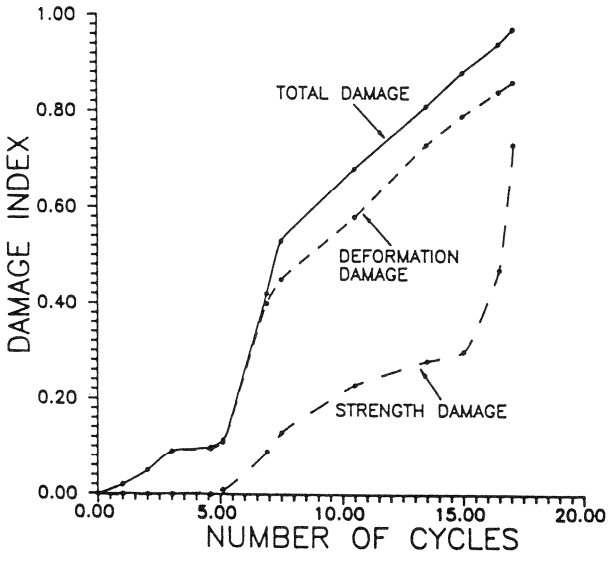

FIGURE 5-5 Progressive Damage
(Option #2, Triangular)

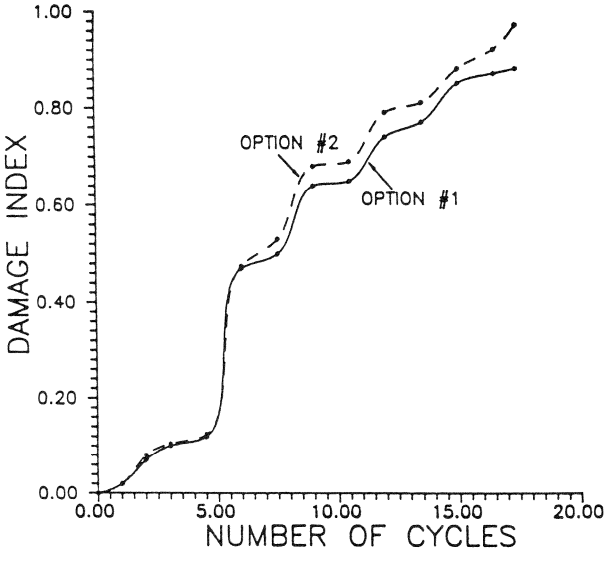

FIGURE 5-6 Total Damage for
Beam #4

Fig. 5-6 shows a comparison of total damage using both the upper bound (triangular, Option #2) and lower bound (transposed bilinear, Option #1). Near failure, the Option #2 is greater than Option #1 due to the increase in strength damage. At failure, the Damage Indices were about 0.90 and 0.97 for Options #1 and Option #2, respectively.

5.2.2 Evaluation of Structural Damage

Fig. 5-7 shows the progressive damage of the structure. Both the component and overall structural damage at different levels of yielding are shown. A close observation of the damage states show good agreement with the experimental test results reported by Yunfei et al.(1986): (1) the significant yielding in beams at the second story level, particularly near failure; (2) the general pattern of damage to columns with most of the yielding concentrated at the bottom level, and in particular the lower left column.

In section 2.3, a self-weighting procedure was presented to combine local damage indices to form a global damage index for a story level or a complete structure. Eq. 2.14 was applied to the three story frame, where the control weighting factor and the importance factor, m and w_i, respectively, were taken as unity for all components. The results of this damage analysis gave an overall structural damage index of 0.64 and 0.69 for Options #1 and #2, respectively.

5.3 Influence of the Importance Factor on the Damage Model

Assessing the quality of damage in a structure requires the designation of importance to members or story levels. From section 2.3, the damage index for a story level and overall structure can be found by using Eq. 2.14 with control weighting factors of unity and using the appropriate importance factor based on the gravity load of the tributary area for each member.

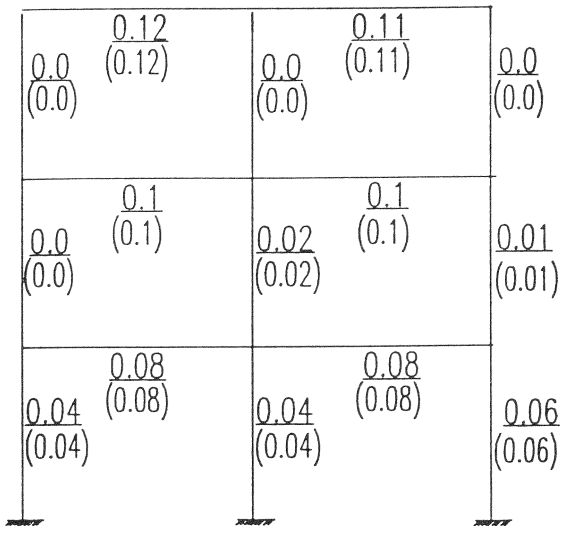

OVERALL DAMAGE INDEX = 0.07 (0.07)

No. of Cycles = 3
Structure Disp. Ductility = 1

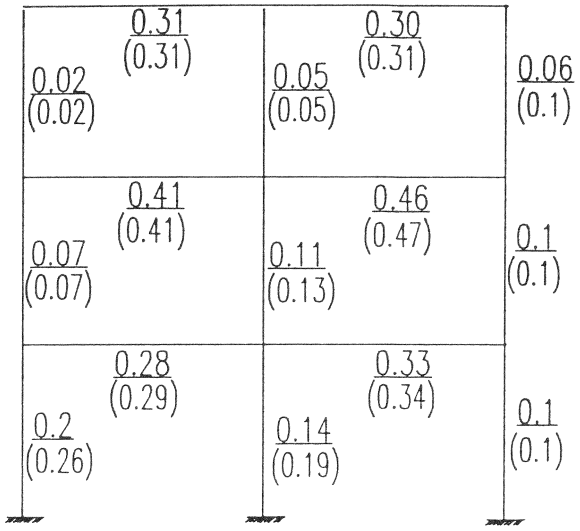

OVERALL DAMAGE INDEX = 0.295 (0.3)

No. of Cycles = 6
Structure Disp. Ductility = 2

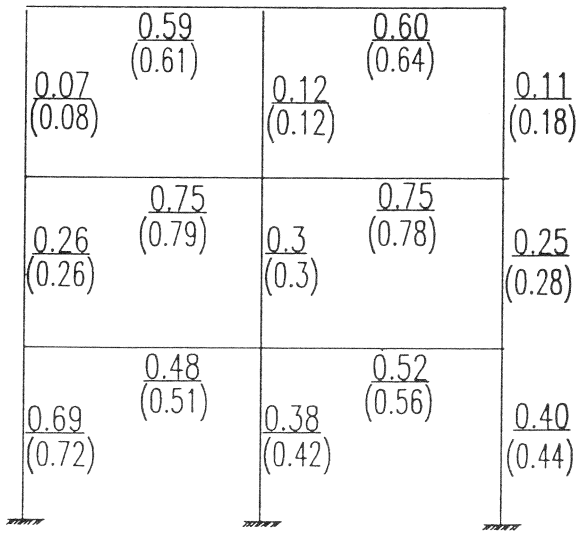

OVERALL DAMAGE INDEX = 0.52 (0.56)

No. of Cycles = 12
Structure Disp. Ductility = 4

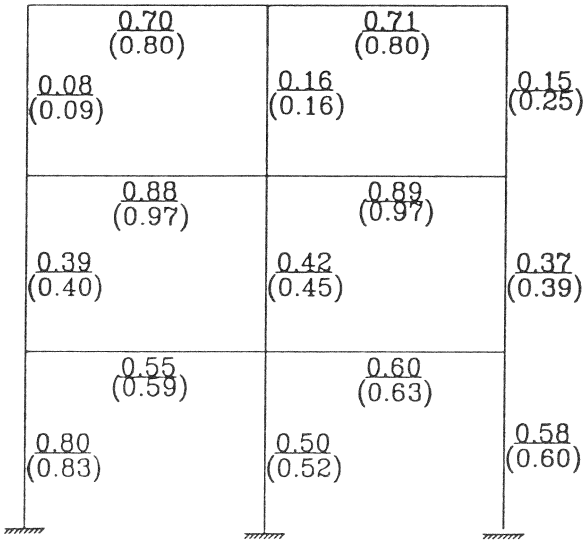

OVERALL DAMAGE INDEX = 0.64 (0.69)

No. of Cycles = 18
Failure

FIGURE 5-7 Progressive Damage of the Structure
Notation: Option #1 (Option #2)

The results of this Damage Analysis using importance factors gave an overall structural damage index of 0.58 and 0.62 for Options #1 and #2, respectively. These results are less than the results achieved with equal importance applied to each member. *The beams on the second story level that were severely damaged and near collapse caused the damage index to be higher for the damage analysis having equal importance factors. By using the gravity load of the tributary area for each member as the importance factor for that member, column members received greater importance than beams. This caused a reduction in the overall damage index due to a reduced importance of the beams on the second story.* On the other hand, if the columns were more severely damaged, the resulting overall damage index would have been higher.

5.4 Conclusions

The quantification of damage, using the proposed damage model in evaluation studies of an actual structure tested under quasi-static cyclic loading, shows good correlation with observed and measured damage by Yunfei et al.(1986). Experimentally, beam #4 had a significant amount of damage. The proposed damage model predicts that this member would be *"ir-repairable"* and close to collapse with a damage index lying between 0.9 and 0.97 depending on the option used for the lower bound curve. The damage model also shows a good representation of damage as observed experimentally on the second story level and damage to columns with most of the yielding concentrated at the bottom level.

The proposed damage model quantifies the amount of damage that occurred in the three story frame that was cyclically loaded. A further step in the qualification of the proposed damage index is to evaluate the damage of a structure under an irregular loading path such as that which is expected in real, rather than experimental, situations.

SECTION 6

DAMAGE MODEL EVALUATION OF A SIX STORY STRUCTURE SUBJECTED TO SIMULATED EARTHQUAKES

6.1 Introduction

In this section, the proposed damage model is applied to a six story reinforced concrete frame structure designed only for gravity loadings, but subjected to a seismic excitation. The structure was designed in accordance with the non-seismic provisions of ACI 318-83 and may be considered typical of construction in the eastern United States. A similar analysis performed by Seidel et al.(1989) was used to compare the calibration of the Park and Ang damage model (1985) with the currently proposed damage model.

The structure used in the analysis was a weak-beam design of a six story reinforced concrete frame structure, designed primarily to sustain gravity loads. Lateral loads from wind or earthquake were not considered in the design. A typical floor plan and elevation of the structure is shown in Fig. 6-1. Due to a complete lack of natural earthquake data for the eastern United States, the ground motion was simulated as a nonstationary process of filtered white noise based on given response spectrum characteristics suitable for this area. The characteristics of the simulated earthquake are a magnitude of 6.5 on the Ritcher Scale with an epicentral distance of 20 km from the structure. The inelastic dynamic analysis was performed using the program IDARC (1988).

6.2 Results of the Comparison of Story Level Damage

A comparison of the proposed damage model with the Park and Ang model (1985) was firstly applied to the vertical distribution of the mean and maximum damage indices. For this case, no importance was assigned to different components in the structure, thus both w_i and m were taken as unity in Eq. 2.14. For twenty simulations of magnitude 6.5 with an epicentral distance

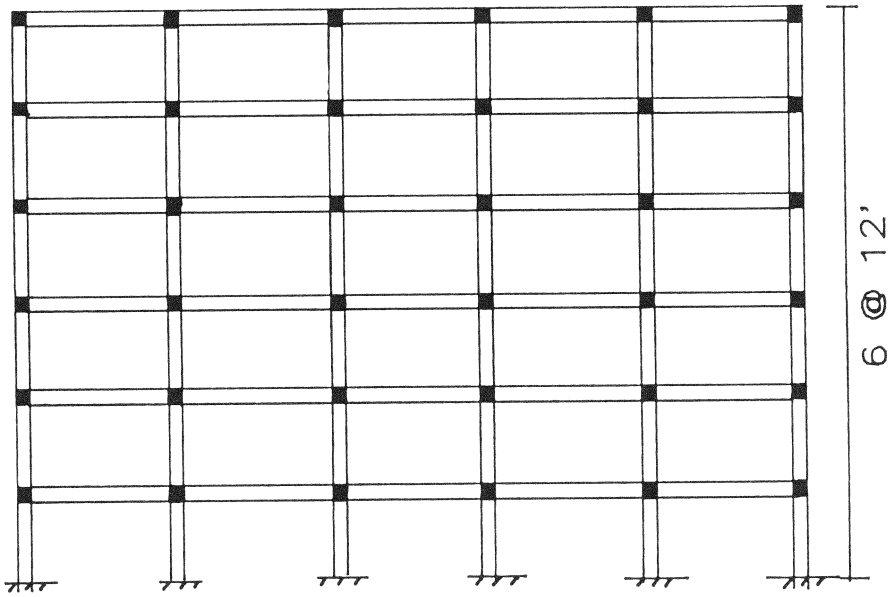

(a) Cross Section

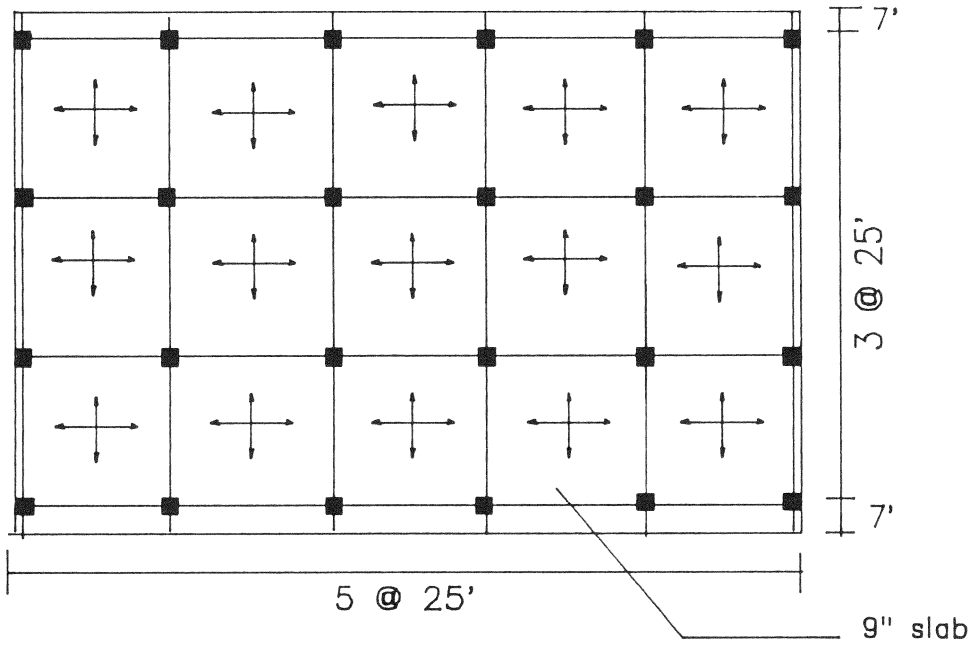

(b) Plan Layout

FIGURE 6-1 Typical Six Story Structure

of 20 km, both damage models produce similar distributions of vertical story level damage for the mean and maximum damages as shown in Fig. 6-2, while the proposed index has values about twice that of the Park and Ang model (1985).

A comparison of the mean and maximum vertical story level damage with the idea of assigning importance to the vertical members according to their total gravity load assigned according to the tributary area of each component are shown in Fig. 6-2. The distribution of vertical story level damage is similar to the Park and Ang model (1985) and approximately identical to that of the proposed damage model with no importance accredited ($w_i = 1.0$). It should be noted that the four interior columns were weighted twice as much as the two exterior columns for any certain damage index evaluation. This caused little aberration in the calculation of the damage index of the proposed model.

6.3 Results of Structural Damage Analysis

The comparison of the proposed model with the Park and Ang model (1985) was made also for the total structural weighted damage analysis. The Park and Ang model (1985) gave mean and maximum structural *damage indices* of 0.211 and 0.374, respectively, while the proposed model gave respective mean and maximum structural *damage indices* of 0.57 and 0.78. The proposed damage model produced a mean structural *damage index* about two and a half times that of the Park and Ang Model (1985), while the maximum *damage index* was approximately twice that of the Park and Ang model (1985). This result corresponds with the vertical distribution of story level *damage indices*, where the proposed damage model predicted about twice the damage of the Park and Ang model (1985).

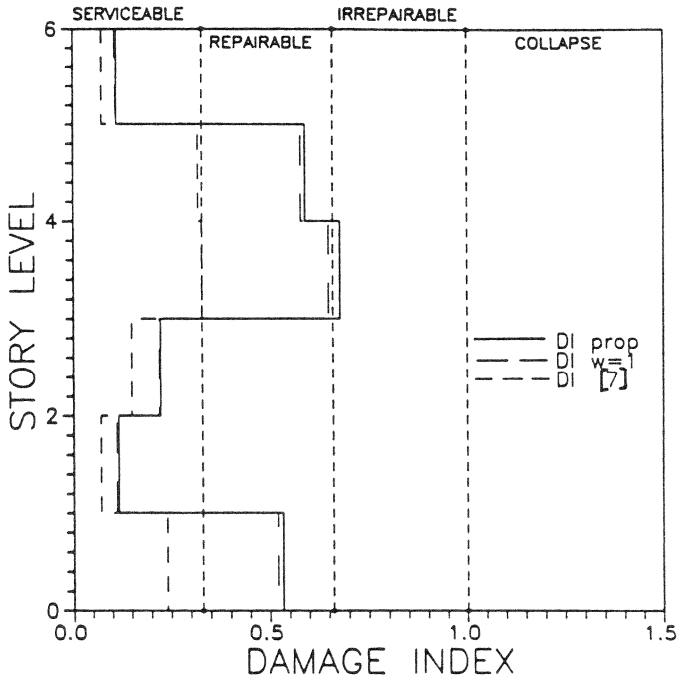

(a) Mean Damage

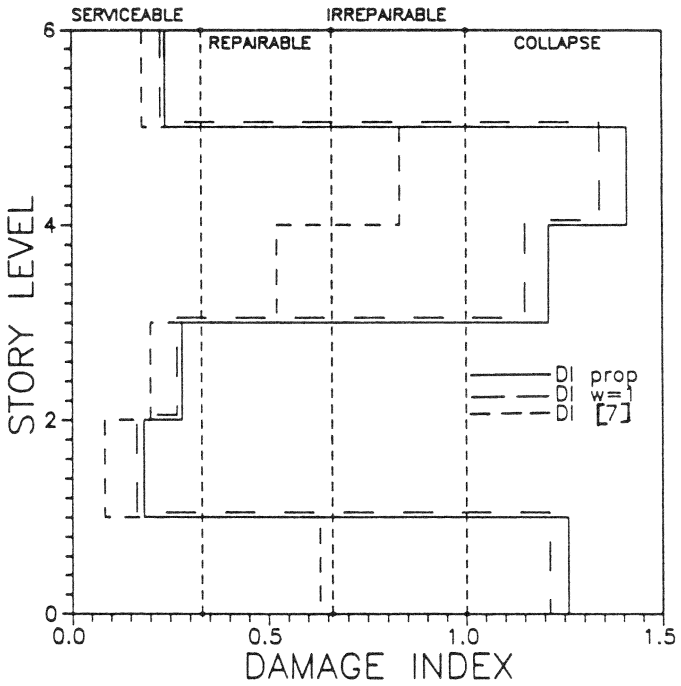

(b) Maximum Damage

FIGURE 6-2 Damage Distribution in Structure

For practical purposes, a simplified expression is desired to relate the damage in a structure to the characteristics (magnitude, M, and focal distance, R) of an earthquake. Seidel et al.(1989) performed simulations of earthquakes ranging from 4.5 to 7.0 in magnitude and focal distances of 20 to 100 km. A relation of the mean Damage Index of the structure to the magnitude of the earthquake (M) and the focal distance (R) was obtained from a regression analysis of the simulation and determined as follows:

$$D.I. = k * 10^{0.6M} / R \qquad (6.1)$$

where k is a constant depending on the structural system. Seidel et al.(1989) determined that k = 0.00108 for the system used in their analysis. Since the comparison of the mean structural damage indices showed that the proposed model predicted damage two and a half times that of the Park and Ang model (1985), the constant k may be modified to be 0.0027 for the proposed damage model. The relation in Eq. 6.1 with the modified constant has a coefficient of variation of 19%.

Eq. 6.1 was applied to formulate contour plots of damage that could be expected in typical six story structures at different levels of magnitude and focal distances of an earthquake (Fig. 6-3). Based on a 90% probability of occurrence, the typical six story structures outside a 65 km radius of an earthquake of magnitude 6.5 will remain serviceable (D.I. $\leq$ 0.33), while structures within a radius of 32 km and 65 km may expect to suffer repairable damage (0.66 $\geq$ D.I. $\geq$ 0.33, respectively). Structures within a 32 km radius may expect to suffer irrepairable damage (D.I. $\geq$ 0.66), with collapse of such structures within a 21 km radius (D.I. $\geq$ 1.0).

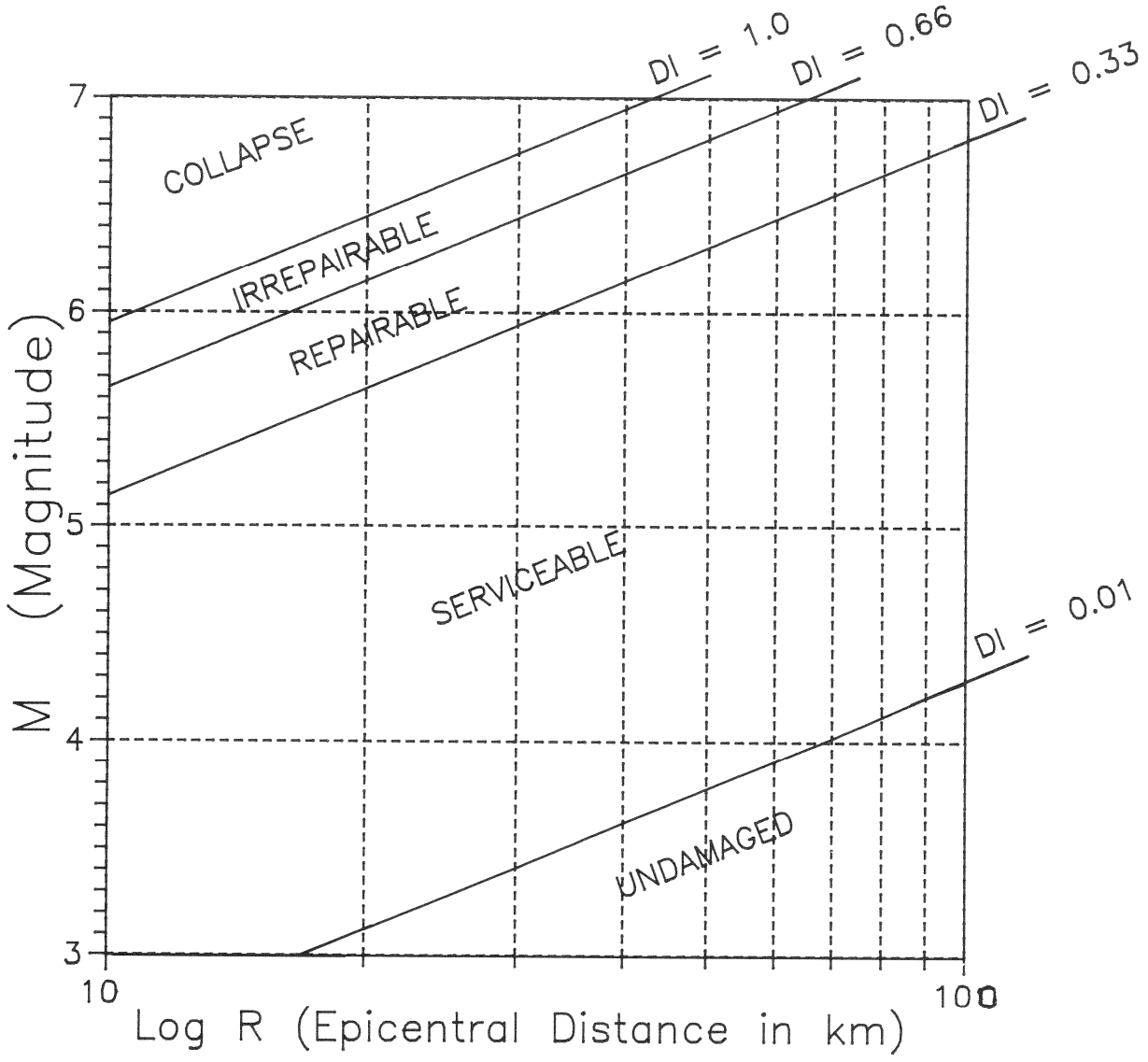

FIGURE 6-3 Proposed Overall Damage Limits for Typical Six-Story Reinforced Concrete Building in Eastern U.S.

6.4 Comparison of State of Damage in the Structure

The interpretation of the state of damage of the structure can also be used for comparison of the proposed damage model with the Park and Ang model (1985). For both the proposed and the Park and Ang (1985) damage models, collapse of the structure occurs at D.I. $\geq$ 1.0. But, the range of *irrepairability* for the proposed and the Park and Ang (1985) damage models were determined to be D.I. $\geq$ 0.66 and D.I. $\geq$ 0.4, respectively. This discrepancy accounts for the greater relative magnitude of the structural damage for the proposed damage model with that of the Park and Ang model (1985), since the structure for the proposed damage model remains repairable until D.I. $\geq$ 0.66. The proposed model provides a wider range for the intermediate states of damage, allowing better differentiation between serviceability, repairability, irrepairability and collapse.

6.5 Conclusions

A successful comparison of the proposed model with the Park and Ang model (1985) was performed for both the vertical story level and structural damage indices for a six story structure typical of design and construction practice in the eastern United States. The results showed that the distribution of vertical story level damage of the proposed damage model was similar to that of the Park and Ang model (1985), but of greater relative magnitude. The mean structural damage of the proposed was two and a half times that of the Park and Ang model (1985). The state of damage of the structure was found to correlate with the appropriate damage index for each model. Also a relation that was formulated by Seidel et al.(1989) was utilized to determine the degree of damage to structures for different levels of earthquake magnitude and focal distance based on the results of the damage states determined in Section 4.

SECTION 7

CONCLUSIONS, APPLICATIONS AND RECOMMENDATIONS

7.1 Conclusions from the Present Study

A conceptual model of damage was developed based on the concept that reinforced concrete members are damaged due to a combined effect of plastic deformation (deformation damage) and cyclic loading (strength damage). These concepts were verified against observed results from columns tested by Mander et al.(1983). The concept of strength damage (low cyclic fatigue) was verified by assuming a lower bound failure curve (transposed bilinear hypothesis) for cyclic loading. Damage states were identified from the observed compressive strains in the concrete core, tensile strains in the transverse hoops and a visual photographic test record. On the basis of an inspecting engineer's observations as part of a post-earthquake reconnaissance, judgements are required regarding the future serviceability of the component in question or the structure as a whole. The results conclude that: $DI \leq 0.33$ represents a serviceable damage state; $0.33 < DI \leq 0.66$ represents a repairable damage state, $0.66 < DI \leq 1.0$ represents an irrepairable damage state and $DI > 1.0$ represents a collapsed state.

The proposed damage model was applied to evaluate a three story frame tested to failure by Yunfei et al.(1986). The model showed good correlation with observed and predicted damage. Observed experimental damage was concentrated on the second story level, which was also concluded by the damage model.

The proposed damage model was also compared with the Park and Ang damage model (1985) in the analysis of a six story structure studied by Seidel et al.(1989). The results showed that the distributions of damage in the proposed damage model were similar, but consistently magnified compared to that of the Park and Ang model (1985). According to Park and Ang,

a structure maybe considered irrepairable when D.I. $\geq$ 0.4 for their model. This compares with D.I. $\geq$ 0.66 identified for the damage model proposed herein. It appears that the severity of damage with the Park model is non-linear between 0.0 and 1.0, with considerable damage implied by small DI values (0.4-0.7). However, the proposed model seems to reflect a more linear distribution of damage between 0.0 and 1.0 by suggesting a repairable damage state in the middle of the damage index range.

7.2 Application of Damage Modeling

The proposed damage model was developed and evaluated from the **post-processing** of damage of actual experimental test results. This development was needed for the comprehensive study for evaluation of vulnerable structures which presently have not experienced strong motions, but need immediate attention and retrofit for future strong motions. Therefore, the damage model could be used in a post-processing environment of time-history response analyses for the following applications:

1. *Evaluation of Existing Building Structures based on Component Properties*

Damage modeling can be used to evaluate the seimic vulnerability of existing buildings. This evaluation requires a reasonable knowledge of the inelastic properties of components of the building structure. The properties of the components can be determined through model testing in the laboratory. The characteristics of the components are simulated as accurately as possible by examining existing drawings of the building and/or by a field inspection. The essential porperties of the component that need to be established are the initial stiffness and yield force level. Also, the inelastic degrading properties (stiffness degradation, strength deterioration and bond-slip) can be determined through either actual component testing or evaluation of existing data of similar components. This data can then be transferred to an inelastic analysis program, such as IDARC (Park et al. 1987), to determine the response of

the building due to seismic excitation. The results of such a response analysis can be used directly for the damage analysis of the building structure based on the model proposed in this report.

2. *A Research Tool*

An accurate pre-test assessment of damage is required for shaking table experiments. The problem always arises with shaking table tests as to the ideal earthquake motion to use as input. If the level of shaking is too intense, the structure may fail early in the test and little may be learned from the experience. On the other hand, a low level earthquake motion could be used resulting in a partially damaged structure. Since the structure would possess a reserve strength capacity, another motion of higher intensity could then be used. Since the previous test would have already yielded the structure, the resulting outcome does not truly represent the original structure.

It is contended that the ideal shaking table test for a reinforced concrete structure is one where a member reaches DI = 1.0 just before the end of the test. The level of shaking and the type of earthquake to achieve this objective can be explored prior to testing by the use of time-history analyses and damage analyses of those simulations. This approach should maximize the results from testing and thus provide the best return on much time and monetary investment in this expensive class of experiment.

3. *A Code Development Tool*

Inelastic Damage Analysis can be used to develop design spectra. At present, design codes use response reduction factors that are based on experience and engineering judgement and this implicity accounts for importance. Design codes are also based on ductility and P-Δ effects. Such response reduction factors could be derived deterministically by constructing equi-damage contours for a given elastic site spectra. Fig. 7-1 shows a speculated form of

response reduction factors based on damage principles. The use of such an approach promises a more rational basis for design. Importance, for example, can be considered explicitly by permitting the designer to choose a damage limit state that is commensurate with the return period of the design earthquake motion. Such design objectives are illustrated in Table 7-1. It is likely that such design objectives will be used in the foreseeable future (Whitman, 1989).

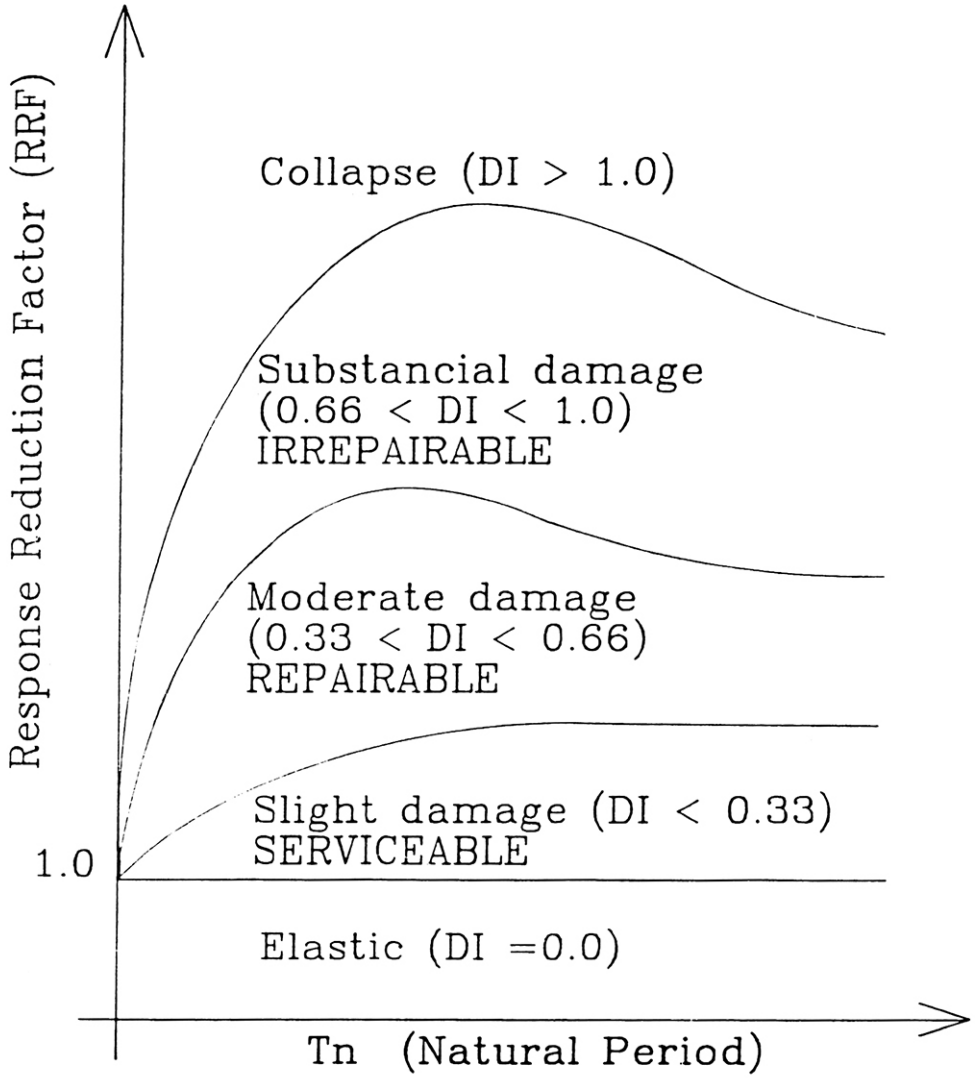

FIGURE 7-1 Probable Form of Response Reduction Factors Determined from an Inelastic Damage Analysis

TABLE 7-1 DAMAGE RESISTANT DESIGN OBJECTIVES

Return Period (years) (probability of yearly exceedence)	Damage Limit State *		
	Ordinary Structures	Essential Facility	Nuclear Structures
50 (0.02)	Undamaged		
100 (0.01)	Serviceable	Undamaged	
500 (0.002)	Repairable	Serviceable	
1000 (0.001)	Irrepairable	Repairable	Undamaged
2000 (0.0005)	Collapse	Irrepairable	Serviceable
5000 (0.0002)		Collapse	Repairable

* Undamaged $D < 0.0$
Serviceable $0.0 \leq D < 0.33$
Repairable $0.33 \leq D < 0.66$
Irrepairable $0.66 \leq D < 1.0$
Collapse $D \geq 1.0$

4. *A Design Evaluation Tool*

Until damage based design using response spectrum techniques becomes routine, it will often be necessary to evaluate important structures more thoroughly. A given structure may be analyzed using a time-history dynamic analysis, such as IDARC (1987), to determine the quality of the design, with respect to damageability, for different classes of earthquakes such as:

1. "Working" Earthquakes, with return periods ranging from 150-450 years.

2. "Maximum" Credible Earthquakes, with return periods ranging from 2000-3000 years.

The classification of a structure, whether it be an ordinary or an essential facility (Hospital, nuclear power plant, etc.), can affect the design criteria and the level of acceptable damage. Table 7.1 shows one set of possible design objectives for different classes of structures subjected to probable ground motions.

7.3 Recommendations

Experimental testing is required to develop the lower bound failure curve for a more accurate prediction of the amount of strength damage caused by cyclic loading.

Upon availability of more experimental test data, the empirically defined strength deterioration factor may need to be modified to include such terms as shear span ratio.

An extensive sensitivity analysis should be undertaken to determine the proper weighting and importance factors for each member in a structure to define a global damage index.

It is recommended that for a code-type design spectra, the relationship between the natural period and the response reduction factor be quantified in terms of damage incurred, rather than ductility implicit in current procedures.

SECTION 8

REFERENCES

1. Atalay, M.B. and Penzien, J., 1975, "The Seismic Behavior of Critical Regions of Reinforced Concrete Components as Influenced by Moment, Shear and Axial Force", National Science Foundation EERC 75-19, University of California at Berkeley.

2. Bertero, V.V., Popov, E.P. and Wang, T.Y., 1974, "Hysteretic Behavior of Reinforced Concrete Flexural Members with Special Web Reinforcement", National Science Foundation EERC 74-9, University of California at Berkeley.

3. Chung, Y.S., Meyer, C. and Shinozuka, M., 1987, "Seismic Damage Assessment of Reinforced Concrete Members", Report NCEER-87-0022, State University of New York at Buffalo.

4. Gill, W.D., Park, R. and Priestley, M.J.N., 1979, "Ductility of Rectangular Reinforced Concrete Columns Under Seismic Loading", Department of Civil Engineering Research Report 79-1, University of Canterbury.

5. Kunnath, S.K., 1988, "Inelastic Analysis of Reinforced Concrete Frame-Wall Structures under Lateral Load Reversals", Special Study Report, Department of Civil Engineering, State University of New York at Buffalo.

6. Mander, J.B., Park, R. and Priestley, M.J.N, 1984, "Seismic Design of Bridge Piers", Research Report 84-2, Department of Civil Engineering, University of Canterbury, Christchurch, New Zealand.

7. Mander, J.B., Priestley, M.J.N and Park, R., 1983, "Behavior of Ductile Holow Reinforced Concrete Columns", *Bulletin of the New Zealand National Society For Earthquake Engineering,* Vol.16, No.4, pp. 273-290.

8. Newmark, N.M. and Rosenblueth, E., (1974) "Fundamental of Earthquake Engineering", Prentice Hall.

9. Nmai, C.K. and Darwin, D, 1984, "Cyclic Behavior of Lightly Reinforced Concrete Beams", National Science Foundation Report PFR 79-24596, University of Kansas Center for Research.

10. Park, R. and Paulay, T., 1975, "Reinforced Concrete Structures", Wiley-Interscience, pp. 195-269.

11. Park, Y.J., Ang, A. H-S. and Wen, Y.K., 1985, "Mechanistic Seismic Damage Model for Reinforced Concrete", *ASCE/Journal of Structural Engineering*, Vol.111, No.4, pp. 722-739.

REFERENCES (Cont'd)

12. Park, Y.J., Reinhorn, A.M., and Kunnath, S.K., 1987, "IDARC: Inelastic Damage Analysis of Reinforced Concrete Frame-Shear Wall Structures", Report NCEER-87-0008, State University of New York at Buffalo.

13. Powell, G.H. and Allahabadi, R., 1988, "Seismic Damage Prediction by Deterministic Methods: Concepts and Procedures", *Earthquake Engineering and Structural Dynamics,* Vol.16, pp. 719-734.

14. Priestley, M.J.N. and Park, R., 1987, "Strength and Ductility of Concrete Bridge Columns Under Seismic Loading", *ACI Structural Journal,* Vol.84, No.1, pp. 61-76.

15. Seidel, M.J., Reinhorn, A.M., and Park, Y.J., 1989, "A Seismic Damageability Assessment of Reinforced Concrete Buildings in Eastern United States", *ASCE/Journal of Structural Engineering,* Vol.115, No.9, pp. 2184-2203.

16. Whitman, R.V., 1989, "Workshop on Ground Motion Parameters for Seismic Hazard Mapping", Technical Report NCEER-89-0038, State University of New York At Buffalo.

17. Yunfei, H., Yufeng, C., Chang, S. and Bainian, H., 1986, "The Experimental Study of a Two-Bay Three-Story Reinforced Concrete Frame Under Cyclic Loading", *Proc., 8th Symposium on Earthquake Engineering,* Roorkee, India.

NATIONAL CENTER FOR EARTHQUAKE ENGINEERING RESEARCH
LIST OF TECHNICAL REPORTS

The National Center for Earthquake Engineering Research (NCEER) publishes technical reports on a variety of subjects related to earthquake engineering written by authors funded through NCEER. These reports are available from both NCEER's Publications Department and the National Technical Information Service (NTIS). Requests for reports should be directed to the Publications Department, National Center for Earthquake Engineering Research, State University of New York at Buffalo, Red Jacket Quadrangle, Buffalo, New York 14261. Reports can also be requested through NTIS, 5285 Port Royal Road, Springfield, Virginia 22161. NTIS accession numbers are shown in parenthesis, if available.

NCEER-87-0001 "First-Year Program in Research, Education and Technology Transfer," 3/5/87, (PB88-134275/AS).

NCEER-87-0002 "Experimental Evaluation of Instantaneous Optimal Algorithms for Structural Control," by R.C. Lin, T.T. Soong and A.M. Reinhorn, 4/20/87, (PB88-134341/AS).

NCEER-87-0003 "Experimentation Using the Earthquake Simulation Facilities at University at Buffalo," by A.M. Reinhorn and R.L. Ketter, to be published.

NCEER-87-0004 "The System Characteristics and Performance of a Shaking Table," by J.S. Hwang, K.C. Chang and G.C. Lee, 6/1/87, (PB88-134259/AS). This report is available only through NTIS (see address given above).

NCEER-87-0005 "A Finite Element Formulation for Nonlinear Viscoplastic Material Using a Q Model," by O. Gyebi and G. Dasgupta, 11/2/87, (PB88-213764/AS).

NCEER-87-0006 "Symbolic Manipulation Program (SMP) - Algebraic Codes for Two and Three Dimensional Finite Element Formulations," by X. Lee and G. Dasgupta, 11/9/87, (PB88-219522/AS).

NCEER-87-0007 "Instantaneous Optimal Control Laws for Tall Buildings Under Seismic Excitations," by J.N. Yang, A. Akbarpour and P. Ghaemmaghami, 6/10/87, (PB88-134333/AS).

NCEER-87-0008 "IDARC: Inelastic Damage Analysis of Reinforced Concrete Frame - Shear-Wall Structures," by Y.J. Park, A.M. Reinhorn and S.K. Kunnath, 7/20/87, (PB88-134325/AS).

NCEER-87-0009 "Liquefaction Potential for New York State: A Preliminary Report on Sites in Manhattan and Buffalo," by M. Budhu, V. Vijayakumar, R.F. Giese and L. Baumgras, 8/31/87, (PB88-163704/AS). This report is available only through NTIS (see address given above).

NCEER-87-0010 "Vertical and Torsional Vibration of Foundations in Inhomogeneous Media," by A.S. Veletsos and K.W. Dotson, 6/1/87, (PB88-134291/AS).

NCEER-87-0011 "Seismic Probabilistic Risk Assessment and Seismic Margins Studies for Nuclear Power Plants," by Howard H.M. Hwang, 6/15/87, (PB88-134267/AS).

NCEER-87-0012 "Parametric Studies of Frequency Response of Secondary Systems Under Ground-Acceleration Excitations," by Y. Yong and Y.K. Lin, 6/10/87, (PB88-134309/AS).

NCEER-87-0013 "Frequency Response of Secondary Systems Under Seismic Excitation," by J.A. HoLung, J. Cai and Y.K. Lin, 7/31/87, (PB88-134317/AS).

NCEER-87-0014 "Modelling Earthquake Ground Motions in Seismically Active Regions Using Parametric Time Series Methods," by G.W. Ellis and A.S. Cakmak, 8/25/87, (PB88-134283/AS).

NCEER-87-0015 "Detection and Assessment of Seismic Structural Damage," by E. DiPasquale and A.S. Cakmak, 8/25/87, (PB88-163712/AS).

NCEER-87-0016 "Pipeline Experiment at Parkfield, California," by J. Isenberg and E. Richardson, 9/15/87, (PB88-163720/AS). This report is available only through NTIS (see address given above).

NCEER-87-0017 "Digital Simulation of Seismic Ground Motion," by M. Shinozuka, G. Deodatis and T. Harada, 8/31/87, (PB88-155197/AS). This report is available only through NTIS (see address given above).

NCEER-87-0018 "Practical Considerations for Structural Control: System Uncertainty, System Time Delay and Truncation of Small Control Forces," J.N. Yang and A. Akbarpour, 8/10/87, (PB88-163738/AS).

NCEER-87-0019 "Modal Analysis of Nonclassically Damped Structural Systems Using Canonical Transformation," by J.N. Yang, S. Sarkani and F.X. Long, 9/27/87, (PB88-187851/AS).

NCEER-87-0020 "A Nonstationary Solution in Random Vibration Theory," by J.R. Red-Horse and P.D. Spanos, 11/3/87, (PB88-163746/AS).

NCEER-87-0021 "Horizontal Impedances for Radially Inhomogeneous Viscoelastic Soil Layers," by A.S. Veletsos and K.W. Dotson, 10/15/87, (PB88-150859/AS).

NCEER-87-0022 "Seismic Damage Assessment of Reinforced Concrete Members," by Y.S. Chung, C. Meyer and M. Shinozuka, 10/9/87, (PB88-150867/AS). This report is available only through NTIS (see address given above).

NCEER-87-0023 "Active Structural Control in Civil Engineering," by T.T. Soong, 11/11/87, (PB88-187778/AS).

NCEER-87-0024 Vertical and Torsional Impedances for Radially Inhomogeneous Viscoelastic Soil Layers," by K.W. Dotson and A.S. Veletsos, 12/87, (PB88-187786/AS).

NCEER-87-0025 "Proceedings from the Symposium on Seismic Hazards, Ground Motions, Soil-Liquefaction and Engineering Practice in Eastern North America," October 20-22, 1987, edited by K.H. Jacob, 12/87, (PB88-188115/AS).

NCEER-87-0026 "Report on the Whittier-Narrows, California, Earthquake of October 1, 1987," by J. Pantelic and A. Reinhorn, 11/87, (PB88-187752/AS). This report is available only through NTIS (see address given above).

NCEER-87-0027 "Design of a Modular Program for Transient Nonlinear Analysis of Large 3-D Building Structures," by S. Srivastav and J.F. Abel, 12/30/87, (PB88-187950/AS).

NCEER-87-0028 "Second-Year Program in Research, Education and Technology Transfer," 3/8/88, (PB88-219480/AS).

NCEER-88-0001 "Workshop on Seismic Computer Analysis and Design of Buildings With Interactive Graphics," by W. McGuire, J.F. Abel and C.H. Conley, 1/18/88, (PB88-187760/AS).

NCEER-88-0002 "Optimal Control of Nonlinear Flexible Structures," by J.N. Yang, F.X. Long and D. Wong, 1/22/88, (PB88-213772/AS).

NCEER-88-0003 "Substructuring Techniques in the Time Domain for Primary-Secondary Structural Systems," by G.D. Manolis and G. Juhn, 2/10/88, (PB88-213780/AS).

NCEER-88-0004 "Iterative Seismic Analysis of Primary-Secondary Systems," by A. Singhal, L.D. Lutes and P.D. Spanos, 2/23/88, (PB88-213798/AS).

NCEER-88-0005 "Stochastic Finite Element Expansion for Random Media," by P.D. Spanos and R. Ghanem, 3/14/88, (PB88-213806/AS).

NCEER-88-0006 "Combining Structural Optimization and Structural Control," by F.Y. Cheng and C.P. Pantelides, 1/10/88, (PB88-213814/AS).

NCEER-88-0007 "Seismic Performance Assessment of Code-Designed Structures," by H.H-M. Hwang, J-W. Jaw and H-J. Shau, 3/20/88, (PB88-219423/AS).

NCEER-88-0008 "Reliability Analysis of Code-Designed Structures Under Natural Hazards," by H.H-M. Hwang, H. Ushiba and M. Shinozuka, 2/29/88, (PB88-229471/AS).

NCEER-88-0009 "Seismic Fragility Analysis of Shear Wall Structures," by J-W Jaw and H.H-M. Hwang, 4/30/88, (PB89-102867/AS).

NCEER-88-0010 "Base Isolation of a Multi-Story Building Under a Harmonic Ground Motion - A Comparison of Performances of Various Systems," by F-G Fan, G. Ahmadi and I.G. Tadjbakhsh, 5/18/88, (PB89-122238/AS).

NCEER-88-0011 "Seismic Floor Response Spectra for a Combined System by Green's Functions," by F.M. Lavelle, L.A. Bergman and P.D. Spanos, 5/1/88, (PB89-102875/AS).

NCEER-88-0012 "A New Solution Technique for Randomly Excited Hysteretic Structures," by G.Q. Cai and Y.K. Lin, 5/16/88, (PB89-102883/AS).

NCEER-88-0013 "A Study of Radiation Damping and Soil-Structure Interaction Effects in the Centrifuge," by K. Weissman, supervised by J.H. Prevost, 5/24/88, (PB89-144703/AS).

NCEER-88-0014 "Parameter Identification and Implementation of a Kinematic Plasticity Model for Frictional Soils," by J.H. Prevost and D.V. Griffiths, to be published.

NCEER-88-0015 "Two- and Three- Dimensional Dynamic Finite Element Analyses of the Long Valley Dam," by D.V. Griffiths and J.H. Prevost, 6/17/88, (PB89-144711/AS).

NCEER-88-0016 "Damage Assessment of Reinforced Concrete Structures in Eastern United States," by A.M. Reinhorn, M.J. Seidel, S.K. Kunnath and Y.J. Park, 6/15/88, (PB89-122220/AS).

NCEER-88-0017 "Dynamic Compliance of Vertically Loaded Strip Foundations in Multilayered Viscoelastic Soils," by S. Ahmad and A.S.M. Israil, 6/17/88, (PB89-102891/AS).

NCEER-88-0018 "An Experimental Study of Seismic Structural Response With Added Viscoelastic Dampers," by R.C. Lin, Z. Liang, T.T. Soong and R.H. Zhang, 6/30/88, (PB89-122212/AS).

NCEER-88-0019 "Experimental Investigation of Primary - Secondary System Interaction," by G.D. Manolis, G. Juhn and A.M. Reinhorn, 5/27/88, (PB89-122204/AS).

NCEER-88-0020 "A Response Spectrum Approach For Analysis of Nonclassically Damped Structures," by J.N. Yang, S. Sarkani and F.X. Long, 4/22/88, (PB89-102909/AS).

NCEER-88-0021 "Seismic Interaction of Structures and Soils: Stochastic Approach," by A.S. Veletsos and A.M. Prasad, 7/21/88, (PB89-122196/AS).

NCEER-88-0022 "Identification of the Serviceability Limit State and Detection of Seismic Structural Damage," by E. DiPasquale and A.S. Cakmak, 6/15/88, (PB89-122188/AS).

NCEER-88-0023 "Multi-Hazard Risk Analysis: Case of a Simple Offshore Structure," by B.K. Bhartia and E.H. Vanmarcke, 7/21/88, (PB89-145213/AS).

NCEER-88-0024 "Automated Seismic Design of Reinforced Concrete Buildings," by Y.S. Chung, C. Meyer and M. Shinozuka, 7/5/88, (PB89-122170/AS).

NCEER-88-0025 "Experimental Study of Active Control of MDOF Structures Under Seismic Excitations," by L.L. Chung, R.C. Lin, T.T. Soong and A.M. Reinhorn, 7/10/88, (PB89-122600/AS).

NCEER-88-0026 "Earthquake Simulation Tests of a Low-Rise Metal Structure," by J.S. Hwang, K.C. Chang, G.C. Lee and R.L. Ketter, 8/1/88, (PB89-102917/AS).

NCEER-88-0027 "Systems Study of Urban Response and Reconstruction Due to Catastrophic Earthquakes," by F. Kozin and H.K. Zhou, 9/22/88, (PB90-162348/AS).

NCEER-88-0028 "Seismic Fragility Analysis of Plane Frame Structures," by H.H-M. Hwang and Y.K. Low, 7/31/88, (PB89-131445/AS).

NCEER-88-0029 "Response Analysis of Stochastic Structures," by A. Kardara, C. Bucher and M. Shinozuka, 9/22/88, (PB89-174429/AS).

NCEER-88-0030 "Nonnormal Accelerations Due to Yielding in a Primary Structure," by D.C.K. Chen and L.D. Lutes, 9/19/88, (PB89-131437/AS).

NCEER-88-0031 "Design Approaches for Soil-Structure Interaction," by A.S. Veletsos, A.M. Prasad and Y. Tang, 12/30/88, (PB89-174437/AS).

NCEER-88-0032 "A Re-evaluation of Design Spectra for Seismic Damage Control," by C.J. Turkstra and A.G. Tallin, 11/7/88, (PB89-145221/AS).

NCEER-88-0033 "The Behavior and Design of Noncontact Lap Splices Subjected to Repeated Inelastic Tensile Loading," by V.E. Sagan, P. Gergely and R.N. White, 12/8/88, (PB89-163737/AS).

NCEER-88-0034 "Seismic Response of Pile Foundations," by S.M. Mamoon, P.K. Banerjee and S. Ahmad, 11/1/88, (PB89-145239/AS).

NCEER-88-0035 "Modeling of R/C Building Structures With Flexible Floor Diaphragms (IDARC2)," by A.M. Reinhorn, S.K. Kunnath and N. Panahshahi, 9/7/88, (PB89-207153/AS).

NCEER-88-0036 "Solution of the Dam-Reservoir Interaction Problem Using a Combination of FEM, BEM with Particular Integrals, Modal Analysis, and Substructuring," by C-S. Tsai, G.C. Lee and R.L. Ketter, 12/31/88, (PB89-207146/AS).

NCEER-88-0037 "Optimal Placement of Actuators for Structural Control," by F.Y. Cheng and C.P. Pantelides, 8/15/88, (PB89-162846/AS).

NCEER-88-0038 "Teflon Bearings in Aseismic Base Isolation: Experimental Studies and Mathematical Modeling," by A. Mokha, M.C. Constantinou and A.M. Reinhorn, 12/5/88, (PB89-218457/AS).

NCEER-88-0039 "Seismic Behavior of Flat Slab High-Rise Buildings in the New York City Area," by P. Weidlinger and M. Ettouney, 10/15/88, (PB90-145681/AS).

NCEER-88-0040 "Evaluation of the Earthquake Resistance of Existing Buildings in New York City," by P. Weidlinger and M. Ettouney, 10/15/88, to be published.

NCEER-88-0041 "Small-Scale Modeling Techniques for Reinforced Concrete Structures Subjected to Seismic Loads," by W. Kim, A. El-Attar and R.N. White, 11/22/88, (PB89-189625/AS).

NCEER-88-0042 "Modeling Strong Ground Motion from Multiple Event Earthquakes," by G.W. Ellis and A.S. Cakmak, 10/15/88, (PB89-174445/AS).

NCEER-88-0043 "Nonstationary Models of Seismic Ground Acceleration," by M. Grigoriu, S.E. Ruiz and E. Rosenblueth, 7/15/88, (PB89-189617/AS).

NCEER-88-0044 "SARCF User's Guide: Seismic Analysis of Reinforced Concrete Frames," by Y.S. Chung, C. Meyer and M. Shinozuka, 11/9/88, (PB89-174452/AS).

NCEER-88-0045 "First Expert Panel Meeting on Disaster Research and Planning," edited by J. Pantelic and J. Stoyle, 9/15/88, (PB89-174460/AS).

NCEER-88-0046 "Preliminary Studies of the Effect of Degrading Infill Walls on the Nonlinear Seismic Response of Steel Frames," by C.Z. Chrysostomou, P. Gergely and J.F. Abel, 12/19/88, (PB89-208383/AS).

NCEER-88-0047 "Reinforced Concrete Frame Component Testing Facility - Design, Construction, Instrumentation and Operation," by S.P. Pessiki, C. Conley, T. Bond, P. Gergely and R.N. White, 12/16/88, (PB89-174478/AS).

NCEER-89-0001 "Effects of Protective Cushion and Soil Compliancy on the Response of Equipment Within a Seismically Excited Building," by J.A. HoLung, 2/16/89, (PB89-207179/AS).

NCEER-89-0002 "Statistical Evaluation of Response Modification Factors for Reinforced Concrete Structures," by H.H-M. Hwang and J-W. Jaw, 2/17/89, (PB89-207187/AS).

NCEER-89-0003 "Hysteretic Columns Under Random Excitation," by G-Q. Cai and Y.K. Lin, 1/9/89, (PB89-196513/AS).

NCEER-89-0004 "Experimental Study of 'Elephant Foot Bulge' Instability of Thin-Walled Metal Tanks," by Z-H. Jia and R.L. Ketter, 2/22/89, (PB89-207195/AS).

NCEER-89-0005 "Experiment on Performance of Buried Pipelines Across San Andreas Fault," by J. Isenberg, E. Richardson and T.D. O'Rourke, 3/10/89, (PB89-218440/AS).

NCEER-89-0006 "A Knowledge-Based Approach to Structural Design of Earthquake-Resistant Buildings," by M. Subramani, P. Gergely, C.H. Conley, J.F. Abel and A.H. Zaghw, 1/15/89, (PB89-218465/AS).

NCEER-89-0007 "Liquefaction Hazards and Their Effects on Buried Pipelines," by T.D. O'Rourke and P.A. Lane, 2/1/89, (PB89-218481).

NCEER-89-0008 "Fundamentals of System Identification in Structural Dynamics," by H. Imai, C-B. Yun, O. Maruyama and M. Shinozuka, 1/26/89, (PB89-207211/AS).

NCEER-89-0009 "Effects of the 1985 Michoacan Earthquake on Water Systems and Other Buried Lifelines in Mexico," by A.G. Ayala and M.J. O'Rourke, 3/8/89, (PB89-207229/AS).

NCEER-89-R010 "NCEER Bibliography of Earthquake Education Materials," by K.E.K. Ross, Second Revision, 9/1/89, (PB90-125352/AS).

NCEER-89-0011 "Inelastic Three-Dimensional Response Analysis of Reinforced Concrete Building Structures (IDARC-3D), Part I - Modeling," by S.K. Kunnath and A.M. Reinhorn, 4/17/89, (PB90-114612/AS).

NCEER-89-0012 "Recommended Modifications to ATC-14," by C.D. Poland and J.O. Malley, 4/12/89, (PB90-108648/AS).

NCEER-89-0013 "Repair and Strengthening of Beam-to-Column Connections Subjected to Earthquake Loading," by M. Corazao and A.J. Durrani, 2/28/89, (PB90-109885/AS).

NCEER-89-0014 "Program EXKAL2 for Identification of Structural Dynamic Systems," by O. Maruyama, C-B. Yun, M. Hoshiya and M. Shinozuka, 5/19/89, (PB90-109877/AS).

NCEER-89-0015 "Response of Frames With Bolted Semi-Rigid Connections, Part I - Experimental Study and Analytical Predictions," by P.J. DiCorso, A.M. Reinhorn, J.R. Dickerson, J.B. Radziminski and W.L. Harper, 6/1/89, to be published.

NCEER-89-0016 "ARMA Monte Carlo Simulation in Probabilistic Structural Analysis," by P.D. Spanos and M.P. Mignolet, 7/10/89, (PB90-109893/AS).

NCEER-89-P017 "Preliminary Proceedings from the Conference on Disaster Preparedness - The Place of Earthquake Education in Our Schools," Edited by K.E.K. Ross, 6/23/89.

NCEER-89-0017 "Proceedings from the Conference on Disaster Preparedness - The Place of Earthquake Education in Our Schools," Edited by K.E.K. Ross, 12/31/89, (PB90-207895).

NCEER-89-0018 "Multidimensional Models of Hysteretic Material Behavior for Vibration Analysis of Shape Memory Energy Absorbing Devices, by E.J. Graesser and F.A. Cozzarelli, 6/7/89, (PB90-164146/AS).

NCEER-89-0019 "Nonlinear Dynamic Analysis of Three-Dimensional Base Isolated Structures (3D-BASIS)," by S. Nagarajaiah, A.M. Reinhorn and M.C. Constantinou, 8/3/89, (PB90-161936/AS).

NCEER-89-0020 "Structural Control Considering Time-Rate of Control Forces and Control Rate Constraints," by F.Y. Cheng and C.P. Pantelides, 8/3/89, (PB90-120445/AS).

NCEER-89-0021 "Subsurface Conditions of Memphis and Shelby County," by K.W. Ng, T-S. Chang and H-H.M. Hwang, 7/26/89, (PB90-120437/AS).

NCEER-89-0022 "Seismic Wave Propagation Effects on Straight Jointed Buried Pipelines," by K. Elhmadi and M.J. O'Rourke, 8/24/89, (PB90-162322/AS).

NCEER-89-0023 "Workshop on Serviceability Analysis of Water Delivery Systems," edited by M. Grigoriu, 3/6/89, (PB90-127424/AS).

NCEER-89-0024 "Shaking Table Study of a 1/5 Scale Steel Frame Composed of Tapered Members," by K.C. Chang, J.S. Hwang and G.C. Lee, 9/18/89, (PB90-160169/AS).

NCEER-89-0025 "DYNA1D: A Computer Program for Nonlinear Seismic Site Response Analysis - Technical Documentation," by Jean H. Prevost, 9/14/89, (PB90-161944/AS).

NCEER-89-0026 "1:4 Scale Model Studies of Active Tendon Systems and Active Mass Dampers for Aseismic Protection," by A.M. Reinhorn, T.T. Soong, R.C. Lin, Y.P. Yang, Y. Fukao, H. Abe and M. Nakai, 9/15/89, (PB90-173246/AS).

NCEER-89-0027 "Scattering of Waves by Inclusions in a Nonhomogeneous Elastic Half Space Solved by Boundary Element Methods," by P.K. Hadley, A. Askar and A.S. Cakmak, 6/15/89, (PB90-145699/AS).

NCEER-89-0028 "Statistical Evaluation of Deflection Amplification Factors for Reinforced Concrete Structures," by H.H.M. Hwang, J-W. Jaw and A.L. Ch'ng, 8/31/89, (PB90-164633/AS).

NCEER-89-0029 "Bedrock Accelerations in Memphis Area Due to Large New Madrid Earthquakes," by H.H.M. Hwang, C.H.S. Chen and G. Yu, 11/7/89, (PB90-162330/AS).

NCEER-89-0030 "Seismic Behavior and Response Sensitivity of Secondary Structural Systems," by Y.Q. Chen and T.T. Soong, 10/23/89, (PB90-164658/AS).

NCEER-89-0031 "Random Vibration and Reliability Analysis of Primary-Secondary Structural Systems," by Y. Ibrahim, M. Grigoriu and T.T. Soong, 11/10/89, (PB90-161951/AS).

NCEER-89-0032 "Proceedings from the Second U.S. - Japan Workshop on Liquefaction, Large Ground Deformation and Their Effects on Lifelines, September 26-29, 1989," Edited by T.D. O'Rourke and M. Hamada, 12/1/89, (PB90-209388/AS).

NCEER-89-0033 "Deterministic Model for Seismic Damage Evaluation of Reinforced Concrete Structures," by J.M. Bracci, A.M. Reinhorn, J.B. Mander and S.K. Kunnath, 9/27/89.

NATIONAL CENTER FOR EARTHQUAKE ENGINEERING RESEARCH

State University of New York at Buffalo
Red Jacket Quadrangle
Buffalo, New York 14261
Telephone: 716/645-3391
FAX: 716/645-3399

ISSN 1088-3800